



UNIVERSITY OF
BIRMINGHAM

**STUDY OF GIGASEAL FORMATION IN PATCH
CLAMPING USING NANOTECHNOLOGY**

By

Majid Malboubi

A thesis submitted to

The University of Birmingham

for the degree of

DOCTOR OF PHILOSOPHY

School of Mechanical Engineering
College of Engineering and Physical Sciences
The University of Birmingham
September 2011

UNIVERSITY OF
BIRMINGHAM

University of Birmingham Research Archive

e-theses repository

This unpublished thesis/dissertation is copyright of the author and/or third parties. The intellectual property rights of the author or third parties in respect of this work are as defined by The Copyright Designs and Patents Act 1988 or as modified by any successor legislation.

Any use made of information contained in this thesis/dissertation must be in accordance with that legislation and must be properly acknowledged. Further distribution or reproduction in any format is prohibited without the permission of the copyright holder.

ABSTRACT

This PhD project is set out to study the mechanism of gigaseal formation and to provide techniques which enable the frequent formation of high resistance seals. Such techniques are highly desirable at both research and industrial levels. Furthermore they can improve the rate of gigaseal formation in high throughput systems to the level which satisfies pharmaceutical industry needs. To tackle the problem of gigaseal formation, the latest micro and nanotechnology have been introduced into the patch clamping technique.

The research can be divided into three main sections. In the first section the most important factors in seal formation were identified. Then a group of novel approaches have been developed to alter these factors and achieve better sealing conditions.

In the second section the effect of each factor on gigaseal formation has been studied. Firstly, the effect of pipette tip roughness was investigated. Scanning Electron Microscope (SEM) stereoscopic technique was used to reconstruct pipette tip and roughness parameters were calculated from the obtained digital elevation model. Patch clamping experiments were carried out using conventional and focused ion beam (FIB) polished pipettes. It is the first time FIB has been used as a polishing tool for glass micropipettes. Finite element modelling of the patch clamp

experiments helped in interpreting the different results obtained from conventional and polished pipettes. Secondly the effect of hydrophilicity of the patching site on gigaseal formation was examined. Piranha solution and oxygen plasma treatments were used to increase the hydrophilicity of the glass micropipettes. Patch clamp experiments were carried out using conventional and chemically treated pipettes. As the final factor, the effect of tip size on seal formation was investigated. Surface properties of pipettes having different sizes were measured using SEM stereoscopic technique. Focused ion beam milling was used to split open the pipettes' head for access to the inner walls. Patch clamp experiments were carried out using different sized pipettes to observe the effect of tip size.

In the third section of this research, glass micropipettes were characterized using various measurement techniques. These measurements provide valuable information on the mechanism of micropipette tip formation, sources of leakage in gigaseal formation and geometry and surface roughness properties of glass micropipettes. Furthermore it also provides ways for controlling the surface roughness properties. The proposed techniques in this thesis not only explain the gigaseal formation in more detail, but also provide techniques to increase both the seal resistance and probability of seal formation. FIB polished pipettes improved the seal resistance significantly and chemically treated pipettes resulted in the formation of seals for more than 80 % of trials. Therefore the research aims have been successfully met.

Dedicated to my wife and my parents for their continuous support

ACKNOWLEDGEMENTS

This research project would not have been possible without the support of many people. In the first place, I would like to express my sincere appreciation and gratitude to my supervisor, Professor Kyle Jiang for his patient guidance, support, encouragement and excellent advice throughout this study. He has challenged me to push beyond what I thought was possible in my research. I would like also to thank Dr Yuchun Gu, Professor Philip Prewett, Professor Farhang Bakhtar, Dr Steve Publicover, Dr Ming Lee, Dr James Bowen and Mr Alan Saywell without whose knowledge and assistance this study would not have been successful. I am very grateful to all members of the Microengineering and Nanotechnology group for their cooperative spirit and the excellent working atmosphere, creating a unique setting for intellectual explorations. Finally, I take this opportunity to express my profound gratitude to my beloved wife, parents and my sister and brothers for their moral support and patience during my study at the University of Birmingham. They have always been there as a sounding board during my hard times and I am deeply and forever indebted to them.

2.4.2	Planar and Lateral Patch Clamping.....	24
2.5	Comparison of patch clamping methods.....	31
2.6	Gigaseal Formation	32
2.6.1	Glass Structure	32
2.6.2	Membrane Structure.....	35
2.6.3	Mechanism of Gigaseal Formation	37
2.6.4	Important Factors in Gigaseal Formation	45
2.6.4.1	Cleanliness	46
2.6.4.2	Roughness.....	46
2.6.4.3	Hydrophilicity.....	47
2.6.4.4	Tip Size	47
2.6.4.5	Roundness.....	48
2.6.4.6	Other Factors	48
2.7	Summary	48
CHAPTER 3 EFFECT OF ROUGHNESS ON GIGASEAL FORMATION		50
3.1	Introduction.....	50
3.2	Glass Micropipette Fabrication.....	51
3.3	Measurement of Roughness	53
3.3.1	SEM Stereoscopic Technique	54
3.4	Polishing Pipette Tips by Focused Ion Beam Milling	59
3.5	Patch Clamping Experiments.....	61
3.6	Finite Element Modelling	66
3.6.1	Patch Clamp Manipulators.....	67
3.6.2	Pipette Tip Profile	68
3.6.3	Finite Element Modelling of Patch Clamping	70
3.7	Summary	74
CHAPTER 4 EFFECT OF HYDROPHILICITY ON GIGASEAL FORMATION..		76
4.1	Introduction.....	76
4.2	Piranha Solution Treatment	77
4.2.1	Treatment Time.....	78
4.2.2	Effect of Piranha Treatment on Pipette Surface Roughness	80
4.2.3	Effect of Piranha Treatment on Pipette Capacitance	81
4.2.4	Piranha Solution Treatment of Glass Micropipettes	81
4.3	Oxygen Plasma Treatment.....	82
4.3.1	Effect of Oxygen Plasma Treatment on Pipette Capacitance	83
4.3.2	Effect of Oxygen Plasma Treatment on Surface Roughness	84
4.3.3	Oxygen Plasma Treatment of Glass Micropipettes.....	85

4.4	Patch Clamping Experiments	85
4.5	Discussion	88
4.6	Summary	89
CHAPTER 5 EFFECT OF TIP SIZE ON GIGASEAL FORMATION		91
5.1	Introduction	91
5.2	Effect of Tip Size in Patch Clamping	92
5.3	Effect of Tip Size on Gigaseal Formation.....	94
5.4	Measuring Surface Properties of Pipettes	95
5.4.1	3D Reconstruction of the Tips	96
5.4.2	Inner Wall	100
5.5	Patch Clamp Experiments	104
5.6	Discussion	106
5.7	Summary	108
CHAPTER 6 STUDY OF GLASS MICROPIPETTES FROM TIP FORMATION TO CHARACTERIZATION		109
6.1	Introduction	109
6.2	Measuring Surface Properties of Glass Tubes	110
6.3	Effect of Pulling Parameters on Pipette Tip Size and Surface Properties	113
6.3.1	Pulling Pipettes	114
6.3.2	3D Reconstruction of Pipette Tips	116
6.3.3	Effect of Pulling Parameters of Pipette Surface Properties	118
6.4	Effect of Pulling Direction on Pipette Surface Properties	122
6.5	3D-Reconstruction of a Pipette Using FIB/SEM Nanotomography	124
6.5.1	Effect of Omega Dot	124
6.5.2	3D Reconstruction of a Pipette	125
6.6	Tip Formation	130
6.7	Summary	135
CHAPTER 7 CONCLUSION AND FUTURE WORK		137
7.1	Conclusions	137
7.2	Suggestions for Future Work	142
REFERENCES		144
APPENDIX A		157

LIST OF FIGURES

Figure 2.1. Structure of cell membrane.....	8
Figure 2.2. Schematic of the patch clamping experiment.....	13
Figure 2.3. Patch clamp configurations (20).....	15
Figure 2.4. Equivalent circuit for the cell-attached patch configuration.....	18
Figure 2.5 Comparison of conventional patch clamping with flyscreen technology.....	22
Figure 2.6 RoboPatch automated system.....	23
Figure 2.7 Replacing the patch clamp pipette with a microstructured chip.....	24
Figure 2.8 Prototype of the CytoPatch™ Chip.....	25
Figure 2.9 A microfabricated planar patch-clamp substrates and PDMS microfluidic components.....	26
Figure 2.10 Fabrication of high aspect ratio pores in quartz films.....	27
Figure 2.11 Patch clamp array on a microfluidic platform.....	29
Figure 2.12 Open-access microfluidic patch-clamp array with raised lateral cell trapping sites.....	30
Figure 2.13 Quartz molecular structure (48).....	33
Figure 2.14 Representation of glass surface in two dimensions (47).....	34
Figure 2.15 Phospholipids.....	35
Figure 2.16 Structure of the cell membrane.....	36
Figure 2.17 Chronological sequence of bleb formation in an enzymatically dissociated single fibre from the mouse flexor digitorum brevis muscle.....	38
Figure 2.18 Two models for tight patch formation, native membrane model and lipid bleb model (55).....	39
FIGURE 2.19 Aspiration of membrane into pipette.....	40
Figure 2.20 Dark-field image of a patch from chick skeletal myotube.....	42
Figure 2.21 Cartoon of patch structure.....	43
Figure 2.22 A cartoon of a patch that showing the channel free “exclusion band” below the dome that may be the basis of the gigaseal (57).....	45
Figure 3.1 Schematic shows different areas of glass micropipette.....	51
Figure 3.2 Flaming/brown micropipette puller machine, Model P-97, Sutter Instruments (66).....	52
Figure 3.3 A typical pull cycle in a program of a puller machine (65).....	53
Figure 3.4 An SEM image of a glass micropipette.....	54
Figure 3.5 Schematic of the configuration of SEM with respect to pipettes and tilting angle (α).....	56
Figure 3.6 Stereo images of the pipette tip for 3D reconstruction.....	57
Figure 3.7 A 3D reconstructed surface of the pipette tip shown at different viewing angles.....	58
Figure 3.8 The configuration of glass micropipette milling in the SEM/FIB chamber.....	60
Figure 3.9 A micro glass pipette before milling (a), the pipette after the milling (b).....	61
Figure 3.10 Schematic and real image of the pipette with respect to the cell at the moment of applying suction.....	63
Figure 3.11 Seal values for conventional and polished pipettes.....	64

Figure 3.12 Single channel recording from HEK cells with conventional pipettes. the leakage current is 2.1 pA.....	65
Figure 3.13 Single channel recording from HEK cells with polished pipettes.....	65
Figure 3.14 Schematic of pipette-membrane interaction.....	66
Figure 3.15 MP-225 micromanipulator from Sutter Instruments (66).....	67
Figure 3.16 Approach of pipette to the cell.....	68
Figure 3.17 Four different profiles of the tip surface across the thickness are shown.....	69
Figure 3.18 Dimensions and boundary conditions used in the FE modelling.....	72
Figure 3.19 Result of the FE modelling of patch clamping process.....	73
Figure 4.1 Contact angle measured before and after piranha treatment for 30 minutes.....	78
Figure 4.2 Pipettes were dipped in ink for 30 seconds.....	80
Figure 4.3 Effect of piranha solution etching time on surface roughness of glass slides.....	80
Figure 4.4 Only the very ends of pipettes were dipped into piranha solution using a micropipette holder to preserve the rest of the micropipettes from being treated.....	81
Figure 4.5 glass surface (a) before and (b) after plasma treatment (redrawn from (92)).....	83
Figure 4.6 Contact angle measured before and after oxygen plasma treatment for 1 minute.....	83
Figure 4.7 Fabrication process of a mould for oxygen plasma treatment of glass micropipettes.....	84
Figure 4.8 Surface roughness of glass as a function of power and exposure time (93).....	84
Figure 4.9 Voltage clamp recordings showing changes in current performed by an oxygen plasma treated pipette.....	86
Figure 4.10 Voltage clamp recordings showing changes in current performed by a piranha solution treated pipette.....	87
Figure 4.11 Seal values for conventional, piranha solution and oxygen plasma treated pipettes.....	87
Figure 4.12 Oxygen plasma treatment of micropipettes.....	89
Figure 5.1 Equivalent circuit for the cell-attached patch configuration (5).....	92
Figure 5.2 Longitudinal section through the tip of a thick-walled hard glass pipette (47).....	94
Figure 5.3 Two contact areas of pipette and membrane in gigaseal formation.....	95
Figure 5.4 Images of pipettes' tips before (a,b) and after (c,d) coating with platinum.....	96
Figure 5.5 SEM stereo images of pipette A (tip diameter (D_t)=8.7 μm).....	97
Figure 5.6 SEM stereo images of pipette B (D_t =2.3 μm).....	98
Figure 5.7 Pipette C (D_t =15.3 μm) before and after focused ion beam milling.....	101
Figure 5.8 Inner wall SEM stereo images of pipette C (D_t = 15.3 μm).....	101
Figure 5.9 Pipette D (D_t =11.8 μm) before and after focused ion beam milling.....	102
Figure 5.10 Inner wall SEM stereo images of pipette D (D_t =11.8 μm).....	102
Figure 5.11 Voltage clamp recordings showing changes in current performed by a bigger pipette (tip diameter = 3.5).....	105
Figure 5.12 Voltage clamp recordings showing changes in current performed by a conventional pipettes (tip diameter = 1.1).....	105
Figure 5.13 Seal values for conventional and big pipettes.....	106

Figure 6.1 Measurement of surface properties of glass tubes using light interferometry	111
Figure 6.2 Pipette pulling experiment records	116
Figure 6.3 SEM stereoscopic images captured from different angles	117
Figure 6.4 The effect of heat on tip diameter and average surface roughness.....	118
Figure 6.5 The effect of velocity on tip diameter and average surface roughness...	119
Figure 6.6 The effect of the pull on tip diameter and average surface roughness..	119
Figure 6.7 The effect of delay on tip diameter and average surface roughness.....	120
Figure 6.8 The effect of pressure on tip diameter and average surface roughness...	120
Figure 6.9 Average surface roughness of pipette tip (S_a) versus tip diameter (D_t)..	121
Figure 6.10 Digital elevation model of the inner wall surface of the pipette shown in figure 5.11.	122
Figure 6.11 Autocorrelation of roughness model of the pipette inner wall	123
Figure 6.12 Cross-sections of micropipettes formed with omega dot either down toward the filament or upward away from it.....	125
Figure 6.13 FIB nanotomography of a glass micropipette.....	126
Figure 6.14 Edge detection by using Canny algorithm.....	127
Figure 6.15 A 3D structure of the pipette tip after reconstruction.	129
Figure 6.16 An image of the first slice and fitted circle.....	129
Figure 6.17 SEM images of some big pipettes ($D_t > 20 \mu\text{m}$).	131
Figure 6.18 SEM images of some small pipettes ($D_t < 2 \mu\text{m}$).....	132
Figure 6.19 A schematic of a micropipette tip.	133
Figure 6.20 Digital elevation model of a small pipette tip ($D_t = 2.7 \mu\text{m}$) and 4 different profiles across the tip thickness.....	133
Figure 6.21 Digital elevation model of a big pipette tip ($D_t = 27.9 \mu\text{m}$) and 4 different profiles across the tip thickness.....	134

LIST OF TABLES

Table 2.1 Comparison of 3 kinds of patch clamping: conventional, planar and lateral.	31
Table 2.2. Physical characteristics of glass (47)	34
Table 3.1 Surface parameters of pipette tip for 3 pipettes (D_t = tip diameter).....	58
Table 3.2 Reconstruction information for 3 pipettes	59
Table 3.3 Profile parameters of 4 different profiles.....	70
Table 3.4 Material properties of cytoplasm and membrane.....	71
Table 4.1 Contact angle for different treatment times. Treatment time of 30s was chosen because it is more effective and the surface can maintain its properties for a longer time.	79
Table 5.1 Reconstruction information for 2 pipettes.	98
Table 5.2 Tip surface properties for two pipettes having different sizes.....	99
Table 5.3 Values of the bearing area curve for two pipette tips having different sizes	99
Table 5.4 Reconstruction information for 2 pipettes.	103
Table 5.5 Inner wall surface properties of two different sized pipettes.....	103
Table 5.6 Values of the bearing area curve for two pipette tips having different sizes	103
Table 6.1 Roughness parameters of the outer wall of glass tubes used in fabrication of glass micropipettes.....	112
Table 6.2 Roughness parameters of the inner wall of glass tubes used in fabrication of glass micropipettes.....	112
Table 6.3 Pulling parameters values	115
Table 6.4 Reconstruction information for 3 pipettes	117
Table 6.5 The surface properties of the biggest and smallest pipettes presented in Table 6.4.....	118

ABBREVIATIONS

AChRs	Acetylcholine receptors
CAGR	Compound Annual Growth Rate
CNG	Cyclic nucleotide-gated
dp/wk	Data point/week
DMEM	Dulbecco's Modified Eagle's medium
FBS	Fetal bovine serum
FIB	Focused Ion Beam
GABA	gamma-aminobutyric acid receptors
GPCRs	G protein-coupled receptors
HEK cells	Human Embryonic Kidney cells
HCN	Hyperpolarization-activated cyclic nucleotide-gated
nAChR	Nicotinic acetylcholine receptors
PDMS	Polydimethylsiloxane
PS	Penicillin Streptomycin
RF	Radio frequency
SEM	Scanning electron microscope

A LIST OF PUBLICATIONS DURING THE PHD STUDY

Book chapters:

1. Malboubi M, Gu Y and Jiang K (2010). Study of the tip surface morphology of glass micropipettes and its effects on gigaseal formation (2010), *Electronic Engineering and Computing Technology*, Springer, 609-619.

Journal Papers:

2. Malboubi M, Gu Y & Jiang K, (2011) Surface properties of glass micropipettes and their effect on biological studies, *Nanoscale Research Letters* 6, 401.
3. Malboubi M, Gu Y & Kyle J (2011). Characterization of surface properties of glass micropipettes using SEM stereoscopic technique, *Microelectronic Engineering*, 88, (8) 2666-2670.
4. Mohammadkhani A, Malboubi M, Anthony C & Jiang K, (2011). Characterization of surface properties of ordered nanostructures using SEM stereoscopic technique, *Microelectronic Engineering*, 88 (8) 2687-2690.
5. Malboubi M, Gu Y & Jiang K (2009). Experimental and simulation study of the effect of pipette roughness on gigaseal formation in patch clamping, *Microelectronic Engineering*, 87, 778-781.
6. Malboubi M, Ostadi H, Wang S, Gu Y & Jiang K (2009). Effects of the surface morphology of pipette tip on gigaseal formation, *Engineering Letters*, 17 (4): 281-285.

7. Ostadi H, Malboubi M, Prewett P D & Jiang K (2008). 3D reconstruction of a micropipette tip, *Microelectronic Engineering*, 86, 868-870.

Conference papers:

8. Chitsaz S, Malboubi M, Anthony C, Preece J, Prewett P D (2011). Design, fabrication and surface treatment of a micropaddle resonator for ultra low mass detection, *Micro Nano Engineering conference*, 36th International Conference, Berlin, Germany.
9. Malboubi M, Gu Y & Jiang K (2010). Surface property characterization of glass μ -pipettes using SEM stereoscopic technique, *Micro Nano Engineering conference*, 36th International Conference, Genoa, Italy.
10. Mohammadkhani A, Malboubi M, Anthony C & Jiang K (2010). 3D-reconstruction of nanostructures made by nano-sphere lithography using SEM stereoscopic technique, *Micro Nano Engineering conference*, 36th International Conference, Genoa, Italy.
11. Malboubi M, Gu Y & Jiang K (2009). Investigation of pipette roughness effects on seal formation in patch clamping, *Micro Nano Engineering*, 35th International Conference, Ghent, Belgium.
12. Malboubi M, Ostadi H, Wang S, Gu Y & Jiang K (2009). The effect of pipette tip roughness on gigaseal formation, *The 2009 international conference of systems biology and bioengineering*, *World Congress on Engineering*, Vol II, pp: 1849-1852, London.
13. H Ostadi, M Malboubi, K Jiang & P D Prewett (2008). FIB/SEM Nano-Tomography of a micropipette, *Micro Nano Engineering*, 34th International Conference, Athens.

CHAPTER 1: INTRODUCTION

1.1 Introduction

This thesis presents an investigation on gigaseal formation in patch clamping using micro/nanotechnology. The gigaseal is a high resistance seal (in order of giga ohms) forming between cell membrane and patching site. The project was driven by the need of high resistance seals in order to be able to measure high quality recordings from cellular ion channels activities. The conventional technique of patch clamping, first introduced by Neher and Sakmann in 1976 (1), uses a glass micropipette to study every single cell individually. The nature of the technique makes it laborious, time consuming and very low in throughput yet providing high quality recordings. The introduction of planar patch clamping has revolutionized the technique (2). The new approach took the advantages of microfabrication techniques, microfluidics and nanotechnology, to overcome many of the difficulties of conventional patch clamping. Numerous different designs were developed all over the world. While these efforts were successful in developing less laborious and higher throughput systems, the low seal resistances of planar patch clamping systems prevent them from becoming an absolute alternative to conventional technique. In fact the superior data quality of conventional patch clamping recordings has made this approach the gold standard for ion channel studies (3), (4). It seems that before to be able to develop high throughput systems successful in forming high resistance seals, in depth studies on the physical and chemical mechanism behind the gigaseal

formation are needed. The proposed approach uses micro/nano technology to study the influence of important factors such as roughness, hydrophilicity, pipette tip size etc on gigaseal formation. 3D reconstruction and nanotomography of glass micropipettes has revealed the details of the surface in contact with cell membrane. Focused Ion Beam (FIB) milling, plasma treatments and piranha solution treatment were used to alter the physical and chemical properties of the glass micropipettes. Extensive patch clamp experiments were conducted to investigate the effect of changes on seal resistance.

1.2 Aims and Objectives

The aims of this PhD project are to better understand the mechanisms of gigaseal formation and to enhance seal formation in patch clamping using micro/nanotechnology. The project also aims to provide techniques which are readily applicable in practice for gigaseal formation improvement.

The research will start by an in-depth review of the state of the art patch clamping. Conventional patch clamping and microfluidics and lab-on-a-chip systems which encompass planar & lateral patch clamping were studied. Gigaseal formation, the heart of the patch clamping technique, was found to be a bottleneck which prevents the technique from further improvements. It is planned to tackle the problem by introducing the latest micro and nanotechnology into patch clamping technique. The major challenges in the project originate from the nature and requirements of main elements present in patch clamping. They fall into four categories. First, there are many factors involved in seal formation which are interrelated. Therefore to study one factor all other factors should be kept unchanged and a large number of experiments are required to assure that recordings correspond to the factor under

study. Second, glass micropipettes used in patch clamping are very fragile. They have a tip diameter of 1-2 μm and shank of several millimetres. Furthermore it is the inner wall of glass micropipette that interacts with cell membrane and is very difficult to access. All of these confine the number of possible processes that can be used for working on the area of micropipettes which is involved in seal formation. Third, cleanliness is the most important factor in gigaseal formation and none of the process which will be used to modify the properties of micropipettes should contaminate their surface. Fourth, glass micropipettes are not conductive and it is not possible to coat them with any conductive materials because of contamination aspects. Therefore FIB milling processes to modify the pipette surface should be done without coating the samples.

In order to achieve the research aims mentioned above, the project objectives are set out as below:

1. Review of the state of patch clamping. This includes reviewing conventional patch clamping and recently developed planar & lateral patch clamping systems to find out the bottle necks in the field.
2. Inspection of areas of micropipettes which are involved in seal formation. This requires 3D reconstruction of pipette tip and pipette inner wall to measure geometrical and surface parameters. Different reconstruction techniques such as scanning electron microscope (SEM) stereoscopy and FIB nanotomography are required for different regions of micropipettes.
3. Using Focused Ion Beam milling to: first, produce ultimately flat and smooth pipette tips, second, opening a window to have access to the inner wall and third, performing nanotomography to measure the roundness of micropipettes.

4. Using oxygen plasma treatment and piranha solution treatment to change the hydrophilicity of patching area of pipettes.
5. Study the effect of pulling parameters on pipette geometry and surface properties to be able to pull optimum pipettes for a given application.
6. Conducting patch clamp experiments to observe the effect of factors such as surface roughness, hydrophilicity, tip size on seal formation.
7. Study the mechanism of micropipette tip formation.

1.3 Thesis outline

This thesis consists of seven chapters. Chapter 1 introduces the project research topic covered by this thesis. It includes the project aims, objectives and thesis outline.

Chapter 2 reviews the current research progress on patch clamping. It starts with the introduction of conventional patch clamping method and is followed by a review of planar and lateral patch clamping systems. A comparison is made between the three kinds of patch clamping and their drawbacks and advantages are summarized.

Chapters 3 to 6 describe research work carried out by the PhD candidate. Chapter 3 studies the effect of roughness on gigaseal formation. First, the roughness of pipette is measured by 3D reconstruction of pipette tip using SEM stereoscopic technique. Principles of the technique are discussed. Second, the rough surface is polished by FIB milling and third, patch clamp experiments were carried out to observe the effect of roughness on seal formation. Finite element modelling of patch clamping is carried out to understand the effect of roughness on gigaseal formation.

Chapter 4 investigate the effect of hydrophilicity on gigaseal formation. Oxygen plasma treatment and piranha solution treatment are used to change the hydrophilicity of patching area of pipette. The effects of treatments on surface

chemistry of glass are discussed. The results from different treatment times are compared and the best is selected. Only tips of micropipettes were treated and the rest of pipette is preserved from treatment by using previously manufactured moulds. Patch clamp experiments were carried out to observe the effect of hydrophilicity on seal formation.

Chapter 5 presents the effect of tip size on gigaseal formation. Surface properties of tips and inner walls of pipettes with different sizes were obtained using SEM stereoscopic technique. Pipette heads were split open using focused ion beam milling for access to the inner walls. Relation between pipette resistance and tip size and its influence on gigaseal formation is discussed. Patch clamp experiments were carried out using different sized pipettes to observe the effect of tip size.

Chapter 6 studies the geometry and surface parameters of micropipettes and mechanism of glass micropipettes tip formation. Inside and outside walls surface parameters of micropipettes before pulling were measured using laser interferometry. Surface parameters after pulling were measured using SEM stereoscopy. The effects of pulling parameters such as heat, velocity, pull, time and pressure are investigated on pipette tip surface roughness and size. Roundness of pipette in contact area with cell is also measured using FIB nanotomography and image processing techniques. The results show that two different mechanisms are involved in glass micropipette tip formation. Measurements made in this chapter are used to explain the sources of leakage and are in good agreement with the experiments made in chapters 3 to 5.

The study of gigaseal formation in patch clamping is finally concluded in Chapter 7. The major findings obtained from the study are summarised. Possible future research topics are suggested.

CHAPTER 2: LITERATURE REVIEW

2.1 Introduction

This chapter presents a literature review of popularly used patch clamping methods and gigaseal formation mechanism. Patch clamping was first introduced in biophysical studies by Neher and Sakmann in 1976 (1) and soon was expanded to many other fields in biology as well as to basic research in medicine and related areas (5). The technique not only allowed the detection of single channel currents in biological membranes for the first time but also enabled higher current resolution, direct membrane patch potential control, and physical isolation of membrane patches (6). The development of the patch clamp method was honoured with a Nobel Prize in 1991. After more than 20 years of refinement patch clamping has been refined and is the gold standard technique for assessing ion channel functions (4). The therapeutic areas in which ion channel modulators are most likely to be used include the largest categories, cardiovascular (with annual sales of \$48 billion) and the central nervous system (with annual sales of \$40 billion) (7). In addition to these areas, ion channel modulators have application in a wide range of other high value areas such as pain (neuropathic pain is estimated to be worth approximately \$550 million per year) (7). In the year 2000 drugs that modulate ion channels represented a valuable class of pharmaceutical agents with a total market value in excess of \$8 billion. The global pharmaceutical market is worth more than \$240 billion annually

with the major markets in the US, Europe and Japan where combined sales exceed \$220 billion (7). The global pharmaceutical market grew to \$808 billion in 2009, at a compound annual growth rate of 9.3% between 1999 and 2009. In 2009 there were a total of 14 cardiovascular blockbuster products with combined sales amounting to \$50.7 billion. The market has been forecast to grow to \$1,033 billion in 2014, an equivalent Compound Annual Growth Rate (CAGR) of 5.0% over the next five years (8). Ion channels, their importance as drug targets and methods for measuring ion channel activities are discussed in section 2.2. The method of patch clamping is introduced in section 2.3. Recent improvements in patch clamping including planar and lateral patch clamping are the subjects of section 2.4. Three types of patch clamping techniques are compared and their advantages are summarized in section 2.5. Gigaseal formation was found to be the area that requires more research. The mechanisms of gigaseal formation and important factors in seal formation are discussed in section 2.6. Finally, the literature review is summarised in Section 2.7.

2.2 Ion Channels

All living cells are covered by a plasma membrane. The membrane consists almost entirely of a lipid bilayer with large numbers of protein molecules in the lipid (Figure 2.1). The lipid bilayer is not miscible with either the extracellular fluid or the intracellular fluid and constitutes an effective barrier to charged molecules. As a result chemical compositions of extracellular and intracellular fluids are very different, which is extremely important to the life of the cell. There are some protein molecules that often penetrate all the way through the membrane which provide

specialized passageways for specific substances and facilitate substance exchanges between intracellular and extracellular fluids (9).

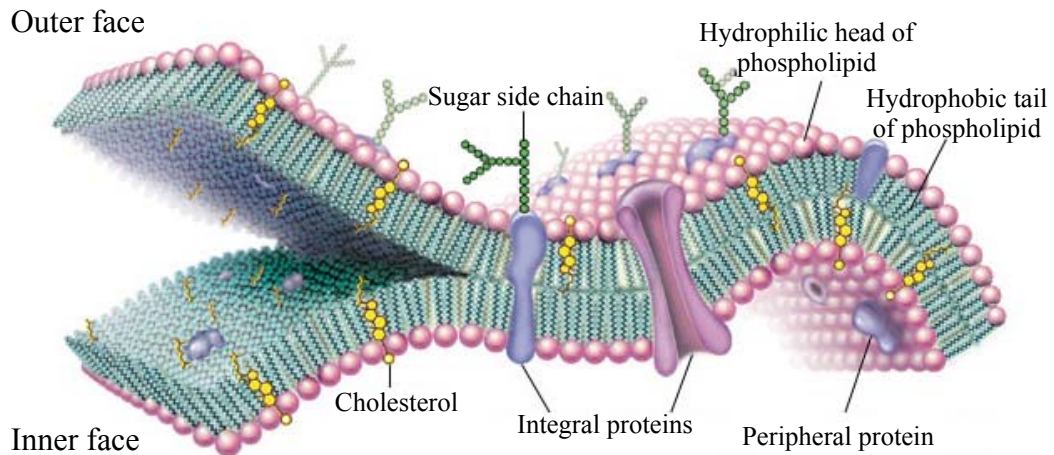


Figure 2.1. Structure of cell membrane. Integral proteins penetrate and bind tightly to the lipid bilayer, which is made up largely of phospholipids and cholesterol. Lipid bilayer is between 4 and 10 nanometers in thickness. Peripheral proteins are loosely bound to the hydrophilic (polar) surfaces, which face the watery medium both inside and outside the cell. Some intrinsic proteins present sugar side chains on the cell's outer surface (10). Section 2.6.2 discusses membrane structure in more detail.

Ion channels are a subset of proteins that span the plasma membrane and control the flow of ions across the membrane. They possess several properties that make them very effective in controlling membrane permeability to small water-soluble molecules. Firstly, they are watery pores that connect one side of the membrane to the other. Therefore substances can diffuse simply through these channels across the membrane. Secondly, they are often selectively permeable to certain substances, which results from the characteristics of the channel itself, such as its diameter, its shape and the nature of the electrical charges along its inside surfaces. Thirdly, channels are opened or closed by gating mechanisms. The opening and closing of ion channels is called gating. Ion channels can be gated by chemical, electrical, or mechanical stimuli (5), (11), and (12). Some of the major ion channels found in the plasma membrane are: Potassium channels, Sodium channels, Calcium channels,

Chloride channels, Hyperpolarization-activated cyclic nucleotide-gated (HCN) channels, Nicotinic acetylcholine receptors (nAChR), neurotransmitter gamma-aminobutyric acid receptors (GABA), Glycine receptors, Kainate receptors, cyclic nucleotide-gated (CNG) channels.

2.2.1 Importance of Ion Channel Studies

Ion channels play a vital role in a huge variety of functions in all cells. In excitable cells such as nerve and muscle, ion channels generate and shape electrical signals leading to action potential propagation, neurotransmitter release and muscle contraction. Ion channels are fundamental in controlling the heart beat and sensory transduction including pain and brain function. In non-excitabile cells, ion channels are involved in hormonal secretion, immune cell responsivity, cell-cycling, ion distribution etc (7), (13).

Ion channels together with G protein-coupled receptors (GPCRs) occupy more than 50% of all the drug discovery targets (14). Nowadays there are around 30 'channelopathies' correlated to ion channel deficiencies including cardiac arrhythmias, diabetes, epilepsy, cystic fibrosis etc making these proteins an important class of therapeutic targets for drug development (15).

2.2.2 Ion Channel Activity Measuring Methods

A major constraint on developing new ion channel-based drugs has been the difficulty in screening ion channels at the throughput required of the modern industry in a cost-effective way and with functionally relevant screens. The main methods of ion channel activity measurement are:

- Patch clamp
- Receptor binding assays
- Flux measurements
- Fluorescence detection.

Undoubtedly the definitive method for studying ion channel function is that of patch clamping. The method can detect signals in the pA range and even measure the current passing through a single ion channel protein in real time. However, patch clamping is very low throughput (~100 data point/week) and doesn't satisfy the pharmaceutical industry needs. Therefore a good deal of effort has been made in developing alternative methods of monitoring ion channel activity that can be integrated into industry-standard compound screening formats with corresponding high throughput (7).

2.2.2.1 High Throughput Ion Channel Screening

The principle methods in ion channel programmes are: receptor binding assays, flux measurements and fluorescence detection techniques. The principle advantage of

these approaches is their medium to high throughput (15-60K dp/wk) albeit at the expense of information content (16).

2.2.2.1.1 Receptor Binding Assays

Cell-based receptor binding assays are a fundamental part of drug discovery programs and a valuable tool for elucidating the mechanisms of a drug's biological effect. To design a binding assay, a high-affinity ligand that binds to the site of interest is needed. For some ligands, the affinity for a particular site has been found to vary according to the channel state (open, closed or inactivated), and hence they exhibit voltage or state-dependent binding. This means that great care is required in designing a meaningful high-throughput assay (17). Ligand binding assays say nothing about functional activity of unknown compounds and are unlikely to detect novel types of modulators by definition (7).

2.2.2.1.2 Flux Assays

Ion channel activity can also be monitored by measuring the ion flux across the cell membrane. In an optimized flux assay, modulation of ion channel activity may produce readily detectable changes in radiolabelled or nonradiolabelled ionic flux. Technologies based on flux assays are currently available in a fully automated high throughput format for efficient screening. This application offers sensitive, precise, and reproducible measurements giving accurate drug rank orders (16). As with

fluorescence, there is no ability to control the membrane potential of the host cell and as such is suited to primary screening in combination with hit validation and lead optimisation using medium to high throughput patch-clamp techniques. Without adequate patch-clamp backup use of the technique, as with fluorescence, should be treated with caution (7).

2.2.2.1.3 Fluorescence Detection

Of the functional assays developed, fluorescence has been seen as the most cutting edge. This methodology exploits changes in fluorescence that occur either with changes in the concentration of ions or changes in the membrane potential of the cell (7), (17). It greatly enabled drug discovery for various types of ligand- and voltage-gated ion channels (18). However, these techniques are limited by their inability to control the membrane potential and thus provide less information about channel activity and conductance than patch-clamp techniques (19).

2.3 Conventional Patch Clamping Technique

In patch clamping a patch of membrane is isolated from the external solution to record the currents flowing into the patch. To achieve this, small glass capillaries are heated and pulled to fabricate glass micropipettes with a tip diameter of 1–2 μm . The pipettes are then backfilled with a conductive solution and pressed against the surface of a cell. To improve the sealing condition a gentle suction is applied to the

backend of the pipette. As it is shown in figure 2.2 there are two electrodes in the patch clamp set-up: a recording electrode inside the pipette and a reference electrode in the bath solution. A high resistance seal between the glass and the patch of membrane reduces the leakage current between the two electrodes and completes the electrical isolation of the membrane patch. It also reduces the current noise of the recording, permitting good time resolution of single-channel currents which are in the order of 1 pA (5). Since the electrical resistance of the seal is in the order of giga ohms, it is called gigaseal.

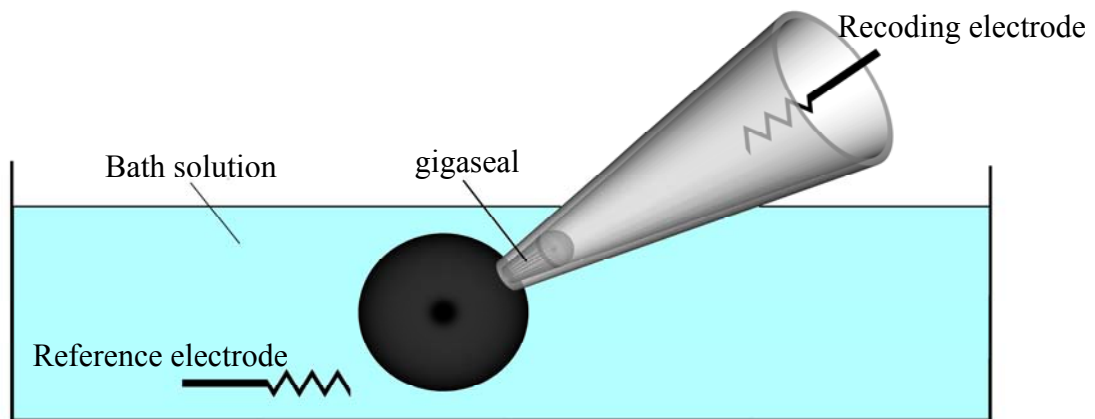


Figure 2.2. Schematic of the patch clamping experiment.

The basic elements present in every patch clamping set up are (5):

- The Platform

Measuring from microscopic samples and moving the manipulator at submicron scale needs a very stable platform. The main task of the platform is to prevent transferring vibrations from the base to the rig. Quick movements or vibrations are fatal to seals.

- The Microscope

There are two important issues about the microscope: optics type and working distance. In patch clamping it is important to visualize the membrane and because living cells are quite transparent Phase-contrast and Nomarski microscopy are usually used for this purpose. Working distance is important because it determines the range angles of approach of the pipette. To make a good seal the angle should be as perpendicular as possible for flat cells. A large working distance provides the greatest flexibility.

- The Manipulator

The main function of the manipulator is to position the micropipette tip onto the cell membrane in a controlled manner. A good micromanipulator should minimize drift and vibration and have a high resolution to be able to result in a good seal formation.

- Electrodes and Micropipettes

A micropipette works as a bridge between microscopic scale biological samples and macroscopic measuring devices. The tip is formed by locally heating and pulling of a glass tube in a micropipette puller. A large section of this thesis concerns the properties of micropipettes and their influence on gigaseal formation.

- Bath and Superfusion System

- Electronics

2.3.1 Conventional Patch Clamp Configurations

There are several configurations of the patch clamping technique (figure 2.3). These configurations enable the technique to: study ion channels at different levels; either whole cell or individual ion channels and manipulate easily the fluid on the extracellular and/or the intracellular side of the membrane during a recording (5), (20). The configurations are:

- Cell attached
- Whole cell
- Inside out
- Outside in
- Perforated

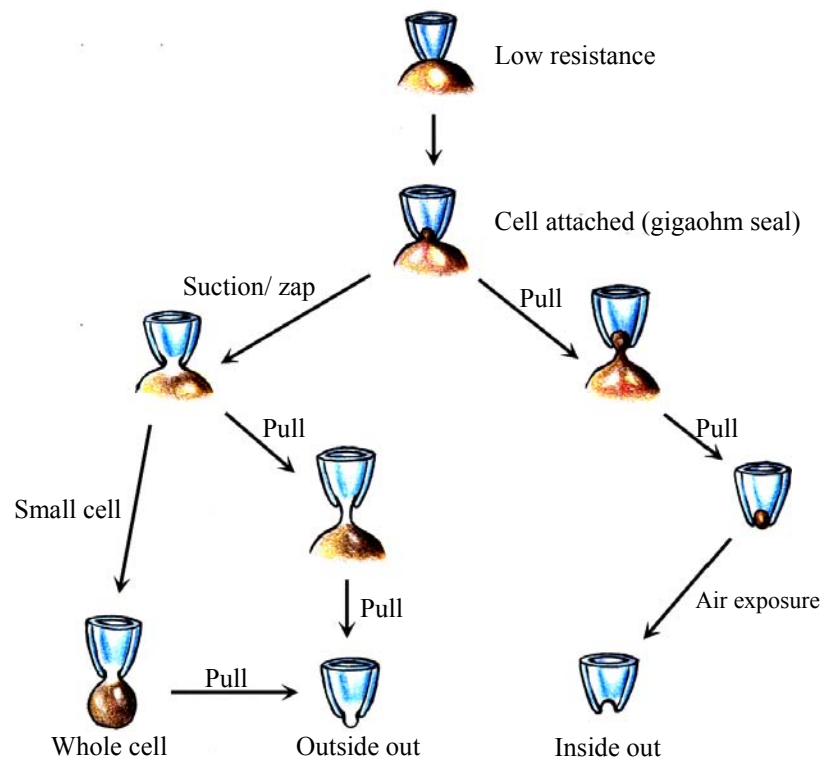


Figure 2.3. Patch clamp configurations (20)

2.3.1.1 Cell Attached Mode

The micropipette is positioned against the cell membrane and suction is applied to the backside of the pipette. A very high resistance seal (known as gigaseal, see section 2.6) forms between glass and cell. Ion channel activity in the tiny patch of membrane surrounded by the tip can be studied. The cell-attached patch mode is a single-channel configuration. This configuration leaves the cell intact, and is the most physiological configuration to study single channels and the simplest to obtain. Every patch clamp experiment starts with this situation.

2.3.1.2 Whole Cell

By applying a higher suction the patch of membrane under the pipette tip in cell-attached mode will rupture and the pipette solution make direct contact with the cytoplasm. The ensemble response of all ion channels within the cell membrane can be studied.

2.3.1.3 Inside Out Mode

By quickly pulling away the pipette from the cell after the cell attached mode is obtained the patch of membrane within the tip of the electrode can be torn from the cell while maintaining the gigaseal. This configuration enables study of the effects of cytosolic factors on channels. This mode is also a single ion channel configuration.

2.3.1.4 Outside Out Mode

By slowly pulling away the patch pipette from the cell in whole cell configuration a bleb of cell separates from the cell and forms a patch on the tip of the pipette. This is a single ion channel configuration and enables study on the effects of extracellular factors on the channels, because the bath composition can be altered easily during recording.

2.3.1.5 Perforated Patch Mode

As the volume of the cell is negligible compared with that of the patch pipette, the cytoplasm is washed out in the whole cell configuration. This is a disadvantage when the experimenter aims to study cytosolic factors. To avoid this problem a membrane-perforating agent is added to the pipette solution in the cell attached mode. The agent perforates the membrane so that only small molecules such as ions can pass through, leaving the cytoplasm's organic composition largely intact. This is referred to as perforated patch clamp mode and allows the study of all ion channels in the cell membrane.

2.3.1.6 The Equivalent Circuit for the Cell-Attached Patch Configuration

Cell attached mode has been chosen to study the gigaseal formation in this research. The equivalent electrical circuit for this mode is illustrated in figure 2.4.

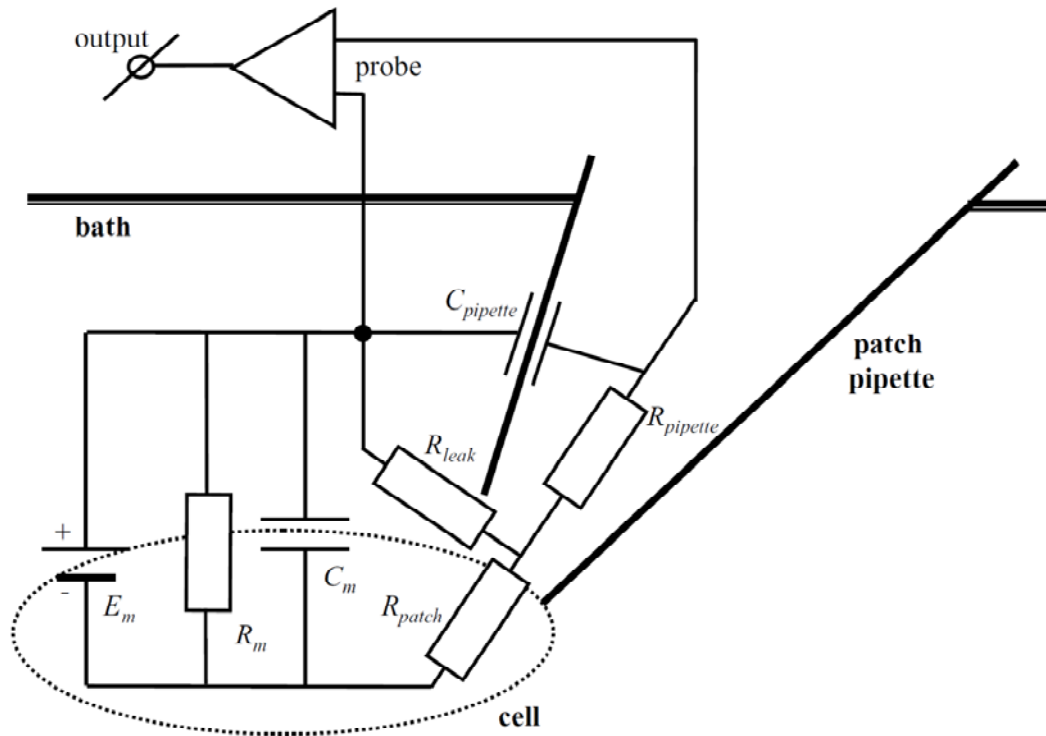


Figure 2.4. Equivalent circuit for the cell-attached patch configuration.

Definitions of the elements in figure 2.4 are as below:

$R_{pipette}$ is pipette resistance.

$C_{pipette}$ is pipette capacitance.

R_{leak} is leak resistance and represents the quality of the seal between the glass micropipette and membrane.

R_{patch} is the resistance of the patch of membrane inside the pipette.

R_m is the whole-cell membrane resistance.

C_m is the whole-cell membrane capacitance. A membrane and the intracellular and extracellular media form a capacitor.

E_m is the potential difference across the membrane.

R_{pipette} , C_{pipette} and R_{leak} are of great importance in patch clamping and are discussed in more detail.

R_{pipette} and R_{leak} : the small size of the tip of the micropipette creates a resistance. The resistance is usually minimised by using a highly conductive solution to fill the pipette and form a connection with the metal junction that leads to the probe. The pipette resistance is relatively low, but the resistance of the patch of membrane is very high. According to Kirchoff's voltage law, the greatest voltage drop in a series circuit will be over the highest resistance, therefore if the R_{patch} is high compared with R_m and R_{pipette} , then the circuit effectively monitors current flow through the patch and any ion channels in it. There is one parallel resistor in the circuit, with the potential of short circuiting, i.e. draining away current. Leak resistance (R_{leak}) represents the quality of the seal between the glass of the micropipette and the membrane. If the seal is good, then R_{leak} is very high and no significant current will leak away. The current through R_{patch} has two pathways to ground (the bath): through the probe and through R_{leak} , therefore R_{leak} should be much higher than the current input resistance of the probe. In addition, good voltage clamp of the R_{patch} can take place only if the parallel R_{leak} is not too low, and a low R_{leak} also significantly increases noise.

C_{pipette} : the relevant capacitances in the circuit are the pipette capacitance (C_{pipette}), membrane capacitance (C_m) and the capacitance of the patch of membrane. The latter is very small and not drawn in the equivalent circuit of figure 2.4. The whole-cell capacitance (C_m) is not so important here because the whole-cell membrane

resistance (R_m) is usually so much smaller than R_{patch} that R_m effectively short-circuits C_m . The pipette capacitance (C_{pipette}), although small, must be well compensated for because the high magnification and fast time scale often required in single-channel recording greatly exacerbate capacitive artefacts. The pipette glass is an insulator between the bath solution and the pipette solution, i.e. it forms a capacitor. Capacitors will delay potential changes and this situation is no exception. In practice, fast membrane potential changes such as action potentials can be distorted by this effect and many amplifiers have circuitry built in that allows for the introduction of negative capacity to counteract it. In sensitive single-channel recording the capacitances formed by the micropipette and possibly the pipette holder can become very significant. These capacitances contribute to thermal noise through RC noise and dielectric noise, and can be minimised by making the pipette and holder short (reducing the capacitor plate area) and/or thick (increasing the capacitor plate distance). A special case of capacitance prevention is to thicken the micropipette wall after pulling, by application of an insulating layer of beeswax or silicone gel. This reduces pipette capacitance by increasing capacitor plate distance but also by preventing a water film from creeping up the outer pipette wall to create more capacitance. The thickening process – or ‘sylgarding’, named after the silicone product that is often used for it – can be tricky because most benefit is gained by treating the pipette close to the tip where the glass is thinnest. It is sometimes more practical to direct effort towards pulling micropipettes with very blunt (fast-tapering) tips.

2.4 Attempts to Improve Patch Clamping

As was discussed earlier, patch clamping is the gold standard for ion channel studies. This technique is capable of studying ion channels at the highest possible resolution (single channel recordings). However patch clamping also suffers from major drawbacks such as being very laborious, time consuming and requiring a lot of experience to get satisfying results. These drawbacks have made conventional patch clamping a very low throughput technique. To overcome these problems automated patch clamp systems have been introduced. Automation can reduce the level of complexity and increase the throughput of conventional patch clamping. Automation of patch clamping has three major obstacles (21):

1. An ultraclean surface on a suitable substrate is required for obtaining the required gigaseals for measuring tiny currents.
2. A single cell should be positioned in micron scale at the patching site without using a microscope and micromanipulator.
3. Complex fluidic and electronic procedures should be carried out to automatically perform the complicated steps involved in a patch clamp experiment.

Efforts to improve and automate the conventional patch-clamp method fall into two categories (22):

- Improved configurations for conventional patch clamping and
- Planar and lateral patch clamp systems.

2.4.1 Improved Configurations for Conventional Patch Clamping

A novel idea is introduced by A. Lepple-Wienhues et al (21) for making seals inside a micropipette (figure 2.5). The configuration has the potential to be automated and inverts the cell-electrode interface. The pipette is backfilled with a solution containing cells and suction is applied to the tip. The cell forms a seal with the inner side of the pipette. The approach uses conventional glass micropipettes for seal formation which have some advantages, such as: cost effectiveness, being easy and reliable to pull pipettes with holes in micrometer scale, good surface properties and good material for seal formation (proven gigaseal substrate). The approach enabled them to develop a fully automated patch clamp robot (22).

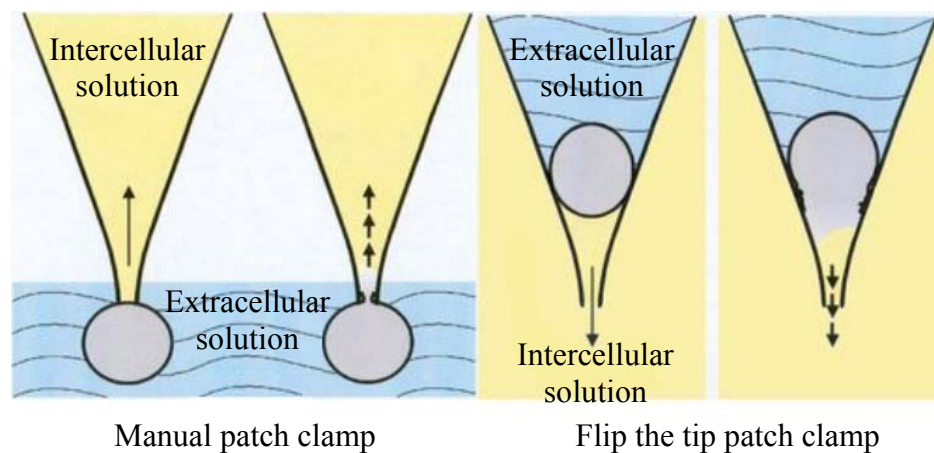


Figure 2.5 Comparison of conventional patch clamping with flyscreen technology. Flushing suspended cells into glass pipette tips automatically achieves stable gigaseals. Microscope and micromanipulator are no longer required in contrast with conventional patch clamping (21), (23).

Another attempt to improve conventional patch clamping was introduced by D. Vasilyev et al and is called RoboPatch (figure 2.6) (3). The pipette is inserted into cell suspension under a positive pressure. A gigaseal is obtained by switching the internal patch pipette pressure from positive to negative (suction). This suction near

the vicinity of the patch pipette tip attracts cells to the opening and eventually results in a physical contact between cellular membrane and patch pipette, allowing the formation of a gigaseal.

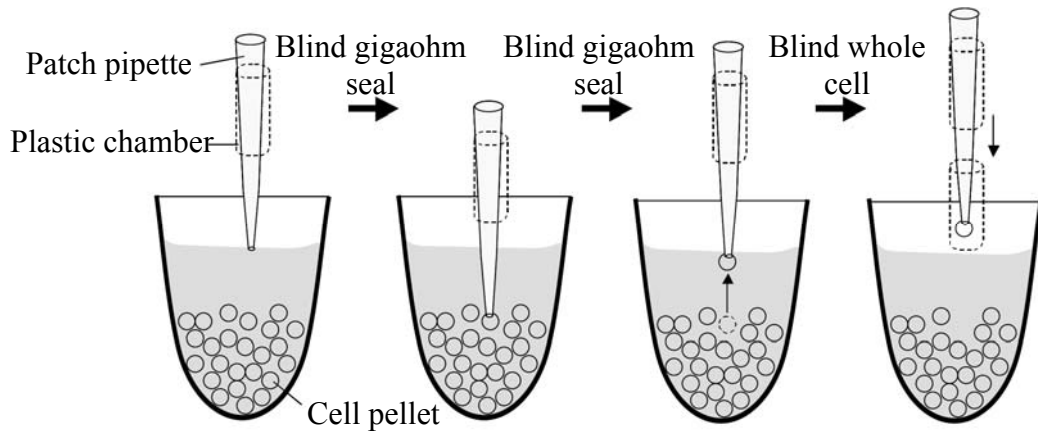


Figure 2.6 RoboPatch automated system. It utilizes a blind patch voltage-clamp recording method for ion channel drug screening (3).

Although these approaches overcome some of the drawbacks of conventional patch clamping they still have some disadvantages, such as: there is no optical access to the cell and the throughput, although higher than conventional patch clamping, doesn't meet pharmaceutical industry needs. The fundamental electrode is still an individual glass pipette which cannot be easily scaled to high throughput applications. At the same time, the heavy reliance on automated sample handling limits applicability at the research level (22).

2.4.2 Planar and Lateral Patch Clamping

In planar patch clamping the pipette is replaced with a microstructured chip. A planar chip with a micron sized pore separates the intracellular and extracellular solutions. The cell is positioned on the pore and suction is applied to encourage gigaseal formation. In comparison with conventional patch clamping, planar patch clamp configuration doesn't need costly equipment such as: a precise manipulator, high magnification microscope and antivibration table.

Fertig et al (2002) conducted one of the earliest attempts in the field of planar patch clamping. Their design is shown figure 2.7. The figure also shows the difference between conventional and planar patch clamp configurations (2).

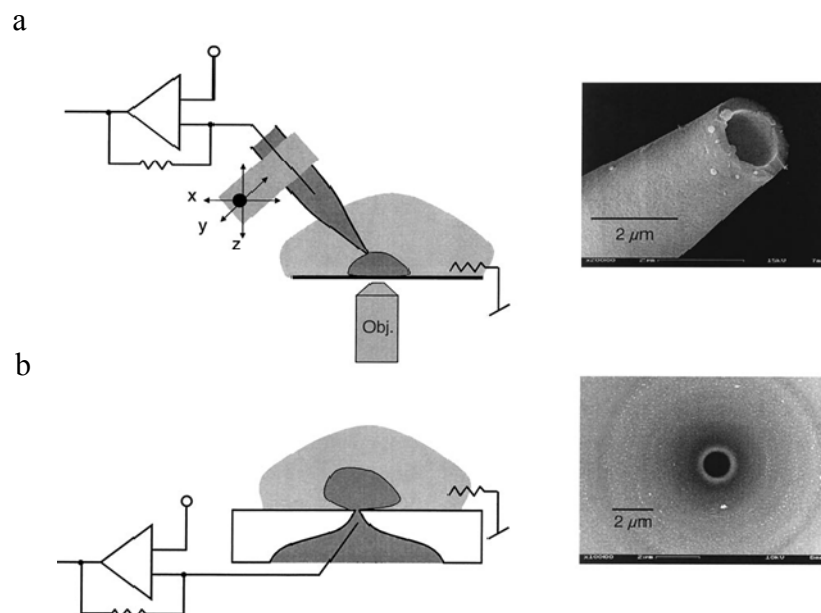


Figure 2.7 Replacing the patch clamp pipette with a microstructured chip. a) Whole cell configuration of the classical patch clamp technique. Using an x-y-z micromanipulator and a binocular microscope, the tip of a glass pipette is positioned onto a cell. b) Whole cell recording using a planar chip device. The quartz chip has an aperture of micrometer dimensions. Cells in suspension are positioned and sealed onto the aperture by brief suction. Further suction establishes electrical contact as in A. No microscope or micromanipulator is needed (2).

The idea of bringing cells to the patching site rather than bringing the pipette to the cells drew the attention of many researchers and hundreds of different designs were developed, each of them has some advantages over the others but are not free from drawbacks. One of the major drawbacks of planar patch clamping is that the same hole is used for both cell positioning and gigaseal formation. This greatly affects the gigaseal quality since debris in the solution may block or contaminate the pore. To overcome this problem, A. Stett. et al (2003) developed a concentric double pipette-like structure (figure 2.8). The outer channel is used for cell positioning and the inner channel for current measurements. Positive pressure is initially applied in the inner channel to prevent debris from approaching its surface. Suction in the outer channel directs a cell to the top of the measurement site, which looks exactly like the tip of a pipette. When a cell is placed at the measurement site, suction is used in the inner channel to encourage seal formation (24).

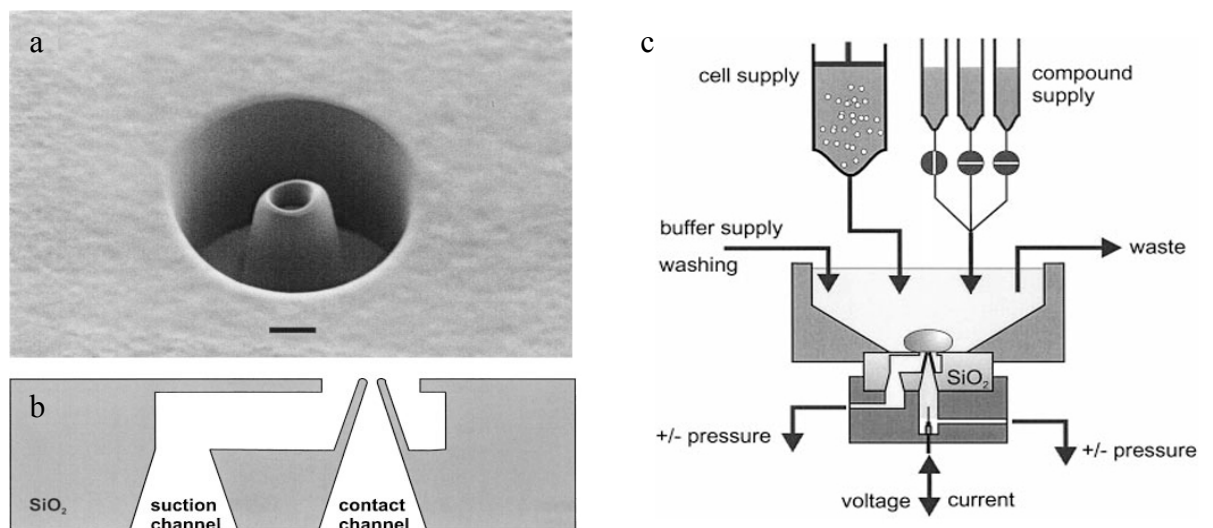


Figure 2.8 Prototype of the CytoPatch™ Chip. a) Design pattern of the cytocentering site with its two concentric openings formed with a focused ion beam in a 10 μm thick quartz layer (Scanning Electron Microscope (SEM) image, scale bar 2 μm), b) schematic drawing of the cytocentering site with suction and contact channels embedded in the bulk of a quartz chip. c) Schematic drawing of a CYTOPATCH™ site, which provides chip, cell and compound supply fully automated for cell-by-cell patch clamping (24).

Planar patch clamping systems increase throughput mainly by taking advantage of their potential to be parallelised and integrated with microfluidic systems. Microfluidic systems facilitate cell manipulation and provide good control on intracellular and extracellular solution exchange. B. Matthews et al (2006) developed a microfabricated planar patch-clamping system with polydimethylsiloxane (PDMS) microfluidic components (figure 2.9) (11).

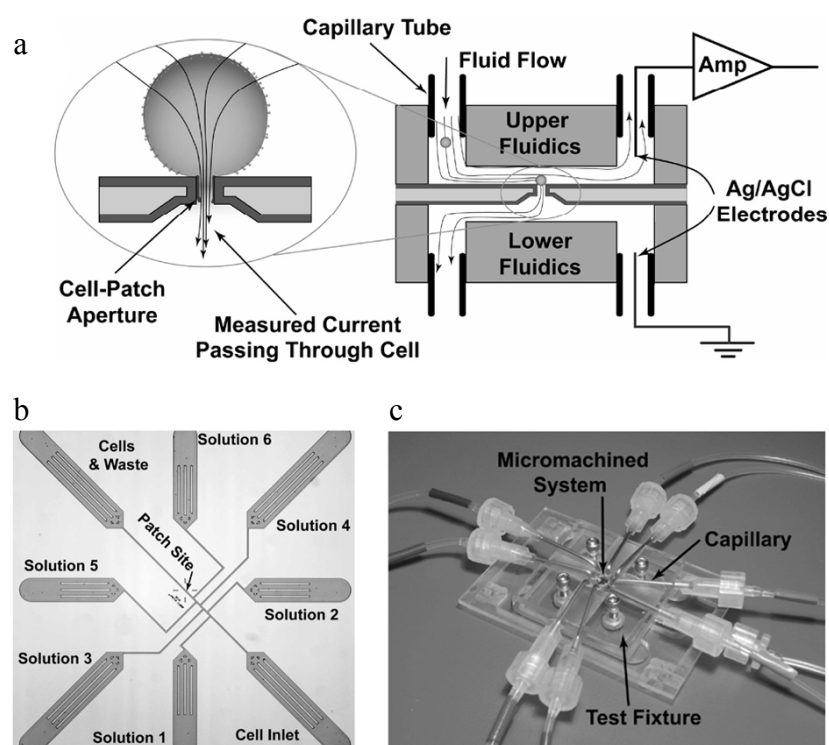


Figure 2.9 A microfabricated planar patch-clamp substrates and polydimethylsiloxane (PDMS) microfluidic components. a) Schematic diagram of a planar patch-clamp dose-response measurement system, b) Overview of the eight-port microfluidic system and c) Photograph of the macroscopic test fixture with eight capillaries connecting to the micromachined planar patch-clamp system.

The design shown in figure 2.9 uses the advantages of PDMS as a transparent, easy to process material. The use of PDMS components has made the exchanging of planar patch clamp chips easier and facilitated quick microfluidic connections. The integration of microfluidics into planar patch-clamp systems can enhance the

solution control by providing laminar- flow conditions, rapid fluid exchange, and micro-scale control elements such as valves and a pump.

The second greatest advantage of planar patch clamping systems is their potential to be parallelised. J. M. Nagarath et al reported the fabrication of quartz films with high aspect ratio pores in order to be used as a planar-patch electrophysiology device (figure 2.10). The smooth surface of pores, the material type and the high depth of pores (which will increase the length of membrane-glass position) resulted in a formation of high resistance seals comparable with those in conventional patch clamping. When interfaced with a microfluidic system, this device has the potential to serve as a low noise, high throughput patch clamp platform (25).

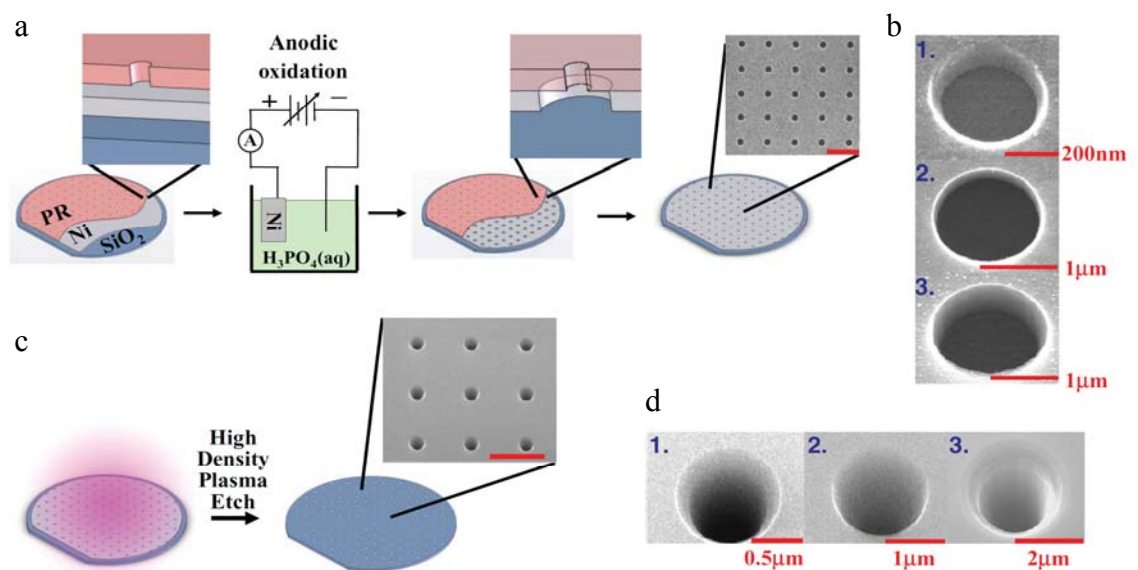


Figure 2.10 Fabrication of high aspect ratio pores in quartz films. a) Pore patterns, smaller than the intended nickel pores, are lithographically defined in a resistant layer above a nickel film. The exposed Ni (anode) is electrochemically etched/polished in concentrated acid to create highly polished Ni patterns undercut from the resistant pattern. SEM image of arrays of pores in a 250 nm thick Ni film is shown. Scale bar = 5 μ m. b) SEM images of pores in Ni films with different thicknesses, #1-3: 100 nm, 300 nm, 500 nm, respectively. c) The Ni pores serve as etch masks during high-density plasma etching of high aspect ratio structures in silicon dioxide. An SEM image of an array of pores etched 5 μ m deep in silicon dioxide. Scale bar = 5 μ m. d) SEM images of high aspect ratio pores in silicon dioxide with very smooth sidewalls. The depth of each pore, #1-3, is 3 μ m, 5 μ m, 8 μ m, respectively. Pores #1-2 are etched in low temperature oxide films while pore #3 is etched in fused quartz.

Although planar patch clamp systems increased the throughput by their ability to be parallelized and automated, they are not free from deficiencies. The main drawback of planar patch clamping systems is that the value of the seal is low, as a result the quality of measurements are not high. Single channel recording is also very difficult to obtain because of the very good sealing conditions which are needed for these recordings. There is no optical access in most of the cases except when the chip is made of transparent material like glass or PDMS (2), (22). Similar to patch clamp pipettes, the planar patch clamp chips cannot be reused once a recording is made. Therefore low cost and easy fabrication processes are desirable. Lateral patch clamping was introduced to overcome some of the drawbacks of the planar patch clamping system. PDMS has been widely used in lateral patch clamping systems. Using PDMS has some advantages such as: the fabrication process is sufficiently simple (requiring only molding and bonding), secondly it is economical to enable the production of single use disposable devices and thirdly it is transparent which enables the visualization of the cells during recording (26).

Figure 2.11 shows a PDMS based lateral patch clamping system developed by P. Lee and his colleagues (26).

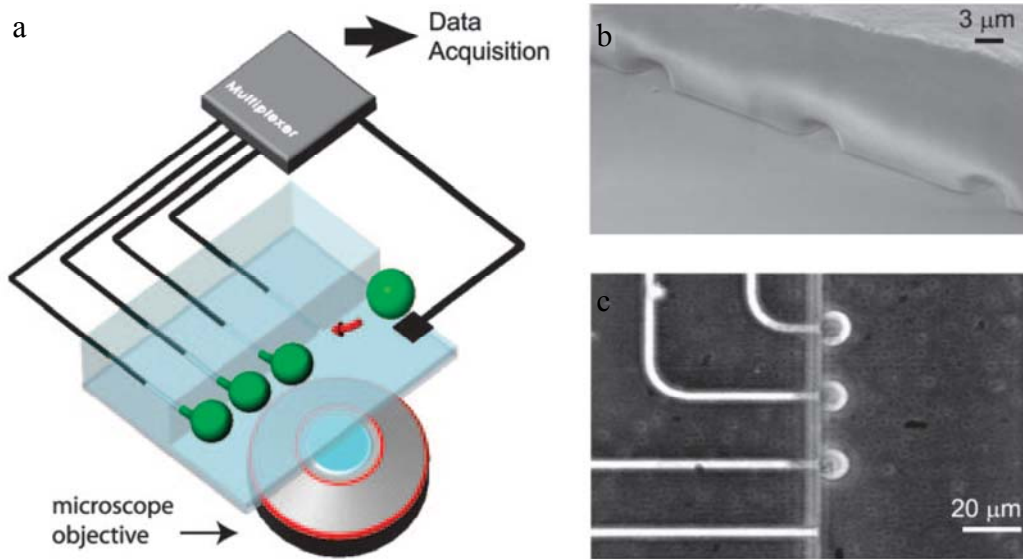


Figure 2.11 Patch clamp array on a microfluidic platform. a) Cell trapping is achieved by applying negative pressure to recording capillaries, which open into a main chamber containing cells in suspension. The device is bonded to a glass coverslip for optical monitoring. b) Scanning electron micrograph of three recording capillary orifices as seen from the main chamber. The capillary dimensions are $4 \times 3 \mu\text{m}$, with a site-to-site distance of $20 \mu\text{m}$. c) Darkfield optical microscope image of cells trapped at three capillary orifices. The device consists of 12 capillaries arrayed 6 along each side of the main chamber fluidic channel, along a $120 \mu\text{m}$ distance (26).

The PDMS microfluidic chip is moulded from microfabricated silicon/SU-8 master. Cells are trapped at the micro-sized lateral channels and gigaseals have been obtained. This geometry allows inherent microfluidic integration, high density patch sites, and the ability to do fluorescence measurement during electrical recording. The success rate to form gigaseals is only about 5%. However, in view of this system's easy integration with microfluidics, it becomes promising for situations where a low-resistance seal is acceptable. Cell trapping sites in this design are at the bottom plane of the chip which gives the patched cell an uncommon deformation. Therefore another design was introduced, by the same group, which has elevated trapping sites (Figure 2.12) (27). In this design a thin layer of PDMS ($20 \mu\text{m}$) is bonded to the main PDMS microfluidic channels by treating both surfaces with oxygen plasma. The PDMS device is peeled off from the silicon wafer and a 4 mm hole is punched at the centre of the device to open an access to the patching sites.

The device is then bonded to a glass cover slip and is ready to use. The success rate of the device is higher than 80% but the low values of seals (250 M Ω) are just sufficient for whole cell recording.

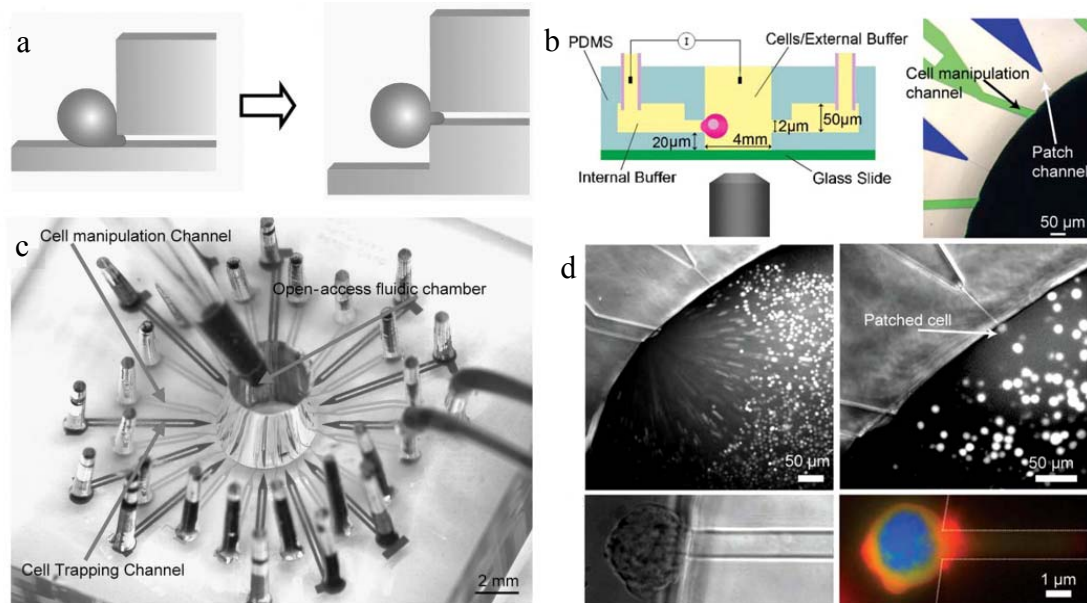


Figure 2.12 Open-access microfluidic patch-clamp array with raised lateral cell trapping sites. a) Cross-sectional illustration showing how the cell is trapped in the new design in comparison with how the cell is trapped in previous lateral patch clamp devices. b) Angled view of the device. Patch channels and cell manipulation channels were filled with two different dyes. The open access chamber is shown in the image, where cells or drug samples can easily be pipetted in. c) Schematic of the set-up showing how the cell is being trapped onto the channel. d) Close-up of a trapped cell on the patch channel in bright field and fluorescent image of the same cell (27).

Many different designs and materials are used in planar and lateral patch clamping, although generally the value of seals are not comparable with seals in conventional patch clamping. Some of the other materials used in planar patch clamping systems are:

- Silicon dioxide (28), (29)
- Quartz glass (2), (30)
- Silicon nitride (31) (32)
- Diamond-on-silicon (33)
- Polyimide (34)

2.5 Comparison of patch clamping methods

In this section a comparison is made between the different kinds of patch clamping.

The advantages and drawbacks of each kind are presented in Table 2.1.

Table 2.1 Comparison of 3 kinds of patch clamping: conventional, planar and lateral.

	Conventional Patch clamping	Planar patch clamping	Lateral patch clamping
Quality of recordings	Superior data quality ^{(3), (25)}	Lower data quality ^{(3), (25)}	Lower data quality
Throughput	Lower throughput ^{(14), (33), (35)}	Higher throughput ^{(4), (36), (22), (11)}	Higher throughput ^{(26), (27)}
Value of gigaseals	Higher ^{(3), (25)}	Lower	Lower ^{(26), (27)}
Optical access	Yes	No* ⁽²²⁾	Yes* ^{(37), (26)}
Microfluidic integration	N/A	Yes ^{(11), (38), (35), (39) (40)}	Yes ^{(37), (26)}
Ability to control pipette and bath solution	More difficult ⁽⁴¹⁾	Easier ^{(11) (39)}	Easier
Density of cell trapping sites	N/A	Lower	Higher ^{(37), (26), (27)}
Level of complexity	Higher ^{(27), (33)}	Lower ⁽²⁾	Lower
Level of user expertise	Higher ^{(27), (33)}	Lower	Lower
Cost	Expensive equipment, cheap pipettes	Expensive single use chips ^{(42), (22)}	Cheaper than planar, more expensive than conventional
Pipettes/chips fabrication processes difficulty	Easy	Difficult	Easier than planar, more difficult than conventional
Time consumption	Higher ^{(27), (33), (2)}	Lower	Lower
Ability to choose the best cell for patching	Yes	No	Yes
Potential for automation	Yes ^{(43), (21), (3), (44)}	Yes ^{(22), (11), (45), (46), (24)}	Yes ^{(26), (27)}

* Unless the substrate is made of glass or other transparent materials.

As it can be understood from the table conventional patch clamping has better data quality and lower throughput while planar and lateral patch clamping have lower data quality and higher throughput. Planar and lateral patch clamping systems have revolutionized the patch clamping technique and took the advantages of microfabrication techniques, microfluidics and nanotechnology. Although they overcome many of the difficulties of conventional patch clamping, it is conventional

patch clamping that has become the gold standard for ion channel studies. The low seal resistances of planar patch clamping systems prevent them from becoming an absolute alternative to the conventional technique. Due to the superior data quality of conventional patch clamping recordings, the confirmation of ion channel recordings is often based on the data obtained by conventional patch clamping (3). It seems that before the development of high throughput systems successful in forming high resistance seals, in-depth studies on the physical and chemical mechanism behind the gigaseal formation are needed. In the next section the mechanism of gigaseal formation is discussed and the important factors in forming a high resistant seal are introduced.

2.6 Gigaseal Formation

Upon applying suction a patch of membrane goes inside the pipette and a seal forms between the glass and membrane. As the electrical resistance of the seal is in the order of giga ohm it is called gigaseal. To have a good understanding of the interactions and forces in gigaseal formation it is necessary to have a close look at the glass and membrane structures.

2.6.1 Glass Structure

Glass have a molecular structure similar to a quartz crystal. In glass the regular arrangement of atoms found in crystalline quartz has been disordered by melting and

by the addition of contamination such as sodium oxide and boric oxide. Quartz is a mineral composed of silicon and oxygen: SiO_2 . Each silicon atom in quartz is surrounded by four tetrahedral disposed oxygens, and each oxygen forms a bridge between two silicon atoms (Figure 2.13) (47).

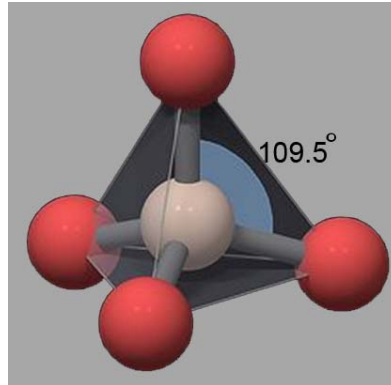


Figure 2.13 Quartz molecular structure (48)

Quartz is transparent and strong but melts at a rather high temperature (1600°C), therefore it is not suitable for fabricating patch clamping pipettes. If the appropriate amount of sodium oxide (Na_2O) is added to quartz a soft glass known as soda glass results, which melts at a lower temperature (800°C). The presence of sodium ions relatively disorder and loose the glass structure and give a higher conductivity to soda glass than fused quartz and hard glass (to be described later). Due to its higher conductivity soft glass is noisier than quartz or hard glass. In fabricating micropipettes for patch clamping, borosilicate glass (hard glass) has long been used and found satisfactory for most purposes. Borosilicate, or hard glass has an intermediate structure and properties, between those of fused quartz and soft glass. It is composed of silicon dioxide, sodium oxide and boric oxide (B_2O_3) in relative proportions of about 80%, 5% and 15%. Hard glass, as compared to soft glass, has a structure more like that of fused quartz. As a result it also has higher mechanical strengths, higher melting point (1200°C), lower electrical conductivity and therefore

is less noisier (47). Some of the physical characteristics of glass are summarized in Table 2.2.

Table 2.2. Physical characteristics of glass (47)

Glass type	Melting temp (°C)	Resistivity (Ω cm)	Coefficient of thermal expansion (cm/cm per °C)	Dielectric constant	Surface charge (e/nm^2)
Quartz	1600	1014	6×10^{-7}	3.75	0
Hard	1200	1010	3×10^{-6}	4.0	0.05
Soft	800	107	1×10^{-5}	7.0	0.3

To understand the glass-membrane interactions involved in the formation of tight seals, surface properties of glass should be considered. The glass surface is composed of silicon atoms and oxygen on one of three configurations: oxygens that form the bridge between pairs of silicon atoms, oxygens bound to hydrogen and charged oxygen with their charge neutralized by a sodium ion (figure 2.14).

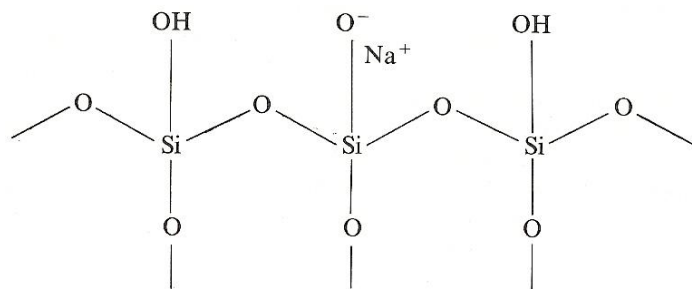


Figure 2.14 Representation of glass surface in two dimensions (47)

Glass has about one oxygen per square nanometre of surface area (47). In soft glass, about one third of these oxygens are charged, producing a surface charge density of approximately $0.3/nm^2$; borosilicate glass has fewer charged oxygen atoms and a

negative surface charge density of about $0.05/\text{nm}^2$. Glass has a negative surface charge and is strongly hydrophilic (47).

2.6.2 Membrane Structure

Liquid bilayer membranes are constructed of phospholipids. The phospholipids contain both hydrophobic (fatty) and hydrophilic (polarised) residues. In a watery environment phospholipids will arrange themselves spontaneously into structures where the hydrophobic residues face each other. The arrangement found in cell membranes is a bilayer of phospholipids (figure 2.15).

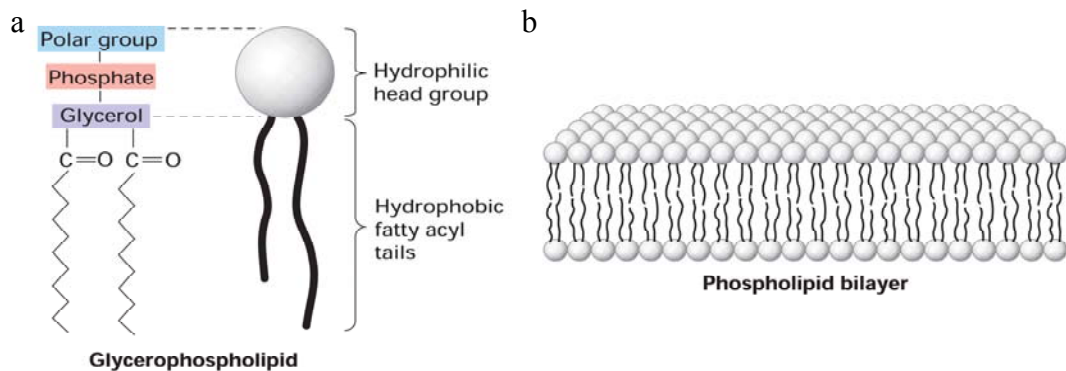


Figure 2.15 Phospholipids. a) Phosphatidyl choline, which is a typical membrane phospholipid, has a polarised head and fatty tails, b) Bilayer arrangement of phospholipids in a watery environment (49).

The most common types of phospholipids present in bilayer are phosphatidylethanolamine, phosphatidylcholine and phosphatidylserine. The first two of these phospholipids have no net charge, because the positive charge on the

alcohol balances the negative charge on phosphate. The third is negatively charged. The net density of surface charges on phospholipid bilayers is about less than one charge per square nanometre. Note that on the 5 to 10 Å scale, phospholipid head groups have both positive and negative charges even when the net surface charge is negative (47).

There are two other general constituents embedded in the lipid bilayer membrane; first, a variable number of membrane proteins whose density ranges from a few hundred per square micrometre up to 10000 per square micrometre and second, a large number of macromolecules associated with the extracellular surface of the membrane (figure 2.16).

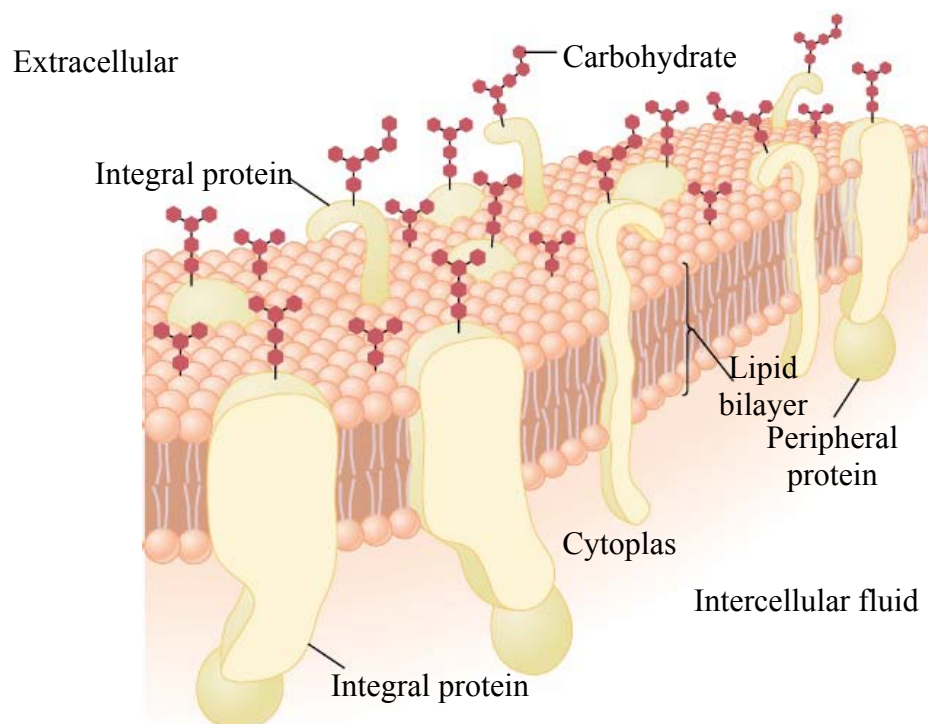


Figure 2.16 Structure of the cell membrane, showing that it is composed mainly of a lipid bilayer of phospholipid molecules, but with large number of protein molecules protruding through the layer (9).

There are two types of proteins in the membrane: integral proteins that protrude all the way through the membrane and peripheral proteins that are attached only to one surface of the membrane and do not penetrate. Many of the integral proteins provide structural channels (or pores) through which water molecules and water-soluble substances, especially ions, can diffuse between the extracellular and intracellular fluid (9) (47).

2.6.3 Mechanism of Gigaseal Formation

After applying suction the membrane patch usually moves 5-100 μm down the inside of the pipette (25), (50), (51), (52). In order to explain the mechanisms of seal formation it is important to find out how do membrane patches form in pipettes and which elements of them are contributed in seal formation. Seals form readily between electrodes and many types of cells in various physiological and developmental states. Such cells have quite different extracellular matrix elements and densities. Furthermore, seals form readily and in an apparently normal fashion between glass electrodes and pure phospholipid membranes of defined composition. The seal interaction seems to be directly between the glass and the lipid bilayer and seems not to involve integral membrane proteins to the extracellular matrix. In fact these elements probably are detrimental to seal formation (47) (53).

There have been many studies on the formation of membrane patches inside pipettes using different techniques such as optical or electron microscopy (51), (52), (53),

(54), (55), (56), (57). The patch and pipette tip are at the limits of resolution of the optical microscope. Only rarely it is possible to see the membrane patch during the experiment and even then quantitative evaluation of its size is impossible or difficult (6). Milton et al have studied seal formation of pipettes with openings around 10 μm which is almost 10 times the size of pipettes used in patch clamping. In their experiments they could reach to resistances as high as 100 $\text{M}\Omega$ and claimed that this is equivalent of gigaseal when doing experiments with normal patch clamping pipettes (55). Figure 2.17 shows the sequence of patch formation in their experiments.

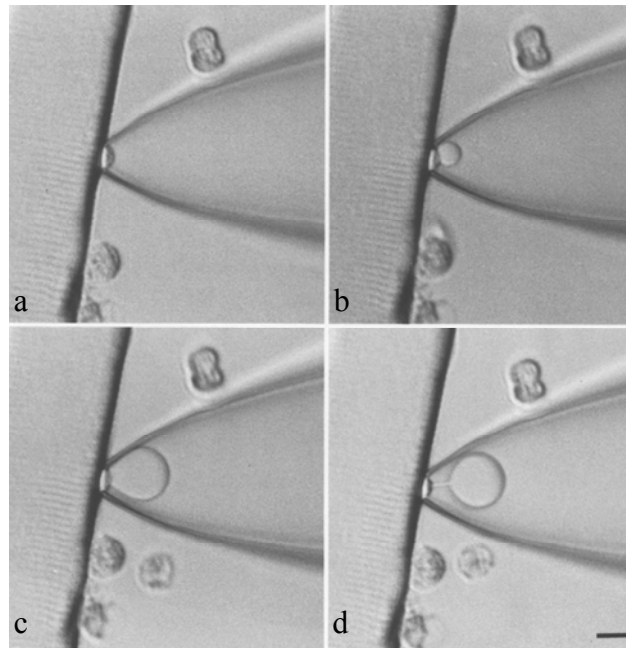


Figure 2.17 Chronological sequence of bleb formation in an enzymatically dissociated single fibre from the mouse flexor digitorum brevis muscle. (a) Upon application of suction, the membrane bulged into the pipette. (b) A bleb appeared abruptly at the rim of the pipette and was almost immediately several micrometres in diameter. (c) Enlargement of the bleb. (d) Sometimes the connection with the cell became a thin tether. The scale bar in d is 10 μm and applies to a-d. The pipette was bent to approach the cell parallel to the cover glass; this view allowed the bleb to be in the same focal plane as the fibre during the formation and growth of the bleb (55).

They have suggested that two models can be assumed for patch formation:

- 1- Native membrane model and
- 2- Lipid bleb model

These two models are shown in figure 2.18.

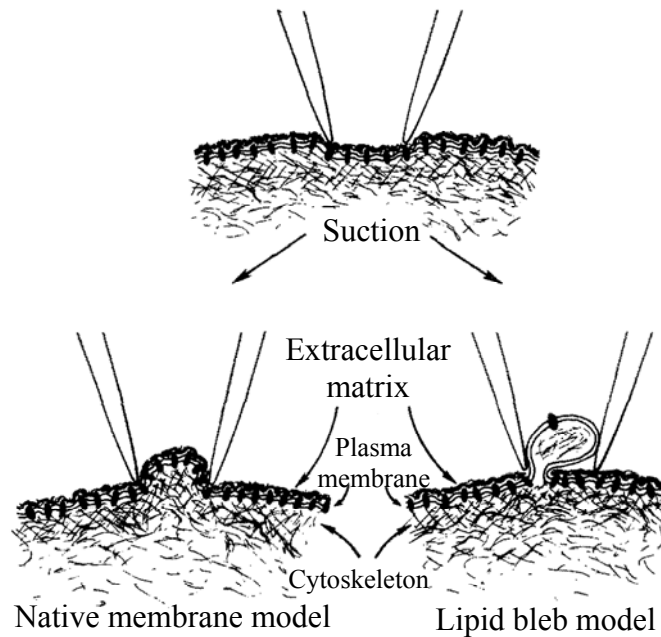


Figure 2.18 Two models for tight patch formation, native membrane model and lipid bleb model (55).

The native membrane model assumes that the surface membrane is distended and forms a seal with the pipette. The lipid bleb model assumes that suction produces a drop in pressure outside the membrane due to fluid flow (a Bernoulli effect) which is greatest under the pipette rim. In addition to the distension of the entire patch, tiny bulges are assumed to occur under the pipette rim where attachments to the cytoskeleton or extracellular matrix are relatively sparse. This bulging creates a shear stress in the membrane at the edges of the bulge. When a critical value of shear stress is reached, a phase separation occurs with phospholipids and highly

mobile membrane proteins flowing into the region of the bulge and forming a bleb. The bleb almost immediately becomes over a micrometre in diameter (Figure 2.17 b) and would form a gigaseal in a small pipette. These bleb membranes tend to have much higher lipid content than a normal surface membrane, with lipid to protein weight ratio of 20:1. This is in good agreement with the fact that seals form readily between electrodes and many types of cells. The bleb is also believed to have less connection with underlying cytoskeleton (figure 2.19) which explains the higher protein motility in blebs (55).

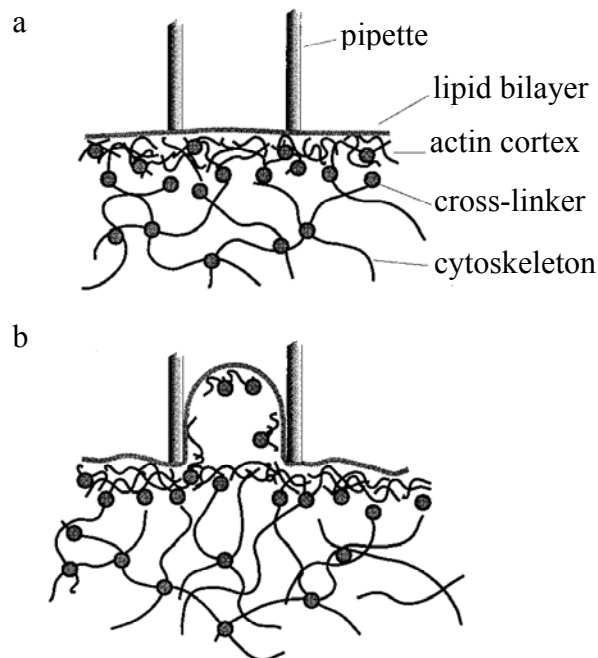


FIGURE 2.19 Aspiration of membrane into pipette. a) Schematic of the first step in an aspiration of membrane into pipette, the formation of a tight seal between pipette and plasma membrane. b) If the suction pressure exceeds the threshold value, a fracture is assumed to occur between lipid bilayer and the underlying actin cortex, including a partial disruption of the latter (58).

Applying higher suction increases the patch area which is because of a flow of lipid (with perhaps small amounts of diffusible protein) along the walls of the pipette into the patch. Using video microscopy as well as capacitance measurements Sokabe et

al. (1991) demonstrated that the area of a membrane patch in a pipette increases up to 10% following the application of suction pressures of up to 3.0 kPa. As this area increase is considerably larger than the 2% elastic limit of lipid membranes, they ruled out membrane stretching as the source of the area change. Capacitance measurements confirmed that the area increase in their video images was the result of a net increase in the amount of material comprising the patch, an increase which they interpreted as evidence for pressure-induced free flow of lipid from the cell into the patch of membrane (52). Lorinda et al have argued that the increase of patch area is not because of the free flow of lipid and is the result of membrane pulling away from the interface of lipid and glass to establish force equilibrium. However even in their model, a seal forms between lipid and glass (53).

Gigaseal forms gradually and this suggests that the seal has distributed resistance rather than a local spot weld (54). Ruknudin et al have studied membrane patches inside pipettes using high voltage electron microscopy. In their experiments patches were formed between 5 to 20 μm from the tip. Figure 2.20 shows an electron microscopy image of a patch inside a pipette. Although they couldn't measure the distance between the membrane and the pipette because of the thick wall of the pipette, they found out that the seal is a distributed rather than a discrete structure. In nearly all of their experiments the interior of the pipette walls were covered with membrane (51).

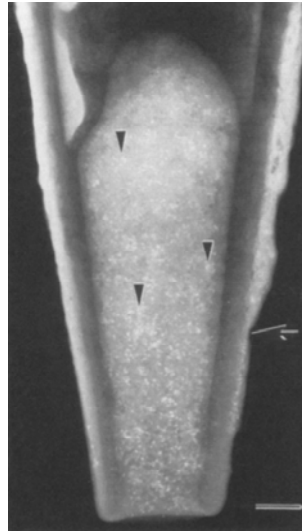


Figure 2.20 Dark-field image of a patch from chick skeletal myotube. The cell was labelled with Con A followed by HRP-gold (15 nm) before the patch was made. Note the classical Ω shape. The gold particles are seen as white dots (arrowheads show representative particles) coating the interior walls of the pipette up to the dome. Arrow shows shreds of membrane with adhering cytoplasm that stick to the outside of the patch pipette after excision. Above the dome is a dense amorphous material that is probably extracellular matrix. Bar, 0.5 μm (51).

Although the membrane and glass are in close opposition in the distributed area of the seal, they do not adhere directly to each other. The extracellular matrix normally extends tens of nanometres beyond the membrane and even membrane proteins extend several nanometres beyond the lipid bilayer (55). Some membrane proteins like acetylcholine receptors (AChRs) protrude >5 nm above the bilayer (57), so that the local phospholipids are prevented from reaching the glass. As a result there is a thin layer of water several molecules thick between lipid bilayer and glass (50). This layer of water acts as lubrication and enables the formation of gigaseals by allowing the membrane to flow up the inner surface of the glass pipette (50). However membrane proteins denature against the glass and can pull the adjacent membrane closer to the glass causing the seal to progress like a zipper (Figure 2.21) (57).

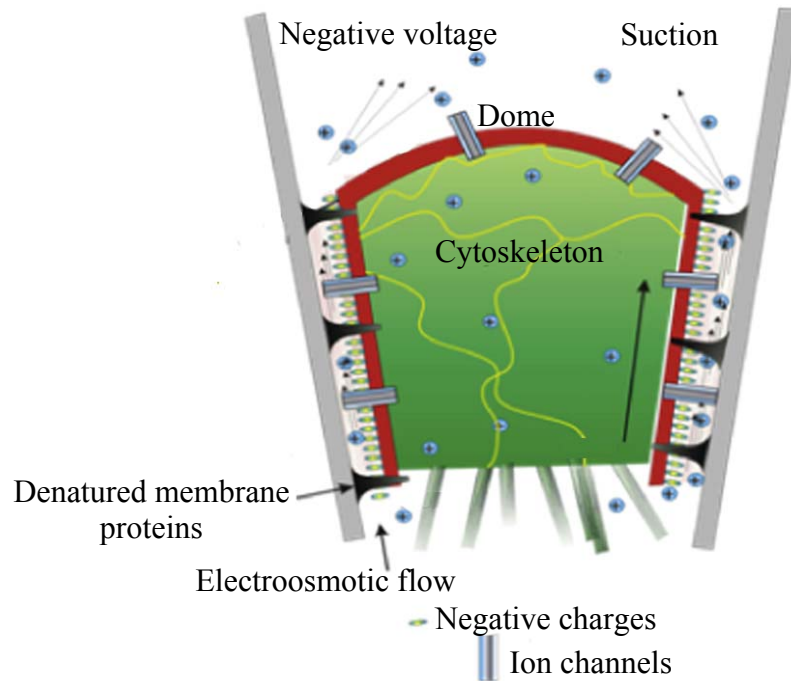


Figure 2.21 Cartoon of patch structure. The patch has three distinct regions: the dome (the characteristic patch of membrane that spans the pipette), the gigaseal between the membrane and the glass that is a cylindrical annulus containing saline and extracellular matrix, and the cytoskeleton that forms a porous matrix behind the dome. A patch consists of a shell of cell cortex (red) containing the bilayer that surrounds a plug of cytoplasm (green). The space between the bilayer and the glass is called the gigaseal (yellow and white). It contains fixed charges (nominally negative) attached to both the membrane and the glass. Proteins sticking far from the bilayer are denatured against the glass (black). Ion channels (blue) that may be mobile and functional are distributed in varying density throughout the dome and the seal (57).

Estimating the distance of separation between the glass and lipid bilayer can help to obtain some clues about the nature of interactions between the elements involved. The resistance per unit length of membrane/glass contact is very high which is the reason that the area of contact between the glass and membrane may be varied without affecting the gigaseal resistance (59). The high resistance of the seals suggests that the approach of glass to the membrane in the area of the seal is in molecular dimensions $\leq 1\text{-}2\text{ nm}$ (50). This close opposition cannot be obtained between lipid bilayer and glass in the presence of integral proteins. Suchyna et al showed that there is a $1\text{-}2\text{ }\mu\text{m}$ region of the seal below the patch dome where

proteins are excluded and this may consist of extracted lipids that form the gigaseal (Figure 2.22) (57). This model is consistent with most of the research described earlier. First, the seal is between lipid and glass, second, the seal is distributed and is not concentrated at a point, and third the seal happens gradually due to the denaturation of membrane proteins. Considering the structure of the membrane and glass surfaces, and the small difference of separation, four sources of interaction can be identified that should participate in the glass-bilayer seal. The first is ionic bonds between positive charges on the membrane and negative charges on the surface. The second is hydrogen bonds between nitrogen or oxygen atoms in the phospholipids and oxygen atoms on the glass surface. A third interaction involves divalent ions such as Ca^{2+} , which can form salt bridges between negatively charged groups on glass and membrane surfaces. Finally the close approach of the glass to the bilayer surface should permit van der Waals' forces to operate. All four of these interactions must occur, and the precise order of importance of each of them is not known. Experience has shown that seals sometimes form much more easily in the presence of high divalent ion concentrations. These observations suggest the importance of salt bridges. Charge-charge interactions appear not to be dominant, since the glass that has been modified with an appropriate silane to give a positive surface charge seems not to seal onto cell membranes (47). The primary attractive force for the gigaseal seems to be van der Waals' attractions. Van der Waals interactions are not a chemically specific force and apply to glass, proteins, polysaccharides and lipids (57). Presumably the seal is formed by a combination of these four forces, with salt bridges, hydrogen bonds and van der Waals' forces being especially important.

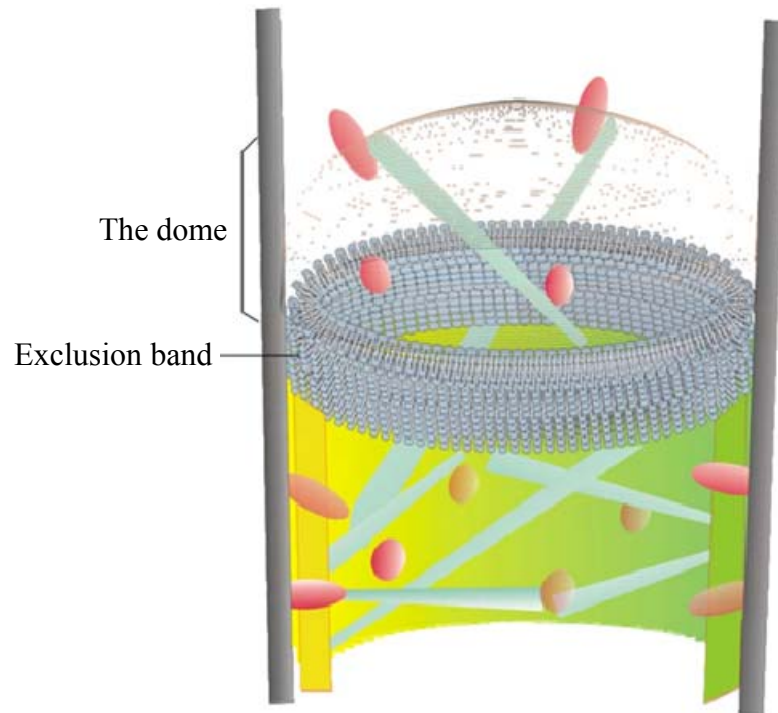


Figure 2.22 A cartoon of a patch that showing the channel free “exclusion band” below the dome that may be the basis of the gigaseal (57).

2.6.4 Important Factors in Gigaseal Formation

A gigaseal in patch clamping will produce improved signal-to-noise ratio and enables ion channel signal measurement to be more accurate. Currently, the formation of a gigaseal in patch clamping occurs in a sudden and all-or-nothing way. A large number of parameters affect the seal formation, making it hard to understand the physical and chemical mechanisms behind it. Although the exact physics behind the gigaseal formation is not clear yet, some important factors have been observed. In this section these factors are summarized.

2.6.4.1 Cleanliness

Cleanliness of glass micropipette and plasma membrane is the most important factor in gigaseal formation which has been emphasized in the literature (6), (20), (24). The crux of a successful seal is that the cell membrane is reached without damage to, or contamination of, the pipette tip and that the contact with the membrane is full and even, therefore there are many considerations to protect pipette from contamination. It is well known that once a cell (or debris in the solution) seals to the tip of a glass pipette or to the aperture of a planar patch-clamp device, a residue, which is very difficult to remove, will stay at the hole and prevent the subsequent formation of another gigaseal. Therefore a positive pressure on the pipette fluid is required to keep the tip from contamination by debris in the bath. In conventional patch clamping before lowering the pipette into the bathing solution, there must be a slight pressure on the pipette fluid to blow any contaminations in the bathing solutions away from the pipette tip. These contaminations often gather in the bathing solution at the fluid-air interface, so pressure must be on before this is crossed (5). The patch pipette should be made and used immediately to reduce tip contamination and subsequent bad sealing properties.

2.6.4.2 Roughness

Roughness is a very important factor in gigaseal formation (2), (4), (60). A rough and sharp pipette can easily destroy the cell. The last pulling cycle in the pipette pulling process is a cold pull which results in a sharp tip with jagged edges. Fire

polishing is used usually to produce a soft and smooth tip (61), (62). Fire polishing also increases the probability of contamination because of a blunting effect on the tip. In planar patch clamping, processes used to fabricate chips were carefully selected or modified to produce a smooth patching site (2), (4), (11), (24), (60). The effect of roughness on gigaseal formation is the subject of the third chapter.

2.6.4.3 Hydrophilicity

Hydrophilicity of the patching site is another important issue in seal formation (35). The hydrophilic cell membrane will not spontaneously interact with the hydrophobic surface in a way to form gigaseals. Different treatment methods were used in the literature to increase the hydrophilicity of the patching site. The effect of hydrophilicity on gigaseal formation is the subject of Chapter 4.

2.6.4.4 Tip Size

It is a practical knowledge that pipettes with a smaller opening form a better seal and lower leakage current. In planar patch clamping tip size has been decreased to increase the seal resistance (22), (33), (63), (64). One also should notice that decreasing the tip size will also decrease the chance of having ion channels in the patch, and it is also more difficult to rupture the membrane to obtain whole cell configuration. The effect of tip size on gigaseal formation is discussed in Chapter 5.

2.6.4.5 Roundness

Roundedness is the next important factor in gigaseal formation. The patching site should have a circular aperture (2), (4), (24), (27), (60). Lau et al show that higher resistances can be achieved by more rounded apertures (27). Roundness of glass micropipettes is measured using the nanotomography technique and results are presented in Chapter 6.

2.6.4.6 Other Factors

There are some other factors that are important in gigaseal formation, such as: biological condition of the cell, PH and presence of divalent ions (50), experience and patience of operator etc.

2.7 Summary

This chapter discusses current research status and the necessity to study gigaseal formation mechanisms to be able to develop high throughput patch clamp measurement devices. The conventional patch clamp technique and its different configurations have been reviewed in Section 2.3. Attempts to improve the technique including automation of conventional patch clamping, planar and lateral patch clamping, are discussed in section 2.4. It has been shown that while convectional patch clamping doesn't have the desired throughput required in

pharmaceutical industries it results in better data quality. Planar and lateral patch clamping have lower data quality and higher throughput. The main advantages, disadvantages and comments of every kind of patch clamping are reported in section 2.5. Planar and lateral patch clamping systems took the advantages of microfabrication techniques, microfluidics and nanotechnology and overcome many of the difficulties of conventional patch clamping. However the low seal resistances of planar and lateral patch clamping systems have prevented them from becoming an absolute alternative to the conventional technique. Due to its superior data quality, it is conventional patch clamping that has become the gold standard for ion channel studies. Based on the comparison of different kinds of patch clamping it can be concluded that, gigaseal formation is the bottleneck in developing high throughput systems capable of producing high quality recordings. Therefore in-depth studies on the physical and chemical mechanism behind the gigaseal formation are needed to be able to develop such systems. The molecular structure of glass and cell membrane, the interactions and forces between them and the mechanisms of gigaseal formation are presented in Section 2.6. The review reported in this chapter has a considerable influence on the direction of this research. The most important factors in gigaseal formation are selected for further studies.

CHAPTER 3: EFFECT OF ROUGHNESS ON GIGASEAL FORMATION

3.1 Introduction

Surface roughness of pipettes is one of the most important factors in gigaseal formation and its effect has been emphasized by various researchers (2), (4), (11), (24), (60). A rough pipette tip in conventional patch clamping or patching site in planar patch clamping can easily destroy the cell. In this chapter the effect of roughness on gigaseal formation has been studied. The fabrication process of glass micropipettes is introduced in section 3.2. In conventional patch clamping pipettes are fabricated in a heating and pulling process. The last pulling step in the pipette pulling process is the cold pull which results in a sharp tip with jagged edges. Pipette roughness is measured using Scanning Electron Microscope (SEM) stereoscopic technique (section 3.3). Focused ion beam (FIB) milling has been used to polish pipette tips and produce a smooth surface. This has been discussed in section 3.4. Patch clamping experiments were carried out using conventional and polished pipettes. Seal values were recorded for both kinds of pipettes and results were compared to observe the effect of roughness (section 3.5). Finite element modelling was carried out to further investigate the effect of roughness. Results of the modelling are in agreement with the experimental results and could explain the

better performance of FIB polished pipettes (section 3.6). Finally the chapter is summarized in section 3.7.

3.2 Glass Micropipette Fabrication

Consistent terminology is required when one discusses micropipettes. To avoid confusion, some terms used in this thesis relating to micropipette terminology are described here (see figure 3.1):

Tip is the very end of the pipette.

Tip size is the inner diameter of the pipette tip.

Shank is the tapered segment of the pipette.

Shaft is the straight portion of the capillary tubing.

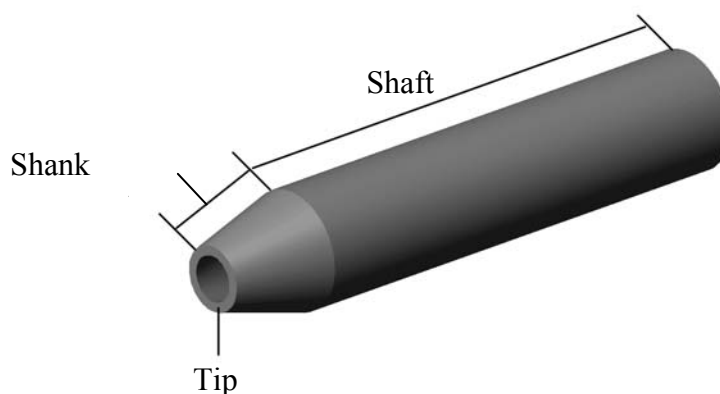


Figure 3.1 Schematic shows different areas of glass micropipette.

Glass micropipettes are fabricated with a heating and pulling process using a puller machine. The glass tube is heated and pulled while it is softened. The process is repeated in several stages until the tube is pulled apart. The connection is then broken by a final hard pull. To have better control of the process the last pull takes

place while the glass is cold and therefore it is called hard pull (65). The glass micropipettes used in the experiments were made of borosilicate glass pipes with an outer diameter of 1.5 mm and an inner diameter of 0.86 mm (BF150-86-10 Sutter Instrument, Novato, CA). They were heated and pulled with a flaming/brown micropipette puller machine (Model P-97, Sutter Instrument, Novato, CA) (figure 3.2). The filament of the puller machine was FB230B (2.0 mm square box filament, 3.0 mm wide, Sutter Instrument).



Figure 3.2 Flaming/brown micropipette puller machine, Model P-97, Sutter Instruments (66).

A typical PULL CYCLE is described below (see figure 3.3) :

- The heat turns on.
- The glass heats up and a weak pull draws the glass out until it reaches the programmed velocity.
- When the programmed velocity has been reached, the heat turns off and the air is turned on.

- If DELAY is >0 the air is activated for 300ms and the hard pull is activated after the specified DELAY.

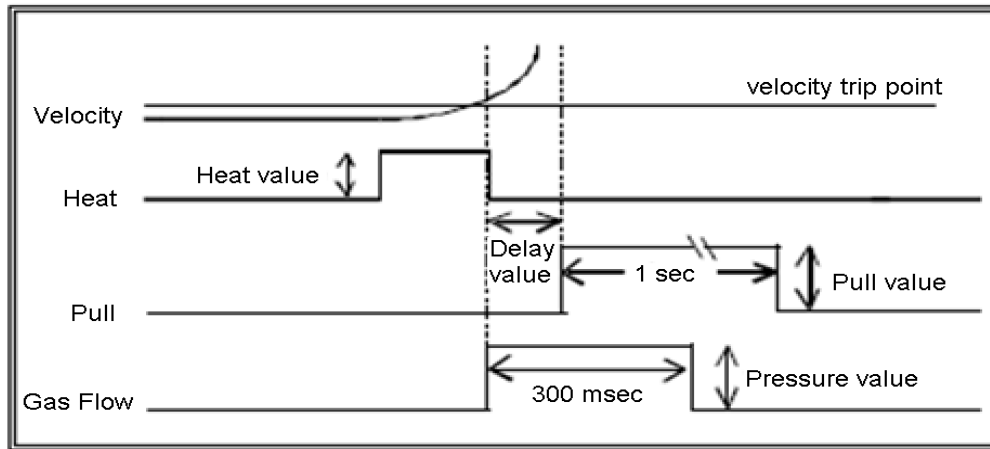


Figure 3.3 A typical pull cycle in a program of a puller machine (65). There are two cooling parameters: delay and time. This illustration represents the pulling cycle when delay is active. For details on glass micropipette pulling and on the definition of each parameter see section 6.3.

3.3 Measurement of Roughness

Hard pull results in a sharp tip with jagged edges. High magnification Scanning Electron Microscope (SEM) images revealed the surface nature of the pipette tip to be in contact with cells (figure 3.4). The first step in investigating the effect of roughness on gigaseal formation is measuring the pipette roughness. This measuring will give a clue about the size of the roughness and how comparable it is with those sizes of cell and its components.

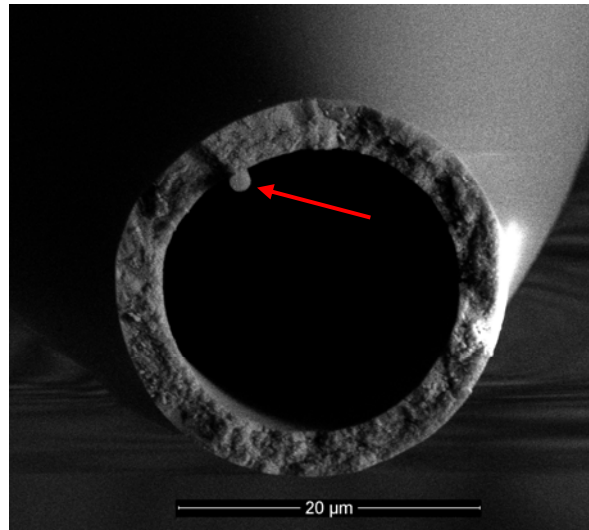


Figure 3.4 An SEM image of a glass micropipette. The tip has a rough surface which is a result of hard pull in the pipette fabrication process. The arrow shows an internal fibre called Omega Dot which is being used to facilitate the filling of micropipette tips (See section 6.5.1 for more details).

One of the challenges of working with glass micropipettes is their fragility. From the patch clamping to microinjection applications, they could have a tip diameter of a few hundreds of nanometres to a couple of micrometers and a shank of several millimetres to a couple of centimetres. This makes micropipettes very fragile and less manoeuvrable. Special care should be taken into account when working with micropipettes. As a result, a non-contact roughness measuring method is needed for measuring the surface roughness properties of micropipettes and the SEM stereoscopic technique is selected for this purpose.

3.3.1 SEM Stereoscopic Technique

The process of scanning a specimen in the scanning electron microscope effectively projects the three-dimensional surface onto a two-dimensional image plane (67). To determine the three dimensional structure of pipette tips, the SEM stereoscopic technique is used (68), (69), (70). The stereoscopic technique scans the same area of

the object from different angles by tilting the object with respect to the fixed optic axis. Surface features in different heights have different lateral displacements and depth can be calculated by measuring the parallax movement of features from their location in the first image, to the new location in the second image (71). For mathematical calculations of obtaining depth from two SEM images see appendix A.

In practice capturing SEM stereo images could be challenging. The quality of images is very important in the calculation of accurate 3D data. Many factors should be taken into account to capture SEM images which satisfy stereoscopic technique requirements, such as (67) :

- Illumination: capture images under optimal illumination. The image shouldn't be too dark or too bright.
- Sharpness: always capture images with maximum sharpness.
- Eucentric tilting: the object should be tilted in an eucentric way. This means that the tilting axis has to be in the middle of the surface.
- Disparity: The software package used here (MeX) calculates the depth image based on the disparity in the stereo image. A large height change in relation to the image diagonal provides better results. Disparity can be increased by higher magnification and higher tilting angle.
- Voltage: the voltage of the electron beam should be well-chosen (the usual range is between 5 to 15 kV). If the chosen electron beam voltage is too high then it is possible for the electron beam to intrude into the surface of the object, so that details which lie inside the object are also received. This circumstance would lead to a wrong reconstruction of the surface.

To capture high quality SEM images which satisfy stereoscopic technique requirements, glass μ -pipettes were coated with a thin layer of platinum (<5 nm). The machine used for capturing SEM images was FEI dual beam focused ion beam system (FEI, Hillsboro, Oregon). Figure 3.5 shows the position of pipettes and electron beam gun with respect to each other.

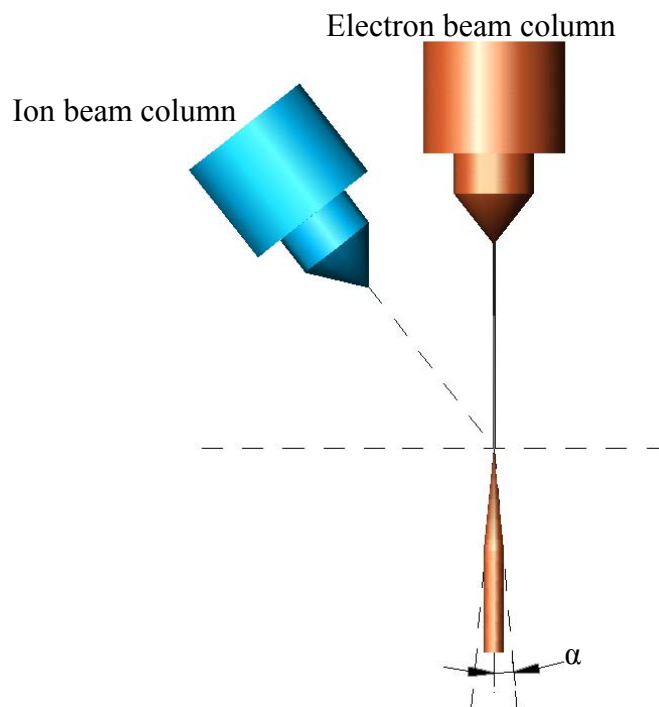


Figure 3.5 Schematic of the configuration of SEM with respect to pipettes and tilting angle (α).

Three SEM images were taken from different angles by tilting the stage with respect to the electron beam direction. Figures 3.6 (a) to (c) show the SEM images taken from the left, middle and right viewpoints of the pipette. The tilting angle between (a-b) and (b-c) of the images is 9 degrees.

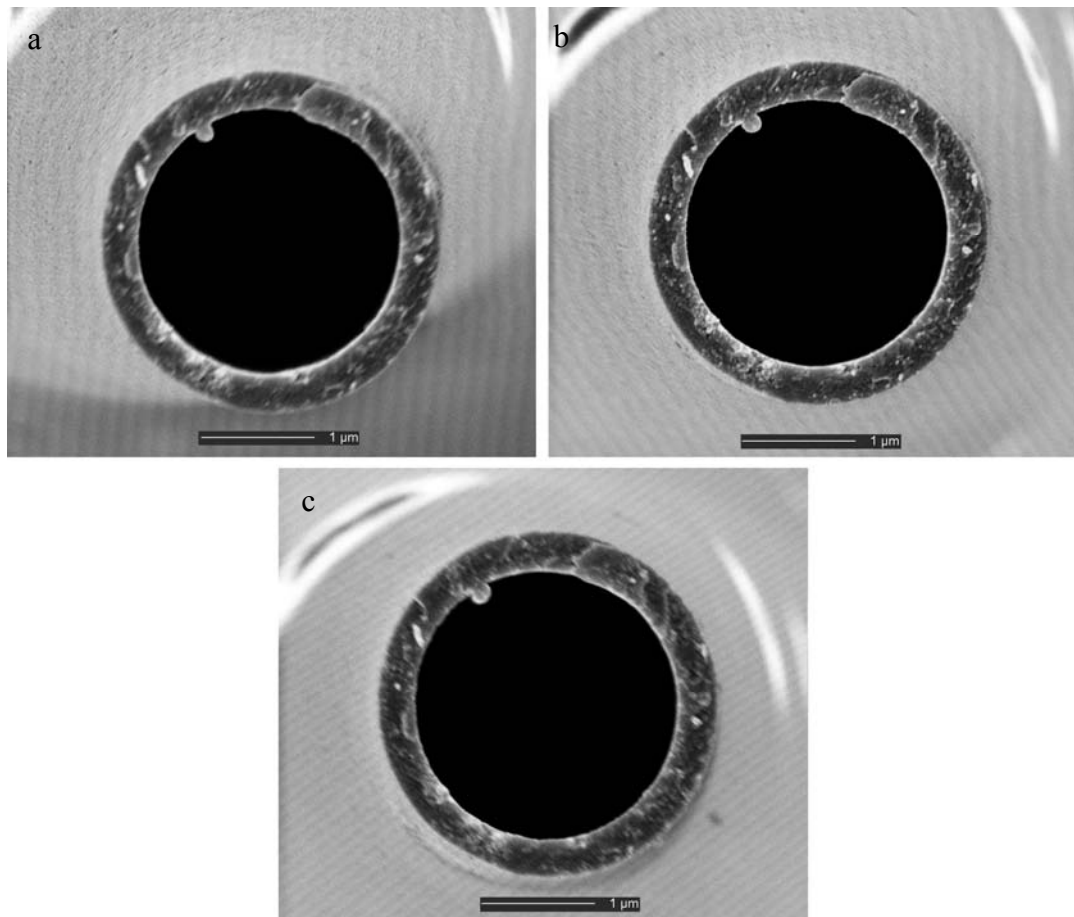


Figure 3.6 Stereo images of the pipette tip for 3D reconstruction; (a) left, (b) middle and (c) right.

The three SEM images were imported to the MeX software (a software package specialized in 3D reconstruction from SEM images) (72) and the digital elevation model of the tip is obtained. Figure 3.7 shows the 3D reconstructed surface of the pipette tip.

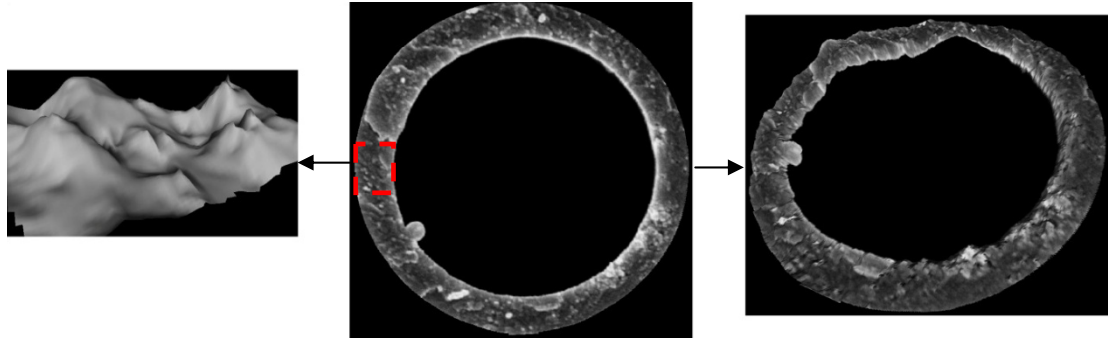


Figure 3.7 A 3D reconstructed surface of the pipette tip shown at different viewing angles; top view (middle), the exploded view of the area showed by dash-line (left), view with an angle (right).

Table 3.1 shows surface parameters of the 3D reconstructed pipettes with different sizes.

Table 3.1 Surface parameters of pipette tip for 3 pipettes (D_t = tip diameter).

Name	Value $D_t=2.2\mu\text{m}$	Value $D_t=1.7\mu\text{m}$	Value $D_t=1.4\mu\text{m}$	Description
S_a	27.3 nm	17.8 nm	8.3 nm	Average height of selected area
S_q	34.6 nm	13.0 nm	10.8 nm	Root-mean-square height of selected area
S_p	104.0 nm	81.5 nm	46.6 nm	Maximum peak of selected area
S_v	150.8 nm	125.5 nm	60.8 nm	Maximum valley depth of selected area
S_z	255.8 nm	207.1 nm	107.5 nm	Maximum height of selected area
S_{10z}	195.2 nm	142.2 nm	88.5 nm	Ten point height of selected area
S_{sk}	-0.225	-0.4857	-0.7099	Skewness of selected area
S_{ku}	3.2623	3.7725	4.5173	Kurtosis of selected area
S_{dq}	0.8774	0.9814	0.8289	Root mean square gradient
S_{dr}	34.986%	45.575%	32.61%	Developed interfacial area ratio

To have the highest lateral and vertical resolution in the 3D reconstructed surface, magnification, tilting angle and resolution should be as high as possible when capturing SEM images. Since the maximum pixel resolution of the machine is limited, different magnifications and tilting angles have been used to reconstruct every pipette's tip with the highest possible resolution. Such a reconstruction could be expected to have the inaccuracy of less than 5% (71). Table 3.2 gives the values

of tip diameter, tilting angle, magnification, lateral resolution and vertical resolution of the several 3D reconstructed pipettes.

Table 3.2 Reconstruction information for 3 pipettes

Pipette number	Tip Diameter (μm)	Tilting angle (left to right)	Magnification	Lateral Resolution	Vertical Resolution
1	2.2	10	65000	18.4 nm	18.4 nm
2	1.7	10	95000	6.2 nm	11.2 nm
3	1.4	10	110000	5.3 nm	7.7 nm

3.4 Polishing Pipette Tips by Focused Ion Beam Milling

As it can be understood from Table 3.1, the surface roughness of the pipette tip is comparable with the thickness of the cell membrane which is 3 to 10 nm (9), (73), (74), (75). In order to study the effect of roughness on gigaseal formation two kinds of pipettes with distinct surface properties are required; rough pipettes (which are pipettes normally pulled by a pulling and heating process) and perfectly smooth pipettes. Focused ion beam (FIB) milling was used to produce pipettes with ideal tip surface conditions. The uneven surface of the pipette tip was corrected by cutting the top of the pipette across using FEI dual FIB system. The configuration of the pipette with respect to the ion beam is illustrated in figure 3.8.

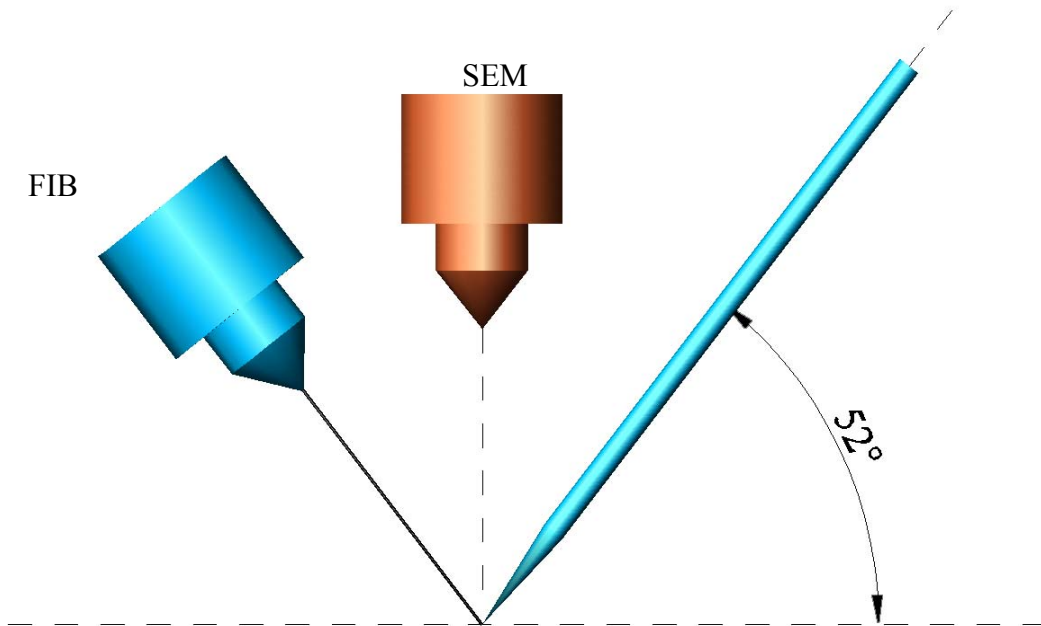


Figure 3.8 The configuration of glass micropipette milling in the SEM/FIB chamber. The stage was tilted by 52 degrees so that the ion beam was perpendicular to the pipettes.

Due to the conic shape of the pipette, cutting the tip changes the tip size, which is an important factor in patch clamping as it determines the pipette resistance (4), (5), (20). It is also well known that a gigaseal is not likely to be achieved with big tip sizes (22), (33), (47), (63), (64) (see Chapter 5). So care was taken not to cut more than 1 μm from the top. Since the roughness of the tip of the pipette was in nanometres cutting 1 μm from the top should be sufficient to remove all rough edges without increasing the tip size significantly. In the FIB milling process, the pipettes' tips were cut using Ga^+ ions with 50 pA current for 100 seconds, dwell time of 1 μs and FIB acceleration voltage of 30 kV. The pipette before and after milling is shown in figure 3.9. The image of the milled pipette, shown in figure 3.9 b, has a resolution of 4.5 nm. No feature could be identified on the milled surface for producing roughness parameters at this magnification. Therefore, the average surface area roughness (S_a) of the milled pipette tip should be well less than 4.5 nm.

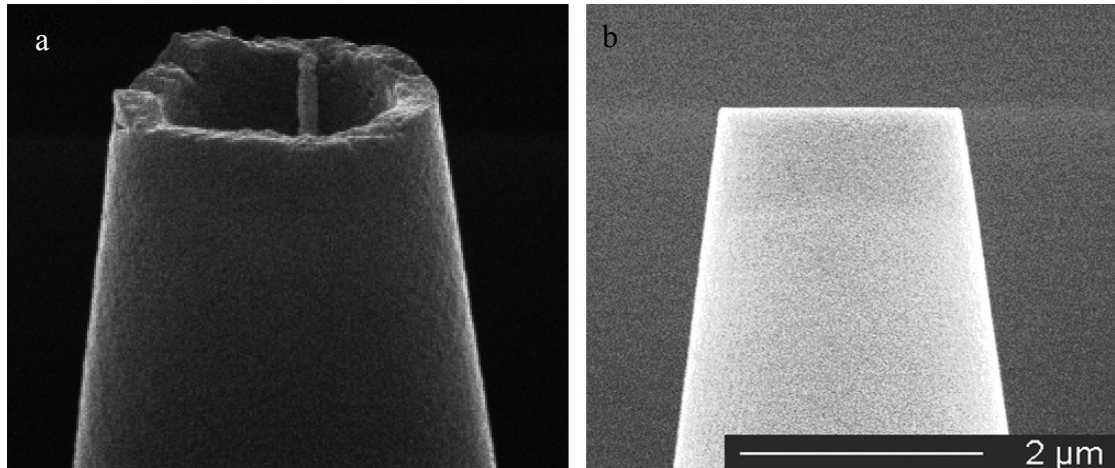


Figure 3.9 A micro glass pipette before milling (a), the pipette after the milling (b). No surface roughness could be identified after milling, so the surface roughness should be smaller than the resolution of the SEM image, which is 4.5nm.

As it is mentioned in Chapter 2, an important step after pipette pulling is fire polishing. We call the process of FIB milling the pipette, “FIB polishing” in comparison with the “fire polishing method”. FIB polishing has some advantages over fire polishing. Firstly, there is more control on the polishing process using FIB, secondly, fire polishing has a blunting effect on the tip, which increases the contamination probability and thirdly, FIB polishing doesn’t change sharpness of pipette which facilitates the pipette travelling through tissues to desired cells.

3.5 Patch Clamping Experiments

To investigate the effect of the roughness of pipette tips, patch clamp experiments were carried out with polished and conventional pipettes under the same conditions and the results were compared. Human Embryonic Kidney (HEK) cells were utilized to investigate the performance of the FIB polished micropipettes in

achieving giga-ohm seals. The cells were cultured on cover slips in HEK cells medium, two to three days before the experiment and incubation was done at 37°C.

The medium has three components:

1. DMEM (Dulbecco's Modified Eagle's medium) 89%
2. FBS (Fetal bovine serum) 10%
3. PS (Penicillin Streptomycin) 1%.

At the time of the experiments, the confluence of the cells was over 80% and all the cells were firmly attached to the bottom of the cover slips. During the experiments, an individual cover slip was directly taken out from the incubator and sited in the recording chamber. The backfilling solution (pipette solution) was composed of 40 mM KCl, 96 mM K-gluconate, 4 mM K₂ATP, 2 mM GTP, 10 mM HEPE and at 7.2 in pH, and the bath solution was composed of 110 mM NaCl, 5 mM KCl, 1 mM MgCl₂, 1 mM CaCl₂, 5 mM HEPEs, 5 mM HEPE–Na, and at 7.2 in pH.

The experimental equipment setup consisted of an Axon multiclamp 700B microelectrode amplifier (Axon Instruments, Union City, CA), Flaming/Brown micropipette puller (Model P-97, Sutter Instrument) and glass micropipettes (BF150-86-10, Sutter Instrument). The puller machine was set to produce pipettes with approximately 1.5 μm in tip diameter. When there was no contact between the recording pipette and the cell membrane, the total pipette resistance ranged from 6.0 to 6.5 M Ω . A 10 mV pulse was constantly applied on the recording electrode from the time that the pipette tip was just immersed in the bath solution till it touched the

cell membrane. A negative pressure was immediately applied to the pipette and then the voltage pulse was raised to 60 mV to monitor the seal resistance precisely (figure 3.10).

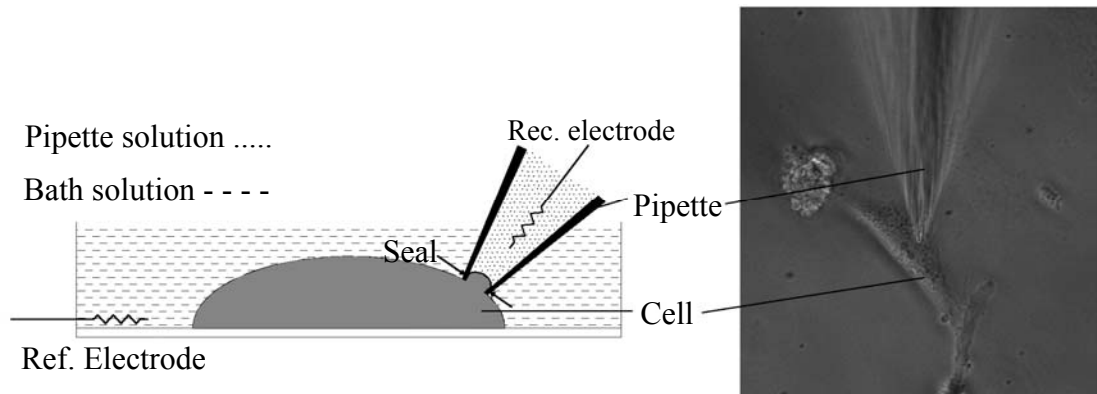


Figure 3.10 Schematic and real image of the pipette with respect to the cell at the moment of applying suction.

Ten recordings were obtained for each type of pipette. Seal resistances are shown in figure 3.11. With the FIB polished pipettes, above 3 Giga ohm seals were achieved in most attempts and the highest seal resistance reached 9 G Ω . The mean value of seal resistances is 4.7 G Ω with the standard deviation of 1.8 G Ω . In comparison, the seal resistances achieved using the conventional pipettes were usually between 1.0 to 2.0 G Ω . The seal resistance could reach 3 G Ω in some excellent cases. The mean value of seal resistances is 1.6 G Ω with the standard deviation of 0.6 G Ω .

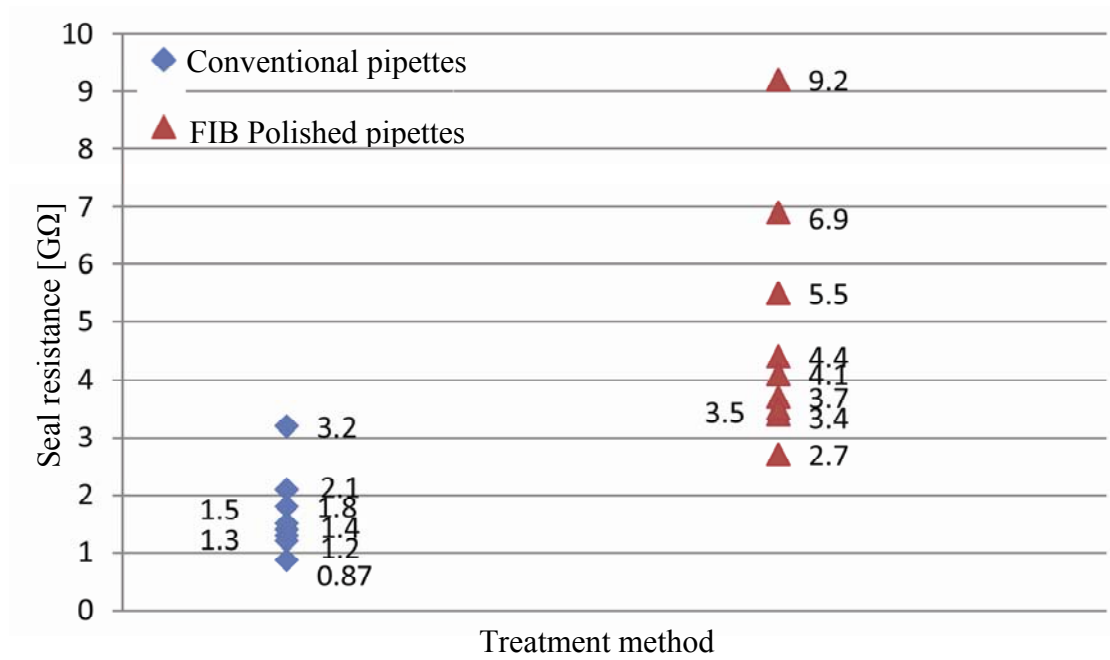


Figure 3.11 Seal values for conventional and polished pipettes.

FIB polished pipettes formed significantly better seals which made it possible to measure single ion channel currents with considerably lower noise. Single-channel currents recorded from conventional and polished pipettes are shown in figures 3.12 and 3.13.

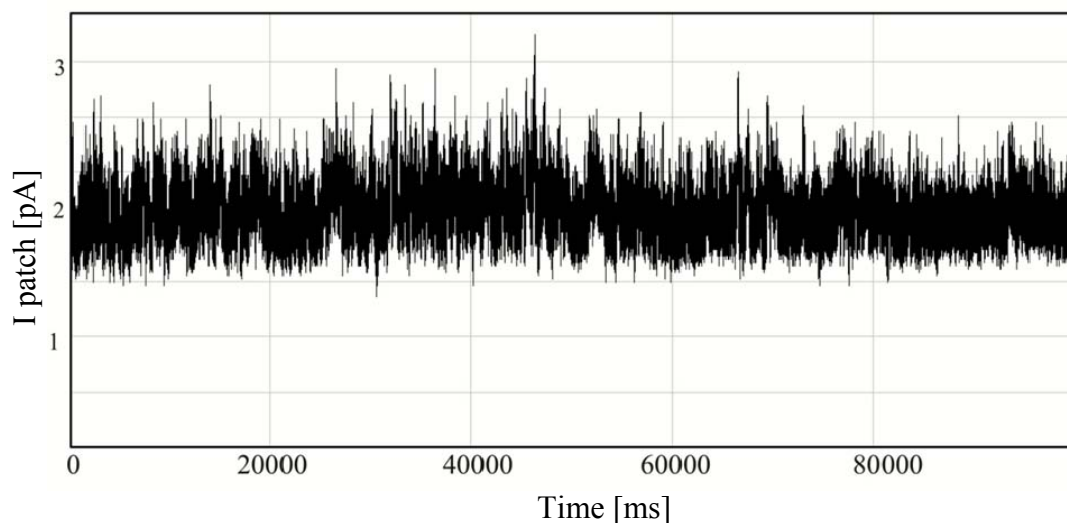


Figure 3.12 Single channel recording from HEK cells with conventional pipettes. the leakage current is 2.1 pA.

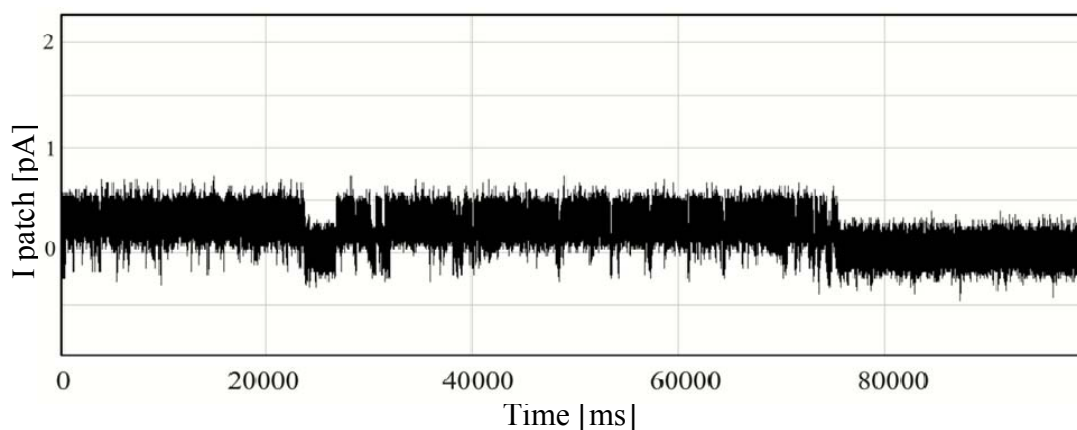


Figure 3.13 Single channel recording from HEK cells with polished pipettes. The improved patch clamping performance with polished pipettes is obtained from better contact conditions of the smoother tip surface with membrane. The leakage current is 0.3 pA, significantly smaller than current for conventional pipettes.

Higher seal resistance for polished pipettes could be explained by their better sealing potential. The ultimately smooth and flat surface of the polished pipette tip leaves no concave area to hold water, as opposed to conventional pipettes, as illustrated in figure (3.14). Contact area between pipette tip and cell membrane is higher for polished pipettes and since there are no peaks or spikes, the membrane can get closer to the tip. As a result it is more difficult for ions to escape from glass-membrane distance and higher seals are achievable. This also implies that the cell cannot fill

the valleys of the rough surface of the conventional pipettes perfectly, which could be possibly the reason for reports on lower seal resistance with rough surfaces in the literature.

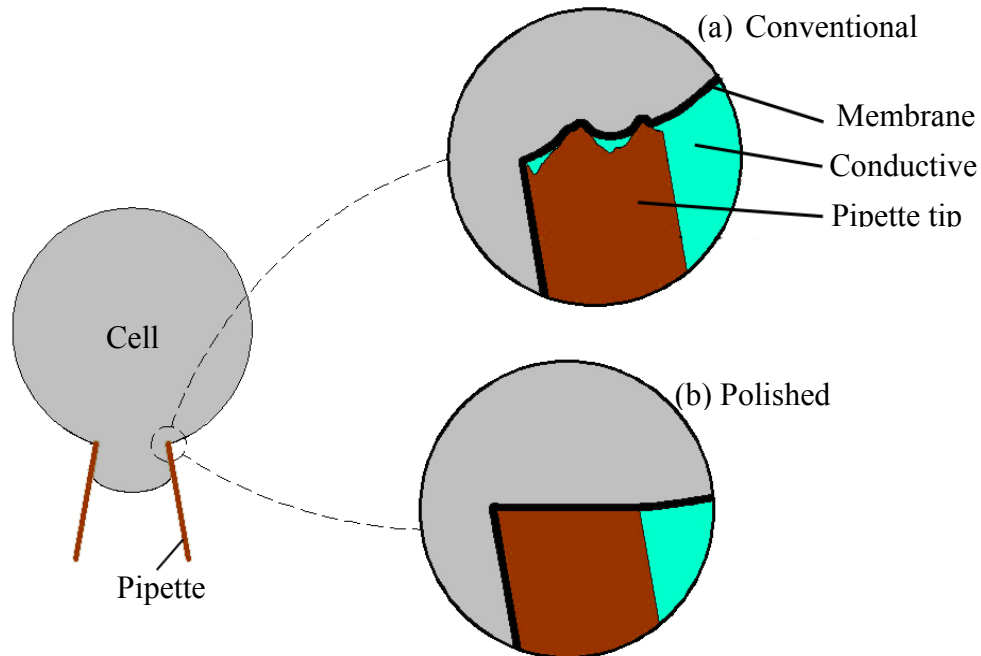


Figure 3.14 Schematic of pipette-membrane interaction: (a) the original pipette tip with a bumpy surface (b) the tip is flat.

3.6 Finite Element Modelling

Finite element modelling is carried out to study the effect of pipette tip roughness on gigaseal formation. How the cell deforms under the rough tip of a pipette has significant importance in gigaseal formation. If the membrane can fill cavities of the rough tip then higher seal resistances are expected due to the higher contact area between the rough pipette and the cell membrane. However if the membrane cannot fill the cavities then the area between two peaks acts like a conductive channel which

connects the inside of the pipette to the outside. FE modelling was carried out using Abaqus/CAE software (76). For the modelling the real profile of a patch clamp pipette tip and the way the pipette approaches the cell are required.

3.6.1 Patch Clamp Manipulators

Patch clamping involves the placement of a glass micropipette onto a cell to form a tight seal. The core function of a micromanipulator in patch clamping set-up is to place the micropipette tip onto the cell surface in a controlled way. The manipulator used in the experiments is MP-225 from Sutter Instruments (figure 3.15), which has a minimal resolution of 62.5 nm for fine movements. As a result the pipette approaches the cell in a step of 62.5 nm. This implies that when a contact is made, the pipette tip is just on the cell surface or presses the cell within tens of nanometres. If the pipette continues its movement, it may penetrate or rupture the cell membrane. Figure 3.16 shows the right moment of applying suction.



Figure 3.15 MP-225 micromanipulator from Sutter Instruments (66).

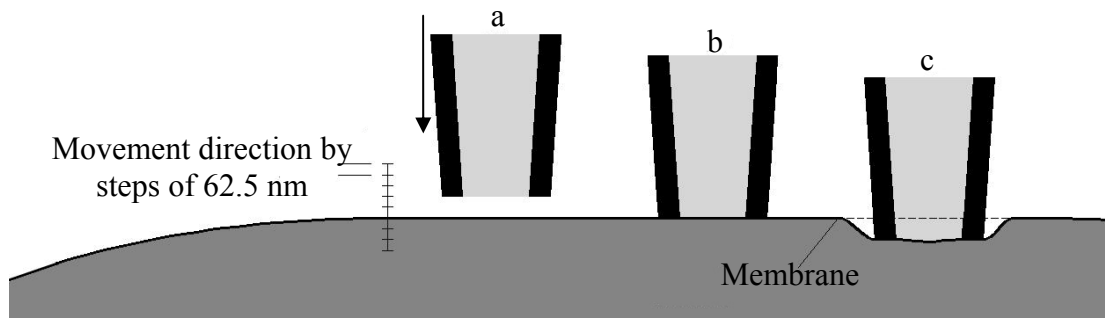


Figure 3.16 Approach of pipette to the cell. The approaches the cell by steps of as long as manipulator resolution. (a) The pipette is far from the membrane, (b) the pipette is on the membrane; this is the best position to apply suction and (c) the pipette presses the membrane by few tens of nanometres; this is the usually occurred case in patch clamping.

In practice the relative position of tip to membrane is estimated by monitoring the change of electrical resistance between the two electrodes. As the pipette comes closer to the membrane the resistance increases; usually an increase of about $1 \text{ M}\Omega$ indicates that the tip has touched the membrane (5). It is not recommended to reach a resistance 1.5 times higher than the pipette resistance as it stresses the membrane and contaminates the tip which is fatal for gigaseal formation. In finite element modelling, once in contact, the pipette is lowered by 500 nm and the suction is then applied.

3.6.2 Pipette Tip Profile

Figure 3.17 shows the digital elevation model image of the pipette used in FE modelling with four different profiles (numbered 1–4) of the tip surface along its thickness. The specifications of the profiles are given in Table 3.3. In order for the

modelled pipette to have the real tip profile of the glass micropipette, coordinates of each profile are extracted and a B-spline is drawn through these points in CATIA. The splines are then transferred to ABAQUS/CAE for finite element simulation. The inner and outer diameters of the pipette tip are $0.7\ \mu\text{m}$ and $1\ \mu\text{m}$, respectively. As can be seen in figure 3.17, there is a large variation in the surface morphology of the tip pipette across its thickness. This increases the chance of ion escape and compromises the formation of high resistance seals.

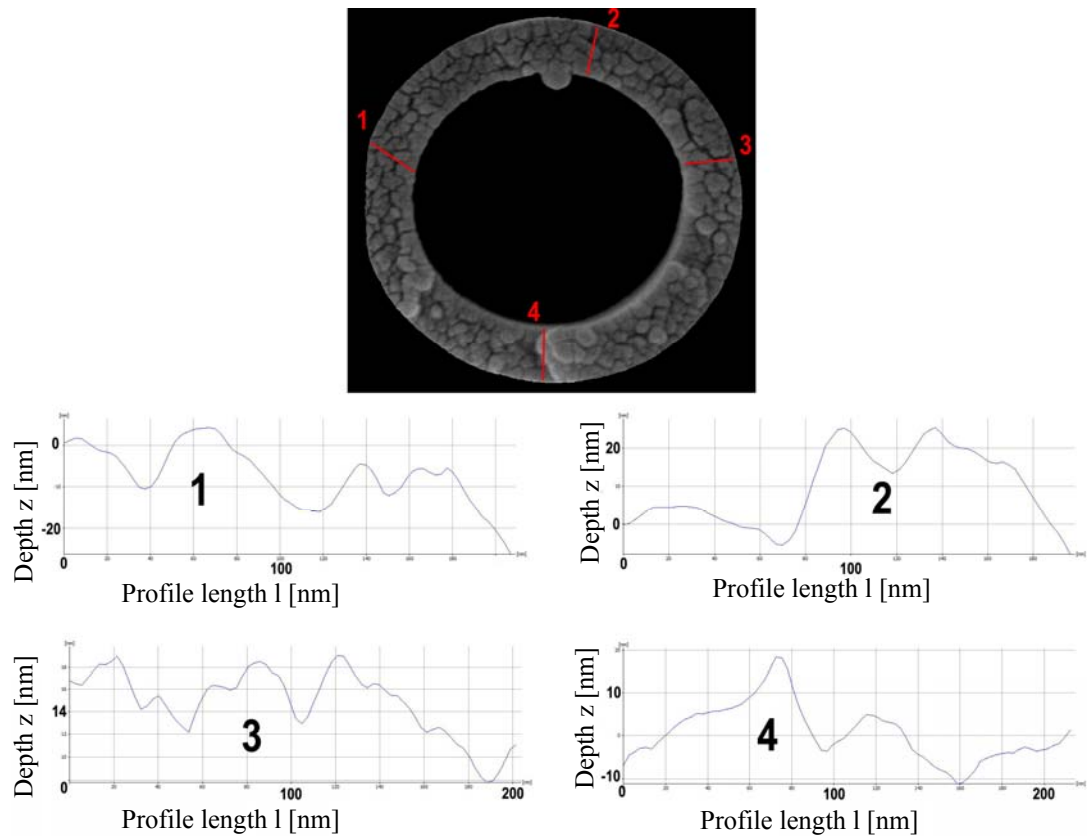


Figure 3.17 Four different profiles of the tip surface across the thickness are shown. The large variation of surface morphology compromises the formation of a high resistance seal.

Table 3.3 Profile parameters of 4 different profiles.

Profile	No.1	No.2	No.3	No.4	Description
P_a	4.0 nm	6.2 nm	2.1nm	4.8 nm	Average height of profile
P_q	4.8 nm	7.8 nm	2.3nm	6.2 nm	Root-mean-square height of profile
P_t	22.1 nm	34.0 nm	9.2 nm	29.2 nm	Maximum peak to valley height of primary profile
P_z	13.0 nm	12.4 nm	5.5 nm	12.6 nm	Mean peak to valley height of primary profile
P_{max}	18.4 nm	20.8 nm	6.7 nm	16.5 nm	Maximum peak to valley height of primary profile within a sampling length
P_p	8.7 nm	14.7 nm	4.8 nm	16.3 nm	Maximum peak height of primary profile
P_v	13.4 nm	19.3 nm	4.4 nm	12.9 nm	Maximum valley height of primary profile
P_c	14.8 nm	26.1 nm	5.4 nm	19.7 nm	Mean height of profile irregularities of primary profile
P_{sm}	92.7 nm	150.54 nm	49.7nm	76.6 nm	Mean spacing of profile irregularities of primary profile
P_{sk}	-0.741	-0.2124	0.08	0.1866	Skewness of primary profile
P_{ku}	2.4831	2.5544	2.272	3.0219	Kurtosis of primary profile
P_{dq}	0.4716	0.6446	0.279	0.5801	Root-mean-square slope of primary profile

3.6.3 Finite Element Modelling of Patch Clamping

There are three elements in this modelling: the glass micropipette, substrate and the cell. The pipette and substrate are modelled as 2D elastic solid bodies. Different pipette tip profiles are used in the modelling.

Two different mechanical models can be applied to cells, and either one allows the simulation of cellular deformations in response to micropipette aspiration in which the cell is sucked into the micropipette by applying negative pressure. The first one describes cells as having a solid membrane and liquid core and has been used to model the aspiration of cells with little or no cytoskeleton (such as red blood cells or unattached leukocytes) into micropipettes. The second one describes cells spread on

a substrate (which is the case in patch clamping) with a well developed cytoskeleton as being elastic solids, and has been applied to the aspiration of cells into micropipettes (73), (77), (78), (79). Cells can be modelled as continuum media if the smallest operative length scale of interest is significantly larger than the distance over which cellular structure or properties may vary (80), (81). A cell is a very complex organized system. Its principal structural elements are the cytoplasm, the membrane and various organelles of which the most prominent is the nucleus (77), (78), (82). In the theoretical models, the system is simplified. Here, the cell is modelled as a continuous, homogeneous, incompressible, isotropic and hyperelastic solid attached to the substrate. The cell consists of two parts: the cytoplasm and membrane. Table 3.4 gives material properties of cell membrane and cytoplasm. The material properties of cytoplasm and membrane used in this modelling are: $E_c=1000 \text{ Pa}$, $\nu_c=0.5$, $\rho_c=1000 \text{ kg/m}^3$, $E_m=100 \text{ Mpa}$, $\nu_m = 0.3$, $\rho_m = 1150 \text{ kg/m}^3$.

Table 3.4 Material properties of cytoplasm and membrane.

	Young modulus (E)	Poisson's ratio (ν)	Density (ρ) kg/m ³
Cytoplasm	75-2500 Pa ^{(78), (79), (75), (83)}	0.5 ^{(74), (78), (84)}	1000 ^{(74), (75), (85)}
Membrane	100-140 MPa ^{(75), (74)}	0.3-0.5 ^{(74), (75), (73)}	1150 ⁽⁷⁵⁾

Since the physical combination of the pipette and cell is completely symmetric, a 2D axisymmetric model is employed instead of using a huge 3D model with a large number of nodes and elements. The cytoplasm is modelled as a semicircle meshed with 4-node bilinear axisymmetric quadrilateral elements. The plasma membrane is modelled as a thin elastic shell. Dimensions and boundary conditions are shown in figure 3.18. In the finite element simulation the pipette is lowered for 500 nm and then the suction is applied to the inside of the pipette. The membrane is tethered to

the cytoplasm using a tie constraint. Contact between pipette and cell is considered frictionless.

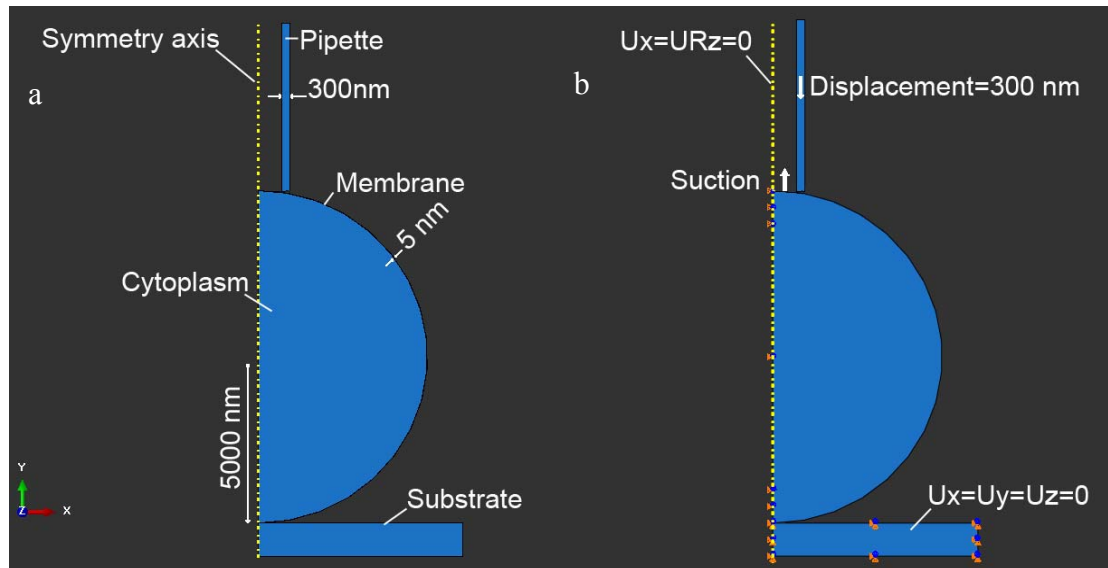


Figure 3.18 Dimensions and boundary conditions used in the FE modelling. Nodes on the symmetry axis are prevented from movement in X direction and rotation around Z axis. The substrate is not allowed to have any movement in any direction.

The result of the finite element modelling is shown in figure 3.19. Although the cytoplasm is soft, the stiffer membrane does not allow the cell to cover all of the cavities of the tip. The highest peaks of the profile push down the membrane. Therefore, the distance between two peaks will not be filled with the patched membrane. This is important because if the membrane fills up all of the room between peaks and valleys, then the contact area between the membrane and the glass will increase. This in turn can result in a better seal. However the result of the FE modelling shows that the membrane cannot go into the valleys. Therefore the space which is left over, acts like channels connecting the inside and outside of the pipette together. These channels are filled with the conductive media, making it easier for ions to escape, therefore increasing the leakage current and compromising

the seal. As can be understood from Table 3.3, the maximum peak to valley height of these channels is about 10-34 nm. The result of the FE modelling is in agreement with experiments carried out with rough and polished pipettes. Polished pipettes make a better seal with cells because their flat tip can make a better contact with the cell surface.

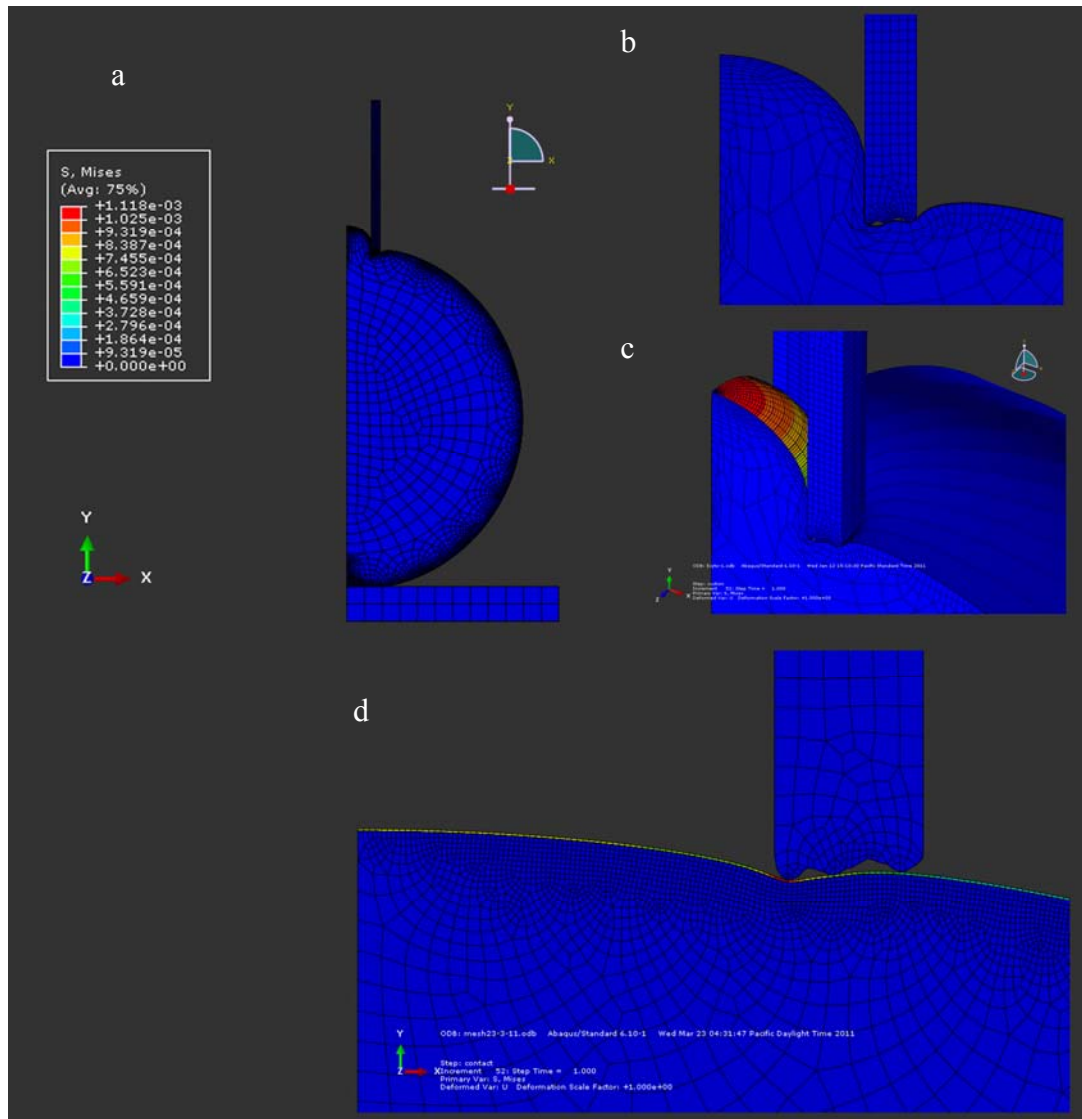


Figure 3.19 Result of the FE modelling of patch clamping process, a) Aspiration of cell into pipette, b) close view of the region underneath the pipette. Stiff cell membrane prevents soft cytoplasm filling the cavities of the tip, c) 3D representation of result, d) cell deformation at the end of indentation process and before applying suction. The material properties of cytoplasm and membrane used in this modelling are: $E_c=1000$ Pa , $\nu_c=0.5$, $\rho_c=1000$ kg/m³ , $E_m=100$ Mpa , $\nu_m = 0.3$, $\rho_m =1150$ kg/m³.

3.7 Summary

In this chapter the effect of pipette tip roughness on gigaseal formation in patch clamping is studied. Micropipettes are fabricated in a heating and pulling process. The fabrication process of glass micropipettes is introduced in section 3.2. High magnification SEM images of pipettes' tips have shown that they are rough and jagged. 3D reconstruction of pipette tips has been discussed in section 3.3. The SEM stereoscopic technique has been used for 3D reconstruction of the pipette tip and roughness parameters were extracted from digital elevation models of the tips. FIB milling is used to cut across the tips, leaving a very smooth surface at the top of the pipettes (section 3.4). Patch clamping experiments were carried out using FIB polished and conventional pipettes (section 3.5).

Seal values were considerably higher in the case of polished pipettes. Above 3 G Ω seals were achieved readily and the highest seal resistance reached was 9 G Ω for polished pipettes. The leakage current in single channel recording was found to be 0.3 pA, significantly smaller than 2-3 pA usually achieved using conventionally treated pipettes. Smaller current is the consequence of higher seal resistance. To further investigate the effect of roughness on gigaseal formation FE modelling of patch clamping was carried out (section 3.6). Results of the FE modelling show that the cell cannot fill up all of the valleys of the tip and therefore in 3-dimensions the inside of the pipette is connected to the outside by nanometre-high channels, facilitating current leakage. This is consistent with the result obtained from patch clamping experiments where smoother tips resulted in higher seal values. FIB

polished glass micropipettes have improved the gigaseal formation in patch clamping.

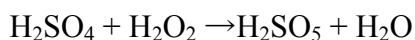
CHAPTER 4: EFFECT OF HYDROPHILICTY ON GIGASEAL FORMATION

4.1 Introduction

As has been discussed in section (2.6.2) the membrane has both hydrophilic and hydrophobic components. The exact contribution of these components in seal formation is not clear. Hydrophilicity of the pipette (or patch site in planar patch clamping) is believed to be a prerequisite for gigaseal formation (6). For many materials, treating the substrate to be more hydrophilic resulted in considerably higher seal values (22), (24), (35), (46). However the twofold structure of the membrane has made it possible for the membrane to form a seal with both hydrophobic and hydrophilic materials, and there has been a report on hydrophobic materials forming seals (26). In this chapter the effect of hydrophilicity on gigaseal formation is discussed. Two treatment methods are used to alter the chemical properties of glass micropipettes: piranha solution treatment and oxygen plasma treatment (section 4.2 and 4.3). Patch clamping experiments were carried out using treated and conventional pipettes to test the effect of hydrophilicity (section 4.4). The results discussed in section 4.5 show the importance of hydrophilicity and hydrogen bonds in seal formation. Finally the chapter is summarized in section 4.6.

4.2 Piranha Solution Treatment

Piranha solution has been in use in the semiconductor industry for decades. The piranha solution is a mixture of concentrated sulphuric acid (H_2SO_4) and hydrogen peroxide (H_2O_2), used to remove organic contaminants from the surface. The solution is a strong oxidizer and will also make the surface more hydrophilic (86). Both cleanliness and hydrophilicity are important factors in seal formation. Many different mixture ratios are commonly used, but a typical piranha solution consists: 3:1 vol/vol 96% H_2SO_4 :30% H_2O_2 . The mixture of the two results in the formation of the strong oxidant H_2SO_5 (87) (88):



As a result piranha solution is a strong oxidizer and will hydroxylate the surface by increasing silanol groups and Si-O- species on the glass support, making the surface more hydrophilic (89).

Glass cover slips were used for characterization of the treatment procedure before application for treating the micropipettes. Cover slips were dipped in piranha solution for 30 minutes and the temperature was kept at 85 °C to maintain the effectiveness of the solution. Figure 4.1 shows the contact angle between the treated glass and water before and after treatments.

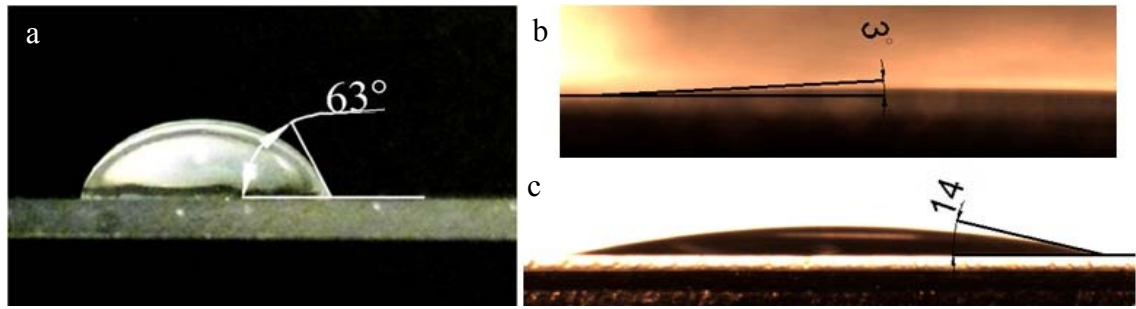


Figure 4.1 Contact angle measured before and after piranha treatment for 30 minutes. Contact angle between water and glass before treatment (a), after treatment (b) and after 2 hours from treatment (c).

Treating micropipettes is different from treating cover slips. In order to apply piranha treatment to glass micropipettes the following issues should be considered carefully:

- Treatment time
- Effect of piranha treatment on pipette capacitance and
- Effect of piranha treatment on pipette surface roughness.

4.2.1 Treatment Time

Figure 4.1 shows that piranha solution treatment is an effective way to increase the hydrophilicity of glass. However, dipping pipettes in piranha solution for 30 minutes causes a considerable amount of piranha solution to be sucked into the pipette by capillary action. Piranha solution is harmful to cells and it must be removed from pipettes before conducting patch clamp experiments. Due to the small tip size of the pipettes (1-2 μm), it takes a long time to remove the piranha solution by applying pressure to the backside of the pipettes. Shorter treatment times were used to overcome this problem by decreasing the amount of the solution which goes

into the pipettes. To observe the effectiveness of treatments, the contact angle between a water droplet and the glass cover slips was measured for different treatment times and presented in Table 4.1. As patch clamp experiments were usually carried out with a delay from treatment, contact angles are measured after treatment and after two hours from treatment to find out if the surface is able to keep its properties for a period of time.

Table 4.1 Contact angle for different treatment times. Treatment time of 30s was chosen because it is more effective and the surface can maintain its properties for a longer time.

Treatment time (sec)	Contact angle measured after treatment	Contact angle measured after 2 hrs.
10	28	48
20	11	37
30	10	19

Based on the values of contact angles in Table 4.1, treatment time of 30 seconds was chosen for pipettes' treatment.

To estimate the influence of capillary action for this treatment time pipettes were dipped in ink for 30 seconds. This gives a good approximation of the length of time required for applying pressure to the pipette to remove the piranha after treatment. Blue ink was used to give a higher contrast as piranha solution is transparent and it is difficult to observe it leaving the pipette. It took 2 minutes and 40 seconds to completely remove ink from the pipette which was sucked in by capillary action in 30 seconds (figure 4.2). Before conducting patch clamp experiments positive pressure is applied to pipettes for three minutes to remove the piranha solution.

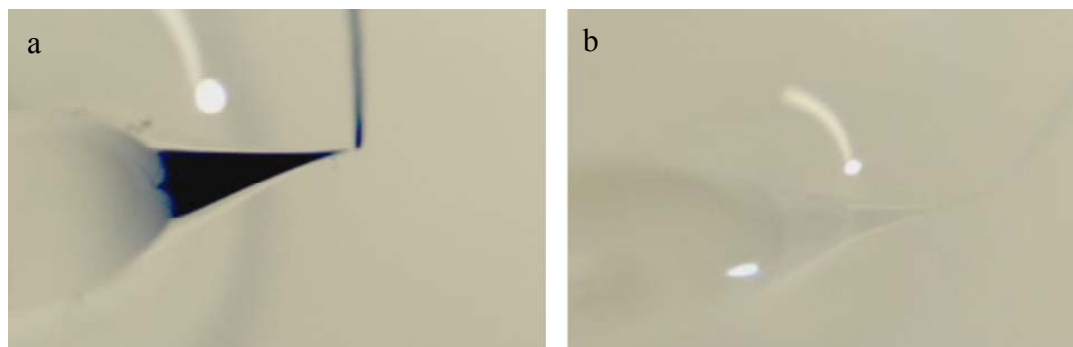


Figure 4.2 Pipettes were dipped in ink for 30 seconds. (a) Positive pressure was applied for 2 minutes and 40 seconds to pipette to remove the ink. The experiments were carried out under water to eliminate surface tension at the tip. (b) Ink has been completely removed from the pipette.

4.2.2 Effect of Piranha Treatment on Pipette Surface Roughness

Piranha solution etches glass. Seu et al have measured the surface roughness of glass slips treated by piranha solution for different times (89). Figure 4.3 shows the surface roughness values of glass after various treatment times. Noticeable roughening can be observed as the etch time is increased.

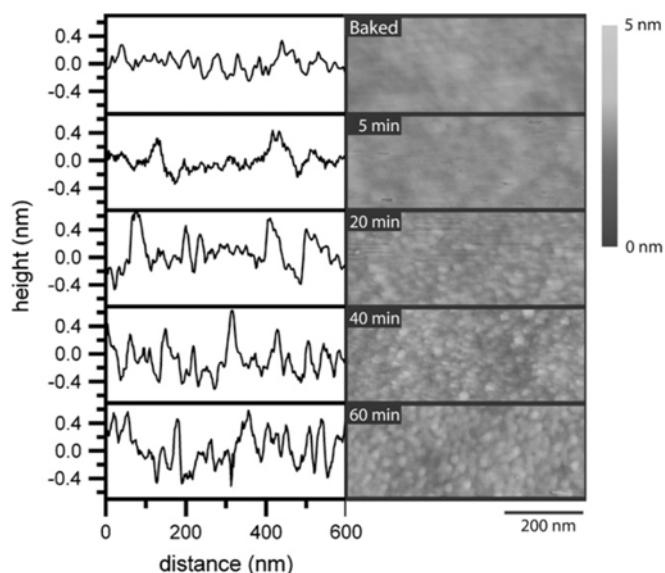


Figure 4.3 Effect of piranha solution etching time on surface roughness of glass slides. AFM images and line scans from five different samples are shown. Surface roughness increases by etching time (89). Surface roughness is detrimental to seal formation (see Chapter 3) and should be kept as low as possible. Decreasing treatment time from several minutes to seconds will greatly reduce etching. Referring to figure 4.3, treating pipettes for 30 seconds with piranha solution should have negligible effect on surface roughness of glass micropipettes.

4.2.3 Effect of Piranha Treatment on Pipette Capacitance

As discussed in section 2.3.1.6, pipette capacitance is an important factor in patch clamp recordings and should be minimized. Treating pipettes with piranha increases the hydrophilicity of the glass surface and facilitates the creep up of conductive watery solution from the pipette wall. This increases the pipette capacitance. Therefore only the very end of pipettes should be treated and the rest of the pipettes should be preserved from treatment. This has been done by dipping only the end of micropipettes in piranha solution using a simple pipette holder (figure 4.4).

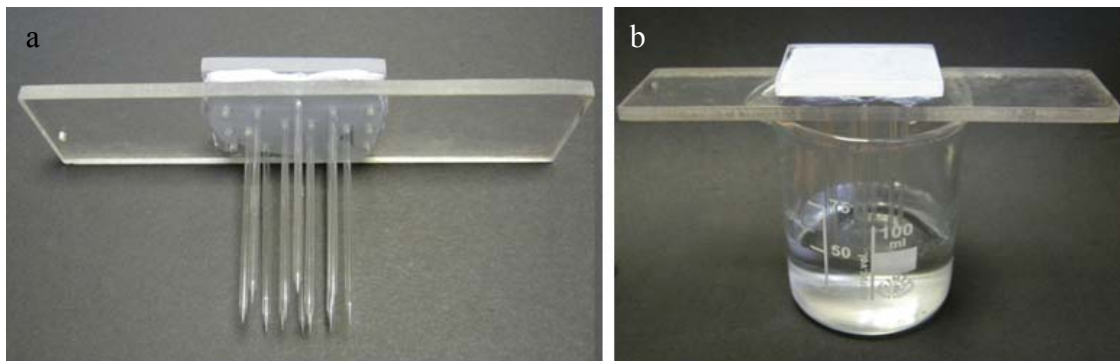


Figure 4.4 Only the very ends of pipettes were dipped into piranha solution using a micropipette holder to preserve the rest of the micropipettes from being treated. (a) The pipette holder with pipettes assembled in the holder, (b) Pipettes were inserted in piranha solution.

4.2.4 Piranha Solution Treatment of Glass Micropipettes

The purpose of treating glass micropipettes with piranha solution is to increase the hydrophilicity of the inner wall of the micropipettes which is in contact with the cell membrane in seal formation. Pipettes were dipped in piranha solution for 30 seconds using the pipette holder. Then pipettes were backfilled with pipette solution and

pressure is applied to them after immersing the tip into bath solution for three minutes. This time is enough to remove harmful solution from the tip. Pipettes are now ready for conducting patch clamp experiments.

4.3 Oxygen Plasma Treatment

The second method used to alter the surface properties of glass micropipettes is oxygen plasma treatment. Plasma treatment increases hydrophilicity and cleans the surface. The plasma affects a surface mainly in two ways: physically and chemically. Physical plasma/surface interaction is due to bombardment of energetic ions. Chemical interaction is driven by chemically active species in the plasma. Plasma is a partially ionized gas with an equal number of positive and negative charges. The ions in the plasma are accelerated through the plasma sheath and bombard the surrounding surfaces. However, by applying an external field the energy of the ions bombarding the substrate can be adjusted (90). Depending on plasma parameters (power, applied voltage, pressure, plasma density etc) and gas chemistry, plasma discharges can be employed for etching, deposition or surface cleaning (90). Oxygen plasma treating leads to the formation of surface ($-OH$) groups (silanol) (figure 4.5) (91). The increased concentration of OH groups at the surface provides a higher number of siloxane bonds. Glass cover slips were used for characterization of the treatment procedure. They were exposed to oxygen plasma for 1 minute. Figure 4.6 shows the contact angle between glass and a droplet of water before and after oxygen plasma treatments.

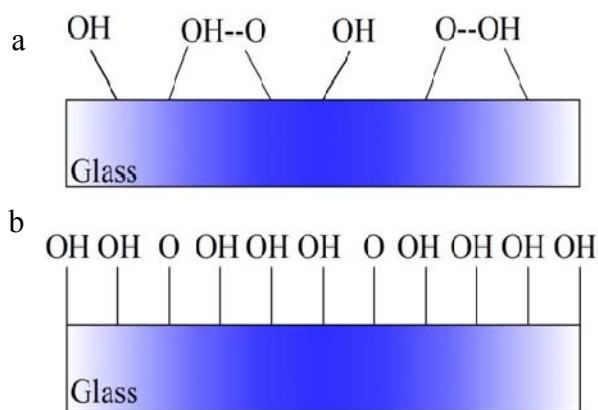


Figure 4.5 Glass surface (a) before and (b) after plasma treatment (redrawn from (92)).

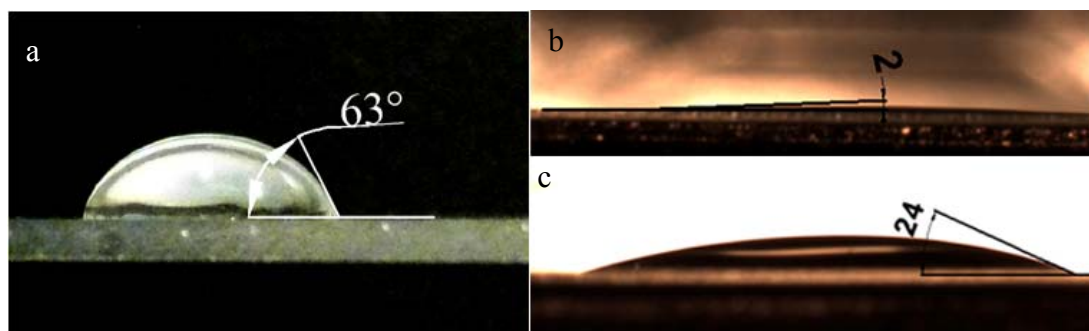


Figure 4.6 Contact angle measured before and after oxygen plasma treatment for 1 minute. Contact angle between water and glass before treatment (a), after treatment (b) and after 2 hours from treatment (c).

Similar to piranha solution treatment, pipette capacitance and surface roughness are important factors which need careful consideration in plasma treatment.

4.3.1 Effect of Oxygen Plasma Treatment on Pipette Capacitance

A mould has been fabricated to be placed into the plasma chamber. Figure 4.7 shows the fabrication process of the mould. As stated earlier, it is only the tips of

micropipettes that need to be treated and the rest of the pipettes should be preserved from treatment.

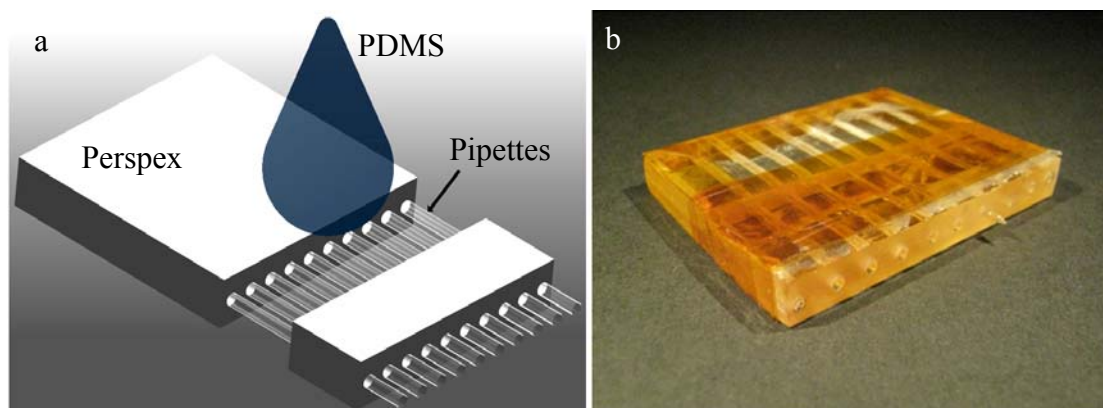


Figure 4.7 Fabrication process of a mould for oxygen plasma treatment of glass micropipettes. a) The holder is fabricated from Perspex and PDMS, b) the image of the holder.

4.3.2 Effect of Oxygen Plasma Treatment on Surface Roughness

Oxygen plasma treatment increases the surface roughness of glass. The amount of roughness is proportional to the magnitude of power and exposure time. The oxygen radicals preferentially remove weak Si-Si bonds and break Si-O bonds at the surface which results in higher surface roughness (93). Figure 4.8 shows surface roughness as a function of power and exposure time.

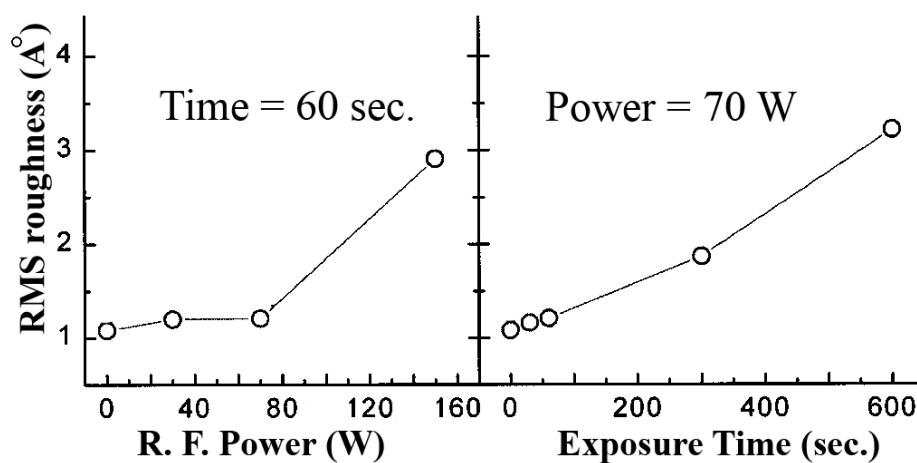


Figure 4.8 Surface roughness of glass as a function of power and exposure time (93).

4.3.3 Oxygen Plasma Treatment of Glass Micropipettes

For oxygen plasma treatment of glass micropipettes, they were inserted into a low-pressure radio frequency (RF) plasma chamber. Ten pipettes were placed in the mould to be treated all at once. The mould was inserted horizontally to the chamber. The plasma treatment was performed at a working pressure of 40 mTorr, an oxygen flow of 50 sccm and 40 degrees. The oxygen plasma power and exposure time were respectively 800 W inductively coupled power, 20 W platen power and 1 min. As can be understood from figure 4.8, for these values the size of roughness is below 2 Å. This amount of change in surface roughness is negligible in comparison with the surface roughness of glass micropipettes (The surface roughness of pipette tip and inner wall is reported in Chapter 5). Therefore oxygen plasma treatment has a minimum effect on surface properties of pipettes.

4.4 Patch Clamping Experiments

Patch clamping experiments were carried out on HEK (Human Embryonic Kidney) cells with piranha solution treated, oxygen plasma treated and conventional pipettes and the results are compared. Cell culture and set up for patch clamping experiments were the same as discussed in Chapter 3. Glass micropipettes used for treatment and patch clamping experiments were pulled from borosilicate glass tubes (BF150-86-10, Sutter Instruments). The puller machine used was the flaming/brown micropipette puller (Model P-97, Sutter Instruments, Novato, CA) and the pulling parameters of the machine were set to produce pipettes with approximately 1.5 µm in tip diameter.

Ten measurements were made for each type of pipette and seal values were recorded. The mean value of seal resistances for conventional pipettes is 1.6 G Ω with the standard deviation of 0.6 G Ω . The mean of seal resistances for piranha treated pipettes is 3.0 G Ω with the standard deviation of 0.9 G Ω . In comparison, the mean value of seal resistance for oxygen plasma treated pipettes is 0.93 G Ω with the standard deviation of 0.3 G Ω . Figures 4.9 and 4.10 show performance of one of the piranha treated and one of the oxygen plasma treated pipettes respectively. Figure 4.11 shows the seal values for oxygen plasma treated, piranha solution treated and conventional pipettes.

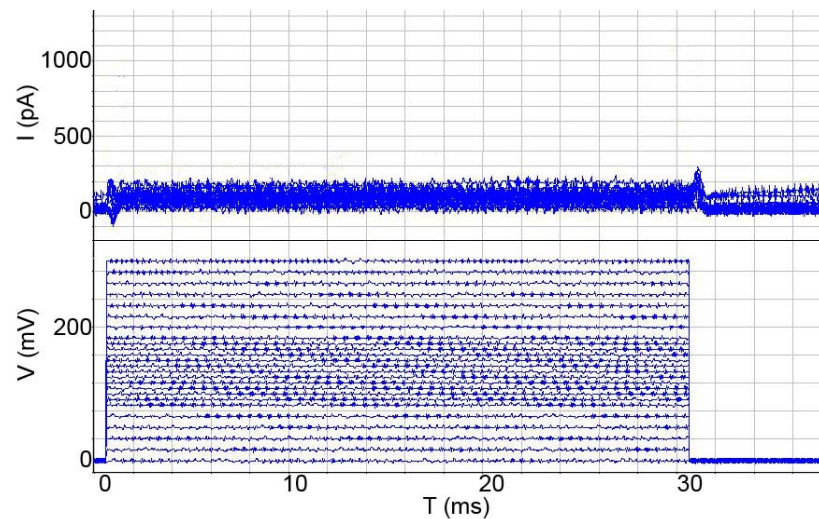


Figure 4.9 Voltage clamp recordings showing changes in current performed by an oxygen plasma treated pipette. The voltage step length is 30 ms, the increment is 25 mV per step. The application of a 350 mV pulse resulted in a recorded current of approximately 210 pA and a calculated seal resistance of approximately 1.6 G Ω .

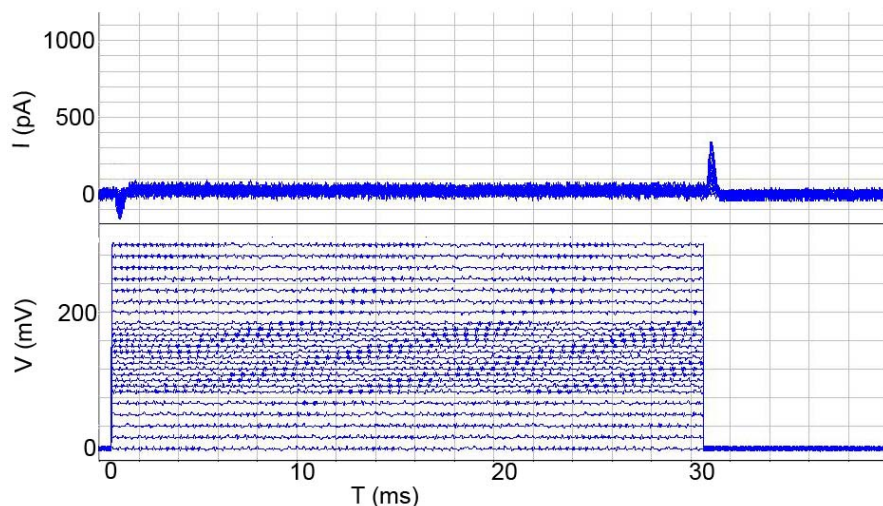


Figure 4.10 Voltage clamp recordings showing changes in current performed by a piranha solution treated pipette. The voltage step length is 30 ms, the increment is 25 mV per step. The application of a 350 mV pulse resulted in a recorded current of approximately 80 pA and a calculated seal resistance of approximately 4.3 G Ω .

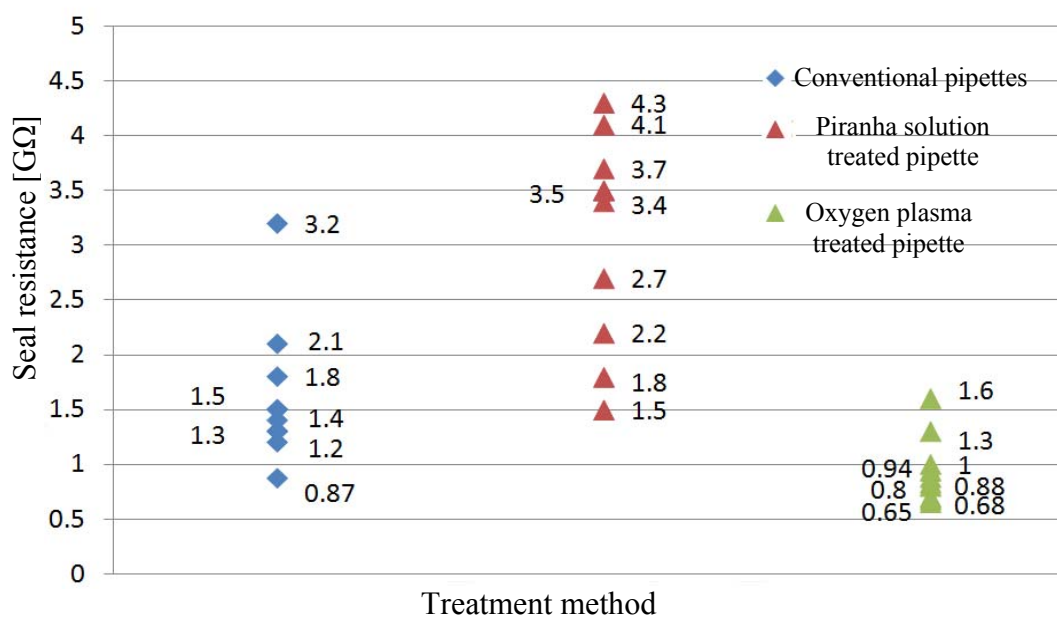


Figure 4.11 Seal values for conventional, piranha solution and oxygen plasma treated pipettes.

4.5 Discussion

The results show that seal values for piranha solution treated pipettes are higher than for conventional pipettes. As discussed in section 2.6.3 four kinds of forces are presented in seal formation: ionic bonds, hydrogen bonds, salt bridges and van der Waals' forces. Of these four, the last three play a more important role. Results from piranha solution treated pipettes show the importance of hydrogen bonds in gigaseal formation. Piranha solution is a strong oxidizer and adds more hydroxyl groups to the surface of the glass, therefore stronger hydrogen bonds can be made between glass and membrane and a stronger seal is obtained. Piranha solution also cleans the surface of the glass of any organic material. Clinginess is a prerequisite for seal formation (6). These two improvements result in a very high probability of gigaseal formation. About 80% of efforts led to gigaseal formation. Piranha solution treatment has been found to be a practical and effective way for pipette treatment, improving gigaseal formation, which is highly desirable in electrophysiology labs.

Oxygen plasma treatment also cleans the surface and makes it more hydrophilic. However oxygen plasma treated pipettes could not form seals as good as piranha or conventional pipettes. This is mainly due to oxygen plasma not being an effective way of treating micropipettes. Firstly, due to the dimensions of the chamber, micropipettes should be placed on a wafer horizontally. This configuration significantly limits the access of plasma to the inside of pipette (Figure 4.12a). Secondly, the inner wall of micropipettes should be treated for the first one hundred micrometers from the pipette tip, as in seal formation the membrane goes from 5 to

100 microns into the pipette. Thirdly, the tip size is very small (1 to 2 microns). As a result plasma cannot reach the desired area effectively. Fourthly, background gases present in the inducting coupled plasma etcher chamber may contaminate the tip (92), thereby preventing seal formation. The combination of these reasons has resulted in lower seal resistances of oxygen plasma treated pipettes. It should also be emphasized that oxygen plasma treatment has been widely used in planar patch clamp systems for treating the patching site (22), (35), (46). The higher seal values after treatment show the importance of hydrophilicity of the patching site and the effectiveness of plasma treatment. In treating planar patch clamp systems, charged species can easily reach to the patching site because it is normally on a flat surface; therefore effectively treating the site (figure 4.12b).

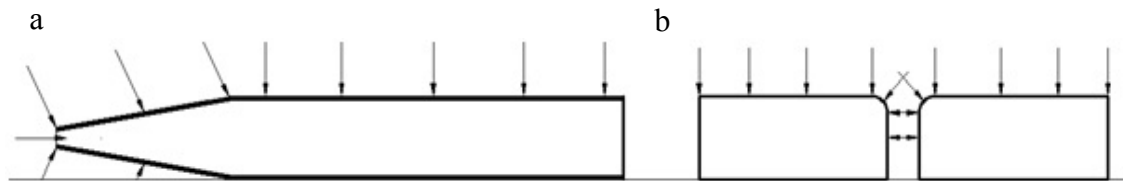


Figure 4.12 Oxygen plasma treatment of micropipettes (a) and planar patch clamp chip (b). Plasma can effectively treat patching site in planar patch clamp systems but the inner wall of pipettes is difficult to access.

4.6 Summary

In this chapter the effect of hydrophilicity on gigaseal formation has been reported. Piranha solution and oxygen plasma treatments are used to change the hydrophilicity of the patching site. Both the piranha solution and oxygen plasma treatment increase surface roughness, but the value of increase is very small and can be neglected.

Results show that piranha treated pipettes form better seals with higher resistance values. The results of this study not only provide better understanding of gigaseal formation but also can be applied in the planar patch clamping design and fabrication process to achieve better cellular recording. These results can be understood by the fact that piranha solution is a strong oxidizer and adds more hydroxyl groups to the surface of the glass. Therefore more hydrogen bonds can be made between glass and membrane and a stronger seal is obtained. Piranha solution also cleans the surface of any organic material. Cleanliness of patching area is a crucial required condition for seal formation (6). Another advantage of piranha solution treatment is that the probability of gigaseal formation is very high. About 80% of efforts led to gigaseal formation. Piranha solution treatment has been found to be a practical and effective way for pipette treating which is highly desirable in electrophysiology labs. Oxygen plasma treated pipettes failed to form high resistance seals. This is mainly because oxygen plasma treatment is not an effective way for treating glass micropipettes. However treatment of planar patch clamping systems with oxygen plasma where there is a good access of plasma to the patching site, has improved seal formation. This shows the importance of hydrophilicity in seal formation.

CHAPTER 5: EFFECT OF TIP SIZE ON GIGASEAL FORMATION

5.1 Introduction

Tip size is perhaps the easiest controllable factor which affects gigaseal formation. It is generally known that the smaller the tip size, the easier it is to achieve a gigaseal. Although tip size has been mentioned in the literature to be an important factor in seal formation and often it has been used in planar patch clamping as a tool to increase the probability of gigaseal formation (22), (33), (47), (63), (64), the reasons remain unclear. This chapter reports on research into the effect of tip size on gigaseal formation. To clarify this matter one needs to study the surface properties of pipettes with different tip sizes and compare the seal resistances obtained by them. However firstly, it is important to know how the tip size affects the patch clamping. The influence of tip size in patch clamping technique and its effect on gigaseal formation is introduced in section 5.2 and 5.3. The areas that make contact with the cell surface in gigaseal formation are the pipette tip and the pipette inner wall. The surface properties of these areas are measured by 3D reconstruction using a Scanning Electron Microscope (SEM) stereoscopic technique and are reported in section 5.4. Results from the 3D reconstruction of different sized pipettes show that smaller pipettes are smoother than bigger pipettes. Section 5.5 reports the results of patch clamp experiments by different sized pipettes. The effect of tip size on gigaseal formation is discussed in section 5.6. Some surface roughness parameters such as

maximum peak to valley distance and developed interfacial area ratio are found to be important in seal formation. Finally the chapter is summarized in section 5.7.

5.2 Effect of Tip Size in Patch Clamping

The small size of the tip of the micropipette creates a resistance. This resistance plays an important role in patch clamping since it constitutes most of the pipette resistance. The other part of pipette resistance is due to the shank of the pipette and is called shank resistance. The equivalent circuit for the cell attached patch configuration was shown in figure 2.4 and is recalled here again (figure 5.1). According to Kirchhoff's voltage law, the greatest voltage drop in a series circuit will be over the highest resistance. It means that the highest resistance in a series circuit determines the current flow; therefore if the patch resistance (R_{patch}) is high compared with the resistance of the rest of the cell (R_m) and the pipette resistance ($R_{pipette}$), then the circuit effectively monitors current flow through the patch and any ion channels in it.

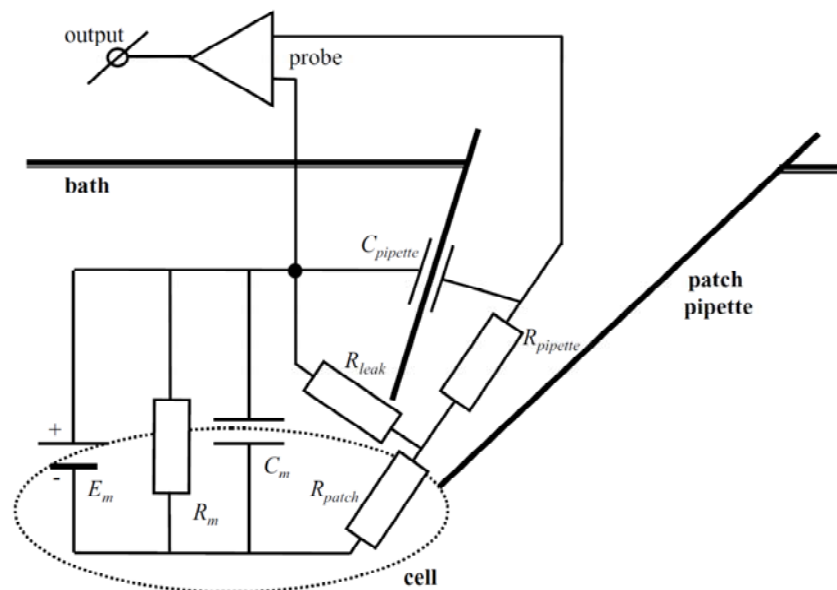


Figure 5.1 Equivalent circuit for the cell-attached patch configuration (5).

Pipette resistance can be obtained theoretically by knowing the geometry of patch pipettes. The geometry of thick walled hard glass patch pipettes (which were the kind of pipettes used in the experiments) is shown in figure 5.2. The tip shape is approximately conical, with an angle φ of 8-12°. When the pipette is modelled as having an approximately cylindrical shank and a conical tip, the total resistance of the pipette is given by the sum of the tip and the shank resistances (47).

$$R = \frac{\rho l}{\pi r_s^2} + \frac{\rho \cot\left(\frac{\varphi}{2}\right)}{\pi} \left(\frac{1}{r_t} - \frac{1}{r_s}\right) \quad (5.1)$$

Where:

ρ is specific resistivity (Ohm.cm)

l is pipette shank length (cm)

r_s is the shank radius (μm)

r_t is the tip radius (μm)

φ is the cone angle.

Since the radius of the cylindrical shank (r_s) is much larger ($>50 \mu\text{m}$) than that of the radius of the tip opening (r_t), the resistance of the tip dominates. Most of the resistance of a patch pipette resides at or very near its tip.

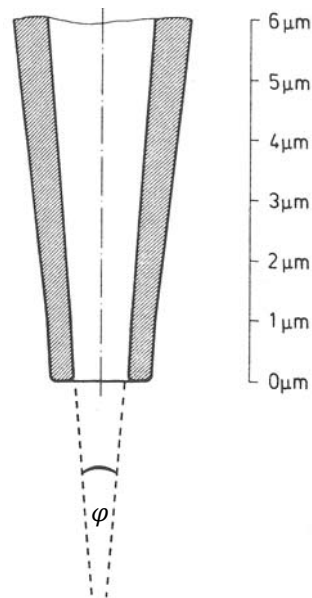


Figure 5.2 Longitudinal section through the tip of a thick-walled hard glass pipette (47).

As was discussed earlier, lower pipette resistance results in more accurate measurement of membrane activity. However the tip size cannot be increased greatly, since it lowers the probability of seal formation. One solution is to minimize shank resistance as much as possible by selecting correct pulling parameters in conventional patch clamping or suitable chip design in planar patch clamping devices.

5.3 Effect of Tip Size on Gigaseal Formation

Tip size affects gigaseal formation. The smaller the tip is, the higher the seal resistance. Length of opposition between cell membrane and pipette is an important factor in gigaseal formation. A cell membrane has contact with the pipette in two areas: pipette tip and pipette inner wall (figure 5.3).

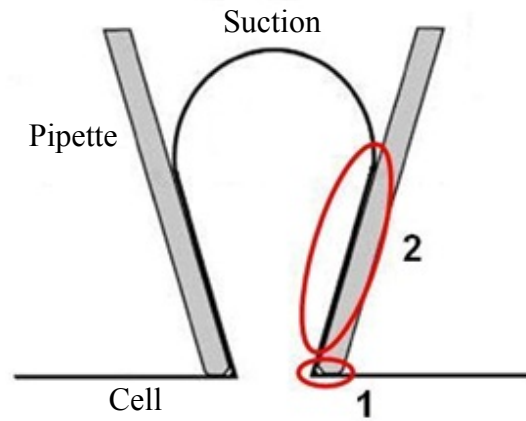


Figure 5.3 Two contact areas of pipette and membrane in gigaseal formation: (1) at the tip and (2) along the inner wall.

In patch clamping, membrane can be sucked into the pipette from 5 to 100 micrometers (50) (51). This implies that as long as the membrane and pipette are in close contact their length of opposition is in the second order of importance. This suggests that membrane can get closer to the pipette surface for smaller pipettes. Measuring surface properties of pipettes with different sizes can help prove this hypothesis.

5.4 Measuring Surface Properties of Pipettes

SEM stereoscopic technique is used to determine three dimensional surface structures of pipettes. Information on SEM stereoscopic technique can be found in Chapter 3 and appendix A.

5.4.1 3D Reconstruction of the Tips

To enhance the quality of images to the level required by the SEM stereoscopic technique, glass micropipettes are coated with a less than 5 nm-thick layer of platinum. Figure 5.4 shows images of pipettes before and after coating. The coating improved significantly the quality of the SEM images. The coating thickness is well below the resolution of the images used in 3D reconstruction. Therefore surface features are not affected from the coating process.

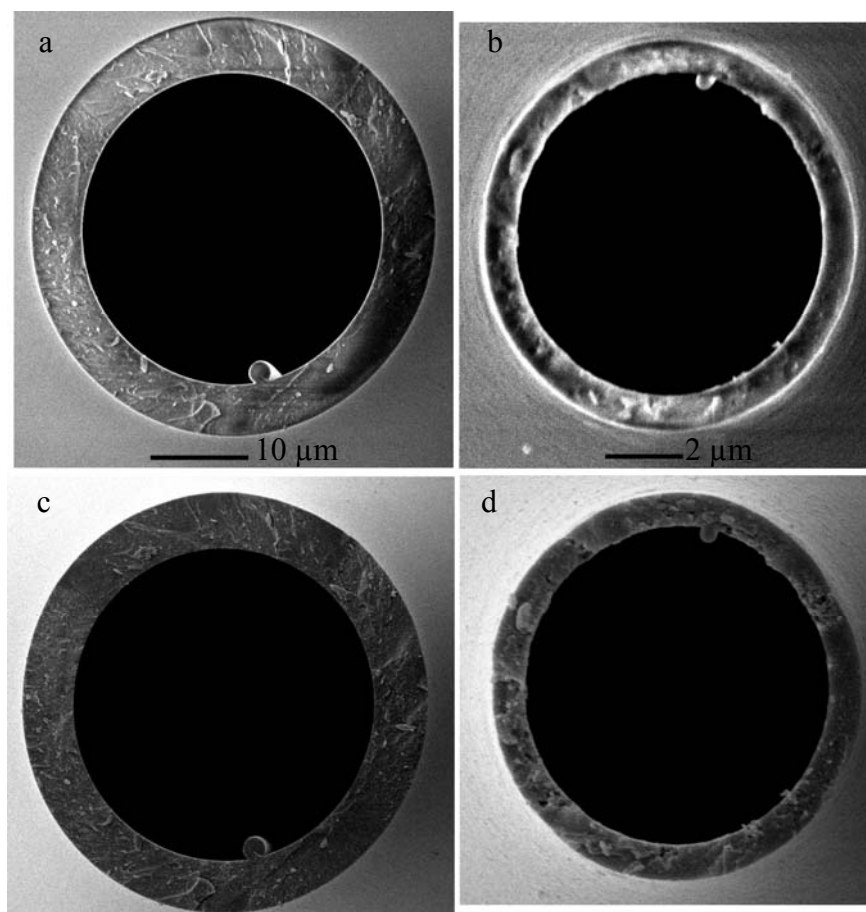


Figure 5.4 Images of pipettes' tips before (a,b) and after (c,d) coating with platinum.

Two pipettes with different tip sizes were chosen for 3D reconstruction:

- Pipette A with the tip diameter of 8.7 μm and
- Pipette B with the tip diameter of 2.3 μm.

To reconstruct the pipettes' tips three high resolution SEM images are obtained from different perspectives. The tilting angle between each pair of stereo images was 5 degrees. The SEM machine used for 3D reconstructions is Strata DB 235 from FEI. MeXTM software (version 5.1) was used for analyses and 3D reconstruction of the pipette surface (72). Figure 5.5 shows the west, the middle and the east SEM images of pipette A and also the digital elevation model created by MeXTM.

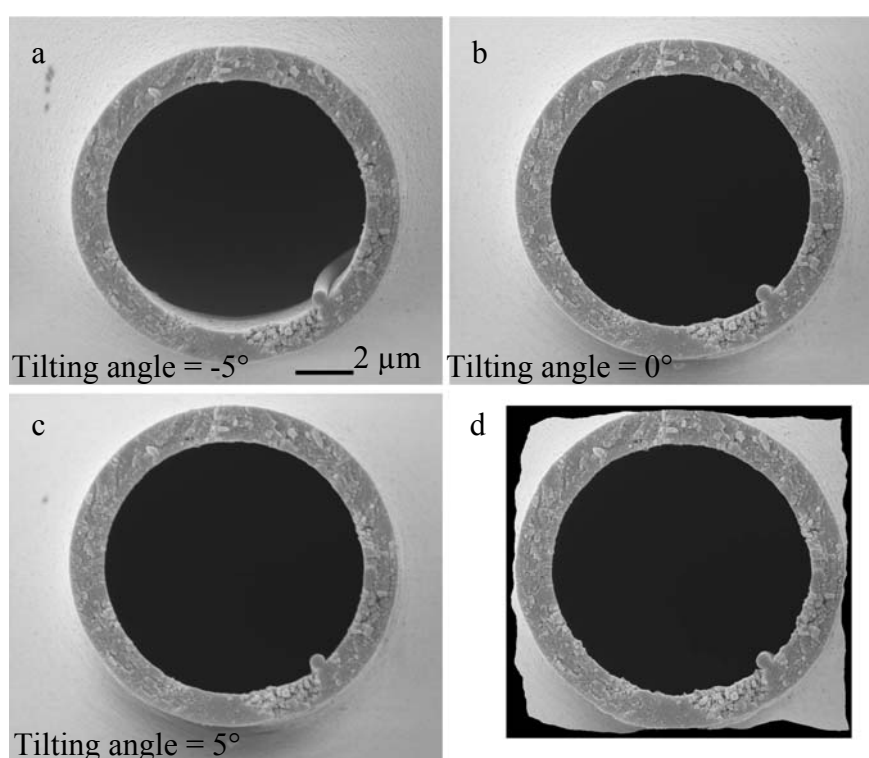


Figure 5.5 SEM stereo images of pipette A (tip diameter (D_t)=8.7 μm): (a) west, (b) middle, (c) east images and (d) the digital elevation model created by MeXTM.

Figure 5.6 shows stereo images and the digital elevation model of pipette B.

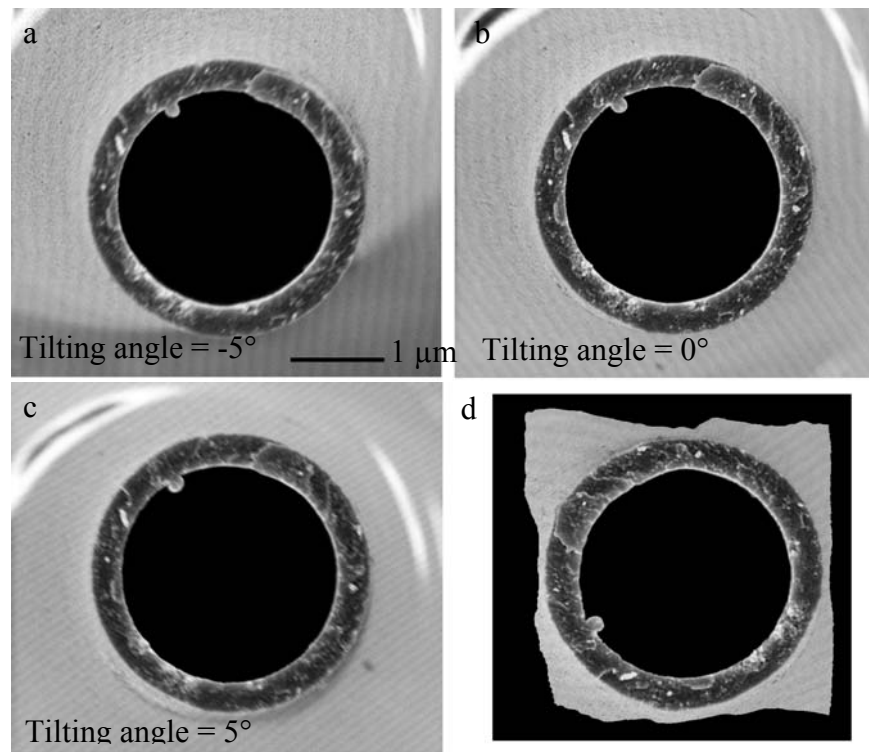


Figure 5.6 SEM stereo images of pipette B ($D_t=2.3 \mu\text{m}$): (a) west, (b) middle, (c) east images and (d) the digital elevation model created by MeXTM.

Table 5.1 gives the values of tip diameters, tilting angles, magnifications, lateral resolutions and vertical resolutions of the two 3D reconstructed pipettes.

Table 5.1 Reconstruction information for 2 pipettes.

Pipette	Tip Diameter (μm)	Tilting Angle (left to right)	Magnification	Lateral Resolution	Vertical Resolution
Pipette A	8.7	10	20000	14.7 nm	42.1 nm
Pipette B	2.3	10	65000	4.6 nm	13.2 nm

Surface properties of pipettes computed from the digital elevation model are presented in Table 5.2. The results show that pipette A is rougher than pipette B. Pipette A (tip diameter (D_t) = $8.7 \mu\text{m}$) has the average surface roughness of 40.8 nm and the maximum peak to valley distance of 585.9 nm . The average surface roughness of pipette B (D_t) = $2.3 \mu\text{m}$) is 17.3 nm and its maximum peak to valley distance is 204.8 nm . Table 5.3 shows the bearing area curve parameters of the

pipettes. These parameters provide useful information about the peak, core and valley volumes and fluid retention ability of the surface (94) which will be used to explain the sources of leakage in seal formation later in this chapter.

Table 5.2 Tip surface properties for two pipettes having different sizes

Name	Value (Pipette A) $D_t = 8.7 \mu\text{m}$	Value (Pipette B) $D_t = 2.3 \mu\text{m}$	Description
S_a	40.8 nm	17.3 nm	Average height of selected area
S_q	54.5 nm	22.6 nm	Root-mean-square height of selected area
S_p	258.7 nm	92.0 nm	Maximum peak height of selected area
S_v	327.2 nm	112.8 nm	Maximum valley depth of selected area
S_z	586 nm	204.8 nm	Maximum height of selected area
S_{10z}	438.7 nm	168.2 nm	Ten point height of selected area
S_{sk}	-0.1515	-0.2774	Skewness of selected area
S_{ku}	4.5606	3.9823	Kurtosis of selected area
S_{dq}	0.7303	0.8654	Root mean square gradient
S_{dr}	27.005%	34.866%	Developed interfacial area ratio

Table 5.3 Values of the bearing area curve for two pipette tips having different sizes

Name	Value (Pipette A) $D_t = 8.7 \mu\text{m}$	Value (Pipette B) $D_t = 2.3 \mu\text{m}$	Description
S_k	358.9 nm	116.9 nm	Core roughness depth, height of the core material
S_{pk}	129.1 nm	67.1 nm	Reduced peak height, mean height of the peaks above the core material
S_{vk}	236.0 nm	47.3 nm	Reduced valley height, mean depth of the valleys below the core material
S_{mr1}	12.4 %	10.18 %	Peak material component, the fraction of the surface which consists of peaks above the core material
S_{mr2}	90.74 %	89.23 %	Peak material component, the fraction of the surface which will carry the load
V_{mp}	0.0059 ml/m ²	0.0033 ml/m ²	Peak material volume of the topographic surface (ml/m ²)
V_{mc}	0.1225 ml/m ²	0.0411 ml/m ²	Core material volume of the topographic surface (ml/m ²)
V_{vc}	0.1816 ml/m ²	0.0563 ml/m ²	Core void volume of the surface (ml/m ²)
V_{vv}	0.021 ml/m ²	0.0056 ml/m ²	Valley void volume of the surface (ml/m ²)
V_{vc}/V_{mc}	1.4817	1.37	Ratio of V_{vc} parameter to V_{mc} parameter

5.4.2 Inner Wall

So far it has been shown that tips of micropipettes are rough and a bigger pipette has a higher average surface roughness. It has been thought that heating and pulling of glass micropipettes produces smooth surfaces (21). Therefore one could expect that inner walls of pipettes are smooth. To measure surface properties of the inner walls of pipettes, focused ion beam and SEM stereoscopic technique were used. Two pipettes with different sizes were chosen:

- Pipette C with the tip diameter of 15.3 μm and
- Pipette D with the tip diameter of 11.8 μm

The pipettes were split and cut open using focused ion beam milling for access to the inner walls. The imaging direction was perpendicular to the cutting plane, avoiding redeposition of sputtered materials from the Focused Ion Beam (FIB) cutting to the area. After cutting, the pipettes were turned 90 degrees by means of a holder which was previously fabricated. Three SEM images were taken from the inside wall and 3D structures of the inner wall were obtained using MeX software. Figure 5.7 shows pipette C ($D_t=15.3 \mu\text{m}$) before and after FIB milling. West, middle and east SEM images of the inner wall of this pipette and its digital elevation model created by MeX are shown in figure 5.8.

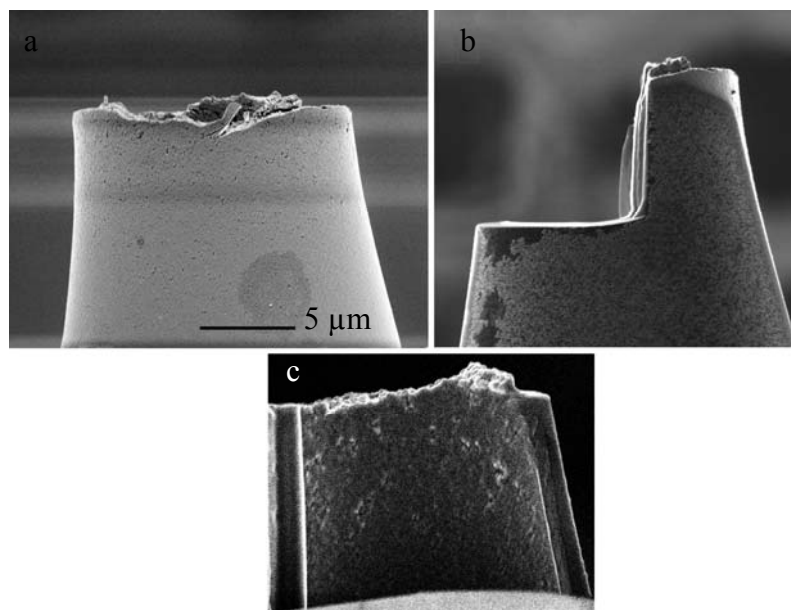


Figure 5.7 Pipette C ($D_t=15.3 \mu\text{m}$) before and after focused ion beam milling.

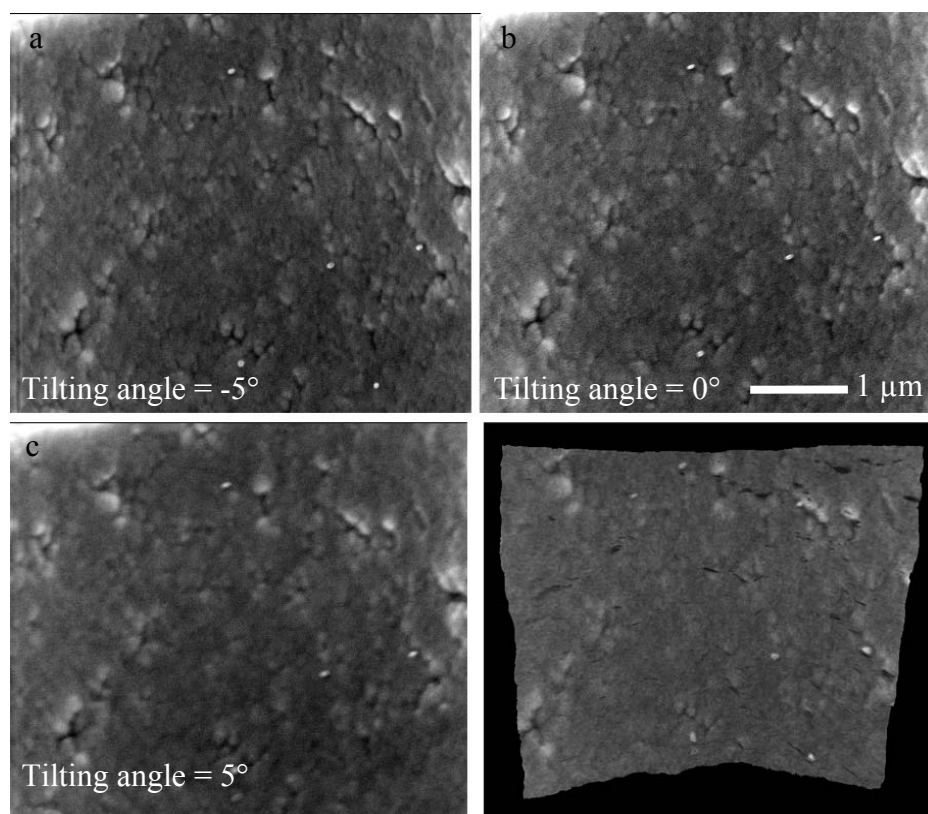


Figure 5.8 Inner wall SEM stereo images of pipette C ($D_t= 15.3 \mu\text{m}$): (a) west, (b) middle, (c) east images and (d) the digital elevation model created by MeXTM.

Figure 5.9 shows pipette D ($D_t=11.8 \mu\text{m}$) before and after FIB milling. West, middle and east SEM images of the inner wall of this pipette and its digital elevation model created by MeX are shown in figure 5.10.

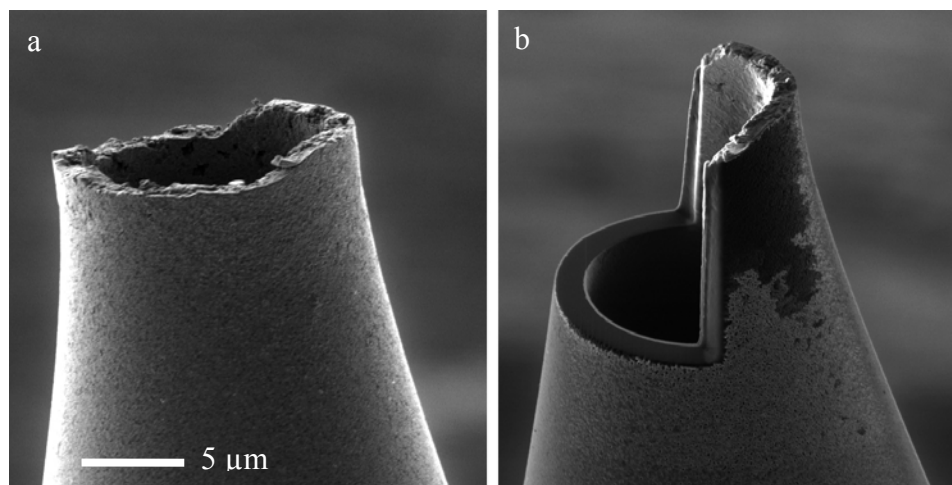


Figure 5.9 Pipette D ($D_t=11.8 \mu\text{m}$) before and after focused ion beam milling.

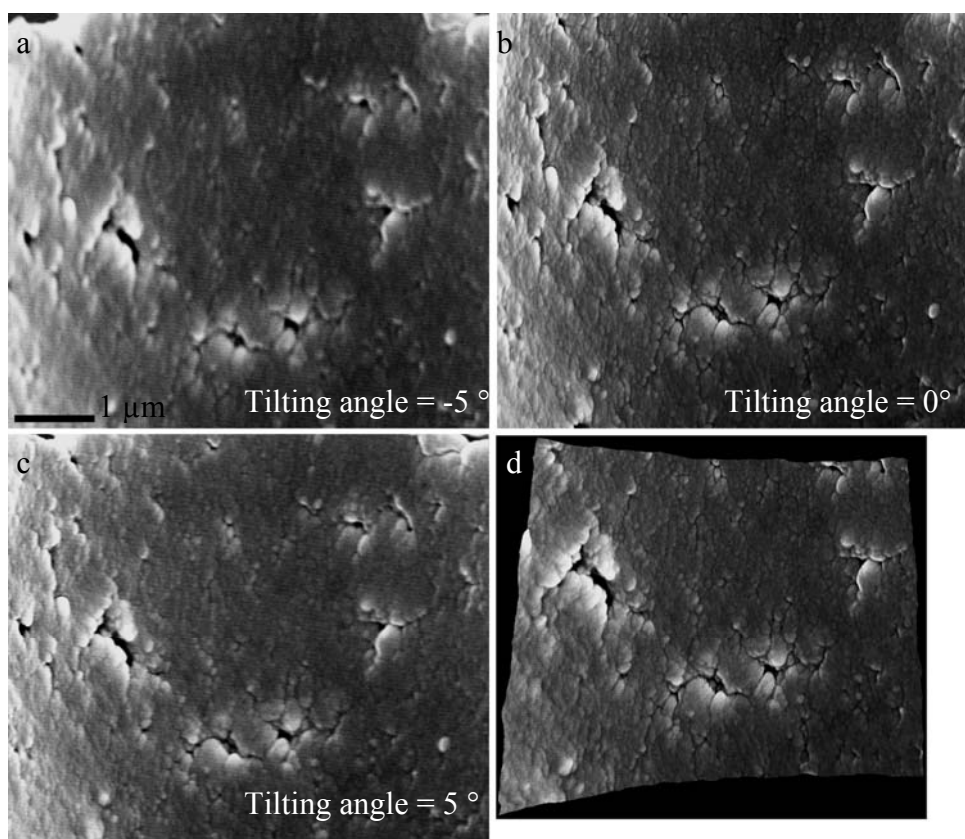


Figure 5.10 Inner wall SEM stereo images of pipette D ($D_t=11.8 \mu\text{m}$): (a) west, (b) middle, (c) east images and (d) the digital elevation model created by MeXTM.

Table 5.4 gives the values of tip diameters, tilting angles, magnifications, lateral resolutions and vertical resolutions of the two 3D reconstructed pipettes.

Table 5.4 Reconstruction information for 2 pipettes.

Pipette	Tip Diameter (μm)	Tilting Angle (left to right)	Magnification	Lateral Resolution	Vertical Resolution
Pipette C	15.3	10	25000	11.7 nm	33.7 nm
Pipette D	11.8	10	50000	5.88 nm	16.8 nm

Surface properties of the pipettes' inner wall surfaces computed from the digital elevation model are presented in Table 5.5. The results show that pipette C is rougher than pipette D. Pipette C ($(D_t) = 15.3 \mu\text{m}$) has the average surface roughness of 30.2 nm. The average surface roughness of pipette D ($(D_t) = 11.8 \mu\text{m}$) is 24.1 nm.

Table 5.5 Inner wall surface properties of two different sized pipettes

Name	Value (Pipette C) $D_t = 15.3 \mu\text{m}$	Value (Pipette D) $D_t = 11.8 \mu\text{m}$	Description
S_a	30.2 nm	24.1 nm	Average height of selected area
S_q	37.9 nm	30.6 nm	Root-mean-square height of selected area
S_p	156.9 nm	183.0 nm	Maximum peak height of selected area
S_v	149.1 nm	172.9 nm	Maximum valley depth of selected area
S_z	361 nm	356 nm	Maximum height of selected area
S_{10z}	270.2 nm	247.0 nm	Ten point height of selected area
S_{sk}	0.0467	0.0696	Skewness of selected area
S_{ku}	2.9718	3.3903	Kurtosis of selected area
S_{dq}	0.6154	0.8312	Root mean square gradient
S_{dr}	17.827%	30.966	Developed interfacial area ratio

Table 5.6 Values of the bearing area curve for two pipette tips having different sizes

Name	Value (Pipette C) $D_t = 15.3 \mu\text{m}$	Value (Pipette D) $D_t = 11.8 \mu\text{m}$	Description
S_k	458.8 nm	340.9 nm	Core roughness depth, height of the core material

S_{pk}	225.4 nm	174.2 nm	Reduced peak height, mean height of the peaks above the core material
S_{vk}	122.4 nm	47.9 nm	Reduced valley height, mean depth of the valleys below the core material
S_{mr1}	19.52 %	17.36 %	Peak material component, the fraction of the surface which consists of peaks above the core material
S_{mr2}	93.79 %	96.72 %	Peak material component, the fraction of the surface which will carry the load
V_{mp}	0.0079 ml/m ²	0.0062 ml/m ²	Peak material volume of the topographic surface (ml/m ²)
V_{mc}	0.1741 ml/m ²	0.1306 ml/m ²	Core material volume of the topographic surface (ml/m ²)
V_{vc}	0.2841 ml/m ²	0.2115 ml/m ²	Core void volume of the surface (ml/m ²)
V_{vv}	0.0155 ml/m ²	0.0073 ml/m ²	Valley void volume of the surface (ml/m ²)
V_{vc}/V_{mc}	1.6326	1.6194	Ratio of V_{vc} parameter to V_{mc} parameter

5.5 Patch Clamp Experiments

Patch clamp experiments were carried out on HEK (Human Embryonic Kidney) cells using two kinds of pipettes:

- Conventional pipettes with tip diameter of 1.1 μm and resistance of 6.5 $\text{M}\Omega$
- Big pipettes with tip diameter of 3.5 μm and resistance of 1.8 $\text{M}\Omega$.

Cell culture and set up for patch clamp experiments were the same as discussed in Chapter 3. Glass micropipettes were pulled from borosilicate glass tubes (BF150-86-10, Sutter Instruments). The puller machine used was a flaming/brown micropipette puller (Model P-97, Sutter Instruments, Novato, CA) and the pulling parameters of the machine were set to produce pipettes with the aforementioned tip diameters. Ten measurements were made for each type of pipette and seal values were recorded. Figures 5.11 and 5.12 show the seal quality for the conventional and bigger pipette respectively. Figure 5.13 shows the seal values for the two kinds of pipettes. The mean value of seal resistance for conventional pipettes is 1.6 $\text{G}\Omega$ with

the standard deviation of 0.6 G Ω . The mean value of seal resistances for bigger pipettes is 0.4 G Ω with the standard deviation of 0.2 G Ω .

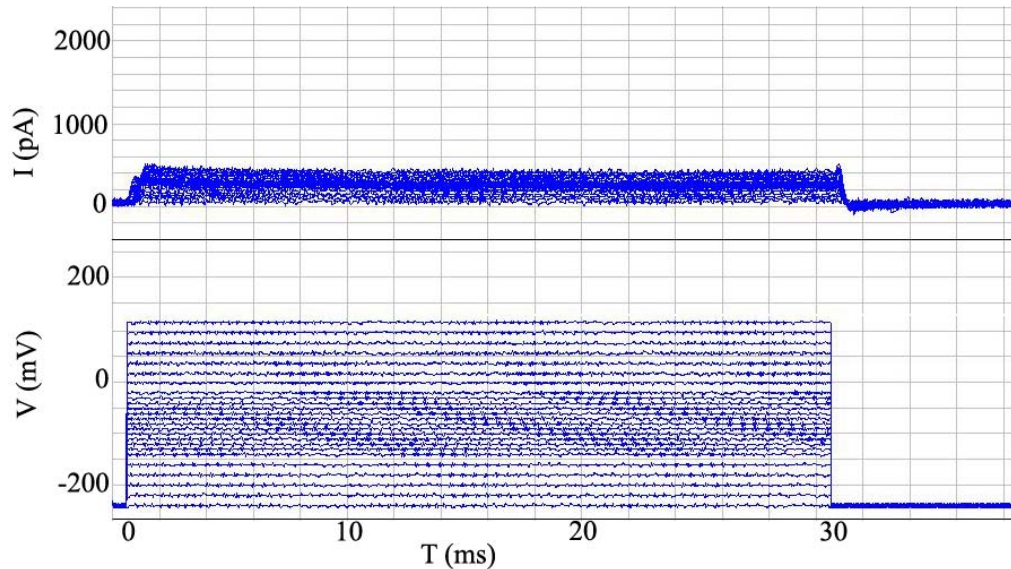


Figure 5.11 Voltage clamp recordings showing changes in current performed by a bigger pipette (tip diameter = 3.5). The voltage step length is 30 ms, the increment is 25 mV per step. The application of a 350 mV pulse resulted in a recorded current of approximately 480 pA and a calculated seal resistance of approximately 0.7 G Ω .

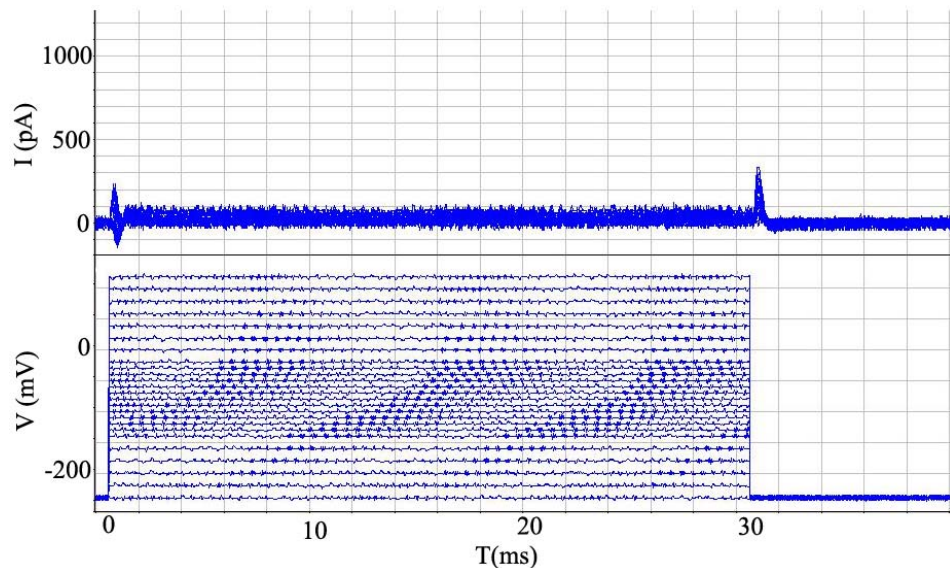


Figure 5.12 Voltage clamp recordings showing changes in current performed by a conventional pipettes (tip diameter = 1.1). The voltage step length is 30 ms, the increment is 25 mV per step. The application of a 350 mV pulse resulted in a recorded current of approximately 110 pA and a calculated seal resistance of approximately 3.2 G Ω .

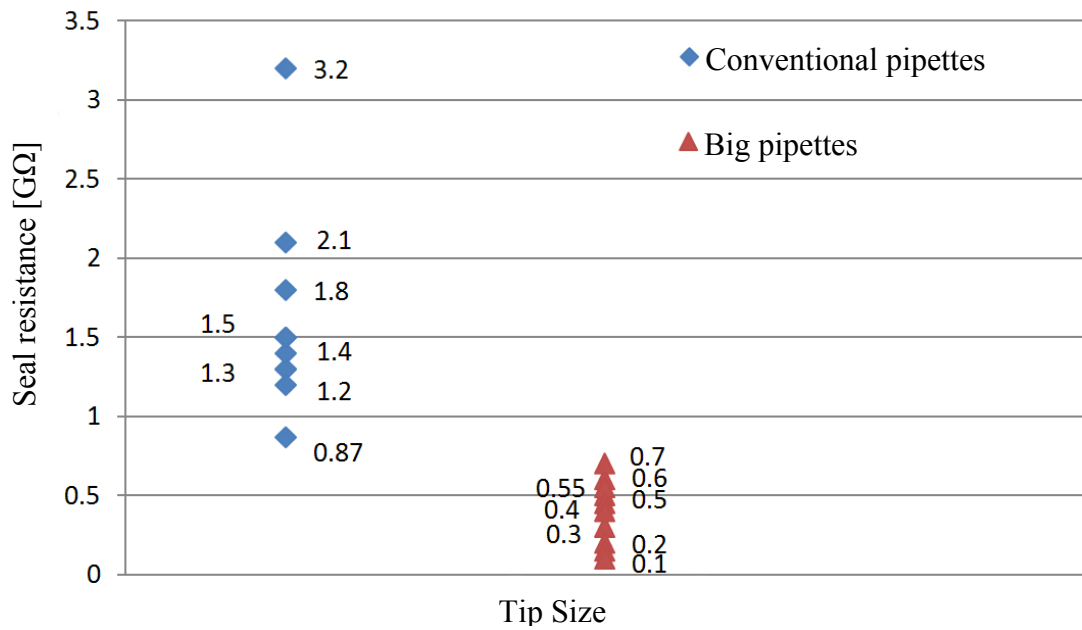


Figure 5.13 Seal values for conventional and big pipettes.

5.6 Discussion

Patch clamping results clearly show that conventional pipettes ($D_t = 1.1 \mu\text{m}$) make better seals. The average seal value is $1.6 \text{ G}\Omega$ for conventional pipettes with standard deviation of $0.6 \text{ G}\Omega$ and is significantly higher than the average seal value of $0.4 \text{ G}\Omega$ for big pipettes with diameter of $3.5 \mu\text{m}$. This can be explained by comparing the roughness parameters of pipettes with different size openings. Tables 5.2 and 5.5 show the surface roughness parameters for pipettes with different tip sizes. The fact that both of the pipette tips and pipette inner walls are rough may help better understanding of the mechanism of gigaseal formation. Bigger pipettes (pipettes A and C) have higher average surface roughness (S_a), higher maximum peak to valley distance and lower developed interfacial ratio (S_{dr}). From Chapter 3, it is known that maximum peak to valley distance determines the height of the channel connecting the inside of the pipette to the outside. Higher maximum peak to valley distances for pipettes A and C show that the inside of pipettes is connected to

the outside by bigger channels facilitating the leakage of ions. The developed interfacial area ratio (S_{dr}) also changes significantly for pipettes having different sizes. S_{dr} is expressed as the percentage of additional surface area contributed by the texture as compared to an ideal plane (94). Higher S_{dr} means that the surface is closer to a flat surface. It has been shown that higher S_{dr} promotes cell adhesion significantly (95) by allowing the membrane to get closer to the glass surface. As a result more bonds can be made between cell surface and glass wall. The fact that pipettes B and D have notably higher S_{dr} at the tip and at the pipette inner wall surface means that a higher percentage of the pipette surface contributes in glass-membrane interactions. This increases the number of membrane proteins sticking to the pipette inner wall and improves the seal. Table 5.3 and 5.6 show that valley void volume (V_{vv}) is considerably high for pipettes A and C (bigger pipettes). This indicates that these pipettes have more fluid retention ability. The ratio of V_{vc}/V_{mc} is also larger for them, which means that there are more voids present compared to pipettes B and D (smaller pipettes). During patch clamp experiments valleys and voids are filled with conductive media facilitating ion escape, increasing the leakage current and compromising the seal. The results suggest that as long as the membrane and pipette surface are close enough, the length of the contact is in the second order of importance. Equation (5.2) shows that although it is more difficult for the membrane to go to the smaller pipettes yet it forms a higher seal with them. This is in good agreement with the practical knowledge in patch clamping that the smaller pipette makes a better seal.

5.7 Summary

In this chapter the effect of tip size on gigaseal formation has been studied. The relationship between pipette resistance and tip size and its influence on gigaseal formation is discussed. Surface roughness parameters of pipettes with different sizes were measured using a SEM stereoscopic technique. In order to have access to the inner wall of the pipette, the pipettes' heads were split and cut open using focused ion beam milling. It is found that the bigger pipettes have higher average surface roughness, higher maximum peak to valley distance, higher valley void volume and lower developed interfacial area ratio. These findings explain the higher leakage current and lower seal resistance in the case of bigger pipettes. The results are in good agreement with the practical knowledge in patch clamping that the smaller pipette makes a better seal.

CHAPTER 6: STUDY OF GLASS MICROPIPETTES FROM TIP FORMATION TO CHARACTERIZATION

6.1 Introduction

In chapter 6 various aspects of glass micropipettes including characterization, mechanisms of tip formation, tip geometry etc are studied. The study is intended both to explain some sources of leakage in patch clamping and to provide useful information for fabricating pipettes with favoured properties. The study may also lead to better understanding of the tip formation mechanisms. The research involves mass fabrication of micropipettes. In section 6.2, the inside and outside walls' surface parameters of glass tubes before pulling, were measured, using laser interferometry. This may be the first step in recognizing the sources of micropipettes' surface roughness. In Chapters 3 and 5 of this thesis, it was shown that tip size and surface roughness have an important effect on gigaseal formation. In section 6.3 the effect of pulling parameters (heat, velocity, pull, time and pressure) on tip size and surface roughness has been studied, which can provide guidelines for fabrication of pipettes with the optimal tip size and surface properties. Section 6.4 discusses the effect of pulling direction on surface properties of pipettes. In section 6.5 the roundness of the pipette along its contact area with the cell is measured using FIB nanotomography. These studies were to lead to new findings about the mechanism of micropipette tip formation (section 6.6). The results explain sources

of leakage in seal formation, but are not limited to patch clamping and can be useful in various applications of glass micropipettes, where surface properties and tip sizes are important.

6.2 Measuring Surface Properties of Glass Tubes

Glass micropipettes are fabricated by the heating and pulling of commercially available glass tubes. Measuring the surface properties of glass tubes from which pipettes are made, may provide information about the sources causing roughness after a pipette has been pulled. Surface properties of glass tubes (BF150-86-10, Sutter Instruments) were measured using light interferometers. White light interferometers allow the rapid acquisition of three-dimensional topographical information in order to create accurate maps of surface architectures. The shape and phase of interferometric fringes created by the optical path differences caused by the sample surface features, when compared to a reference mirror, allows the measurement of topographic information as the sample is scanned vertically relative to the instrument lens. Interferometric measurements of micropipettes were performed using a MicroXAM2 interferometer (Omniscan, UK), operating using a white light source. Pipettes were imaged at a magnification of 100X. Scanning Probe Image Processor software (Image Metrology, Denmark) was employed for the analysis of the acquired images and obtaining surface roughness parameters. Figure 6.1 a-c shows the images of the outer wall of the pipette. Table 6.1 and 6.2 show roughness parameters of the outer and inner wall of glass tubes.

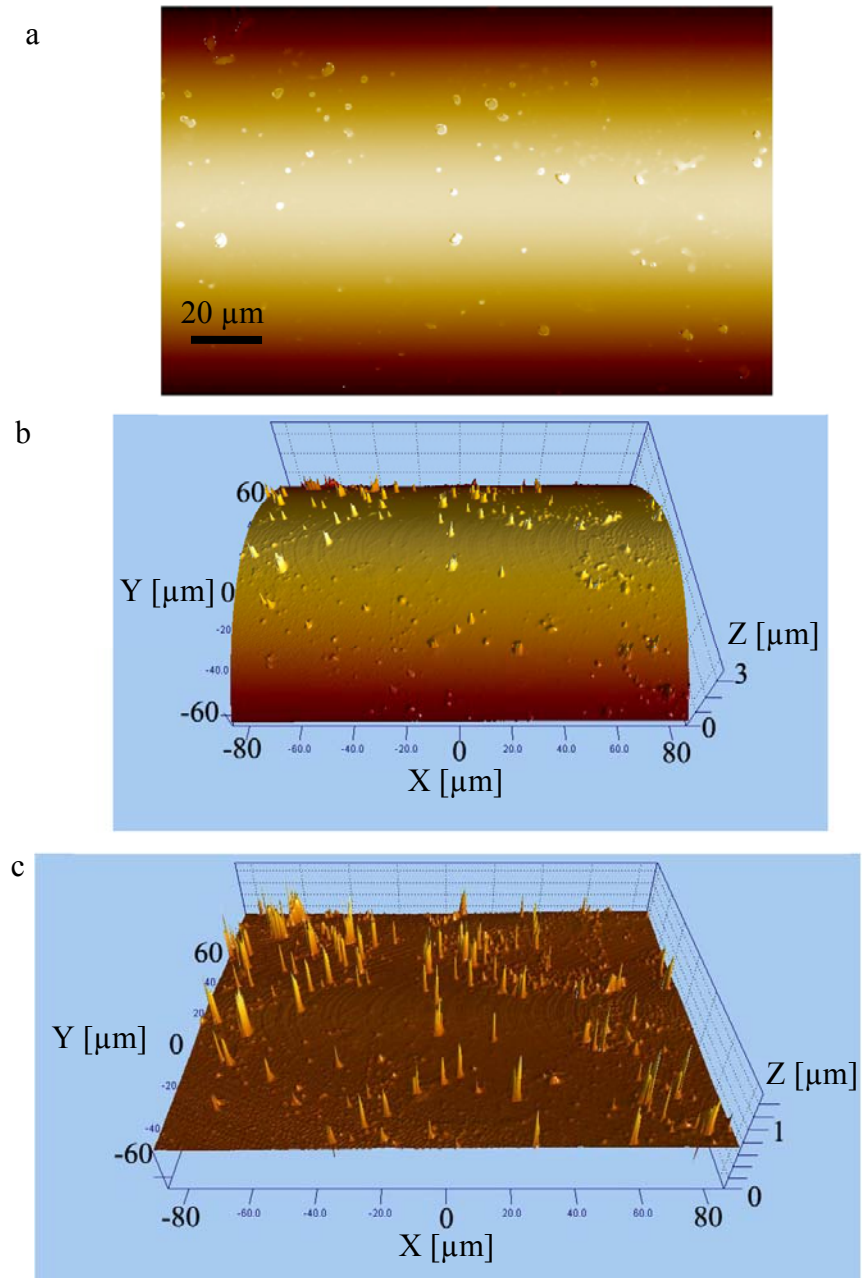


Figure 6.1 Measurement of surface properties of glass tubes using light interferometry (a,b) 2D and 3D representation of topology of pipette outer wall respectively, (c) representation of the pipette surface defects.

Table 6.1 Roughness parameters of the outer wall of glass tubes used in fabrication of glass micropipettes.

Name	Value	Unit	Description
S_a	0.0197	μm	Average surface height of selected area
S_q	0.0431	μm	Root-mean-square height of selected area
S_{sk}	6.66		Skewness of selected area
S_{ku}	70.4		Kurtosis of selected area
S_y	1.54	μm	Largest peak to valley height
S_z	1.26	μm	Ten point height
S_{ds}	0.403	$1/\mu\text{m}^2$	Density of summits - number of summits of a unit sampling area
S_{sc}	0.0141	$1/\mu\text{m}$	Arithmetic mean summit curvature of the surface- average of the principal curvatures of the summits within the sampling area
S_{max}	1.54	μm	Maximum height of selected area
S_{2A}	22071	μm^2	Projected area
S_{3A}	22163	μm^2	Actual surface area

Table 6.2 Roughness parameters of the inner wall of glass tubes used in fabrication of glass micropipettes.

Name	Value	Unit	Description
S_a	0.0188	μm	Average surface height of selected area
S_q	0.0294	μm	Root-Mean-Square height of selected area
S_{sk}	11.9		Skewness of selected area
S_{ku}	575		Kurtosis of selected area
S_y	2.80	μm	Largest peak to valley height
S_z	1.54	μm	Ten point height
S_{ds}	0.549	$1/\mu\text{m}^2$	Density of summits - number of summits of a unit sampling area
S_{sc}	0.0049	$1/\mu\text{m}$	Arithmetic mean summit curvature of the surface- average of the principal curvatures of the summits within the sampling area
S_{max}	2.80	μm	Maximum height of selected area
S_{2A}	22075	μm^2	Projected area
S_{3A}	22100	μm^2	Actual surface area

These measurements clearly show that both of the outer and inner surfaces of glass tubes are rough before pulling. The roughness could come from the manufacturing process of the glass tubes.

6.3 Effect of Pulling Parameters on Pipette Tip Size and Surface Properties

The effect of pipette tip roughness and size on gigaseal formation has been studied in Chapters 3 and 5 respectively. Here the effect of pulling parameters on these factors has been studied. The study provides means for controlling the size and roughness of micropipette tips which in addition to facilitating seal formation, can also be useful in many other applications. Glass micropipettes have been frequently used in applications such as: controlled delivery of liquids, genes or sperm to the target (96; 97; 98), fertilization studies (62), intracellular measurements (99), voltage and current clamp studies (1) (100). Recent development in micro engineering and nanosciences has also found new applications of micro/nanopipettes, such as generating micro droplets (100), single-molecule fluorescence tracking (96), creating nanoscale features by nanolithography and nanowriting methods (101), and nanosensing in scanning probe microscopy (102). In many of these applications a smooth tip is preferred because it reduces the chance of tip contamination and damage to delicate biological samples (62). Dozens of pipettes may be used by an individual in a single day. A small improvement in the conditions of the pipette may have great influence on the outcome. Despite their wide applications, there have been no reports about numerical analysis on the effect of pulling parameters on surface roughness properties of glass micropipettes.

6.3.1 Pulling Pipettes

The puller used in the experiments was Flaming/Brown micropipette puller (Model P-97, Sutter Instruments, Novato, CA). The six parameters on this machine for controlling the shape and size of micropipettes are heat, pull, velocity, delay, time and pressure. These parameters are briefly introduced here and full details of them can be found in the manufacturer's catalogue (65).

- **HEAT** (Range 0-999): HEAT controls the level of electrical current supplied to the filament. The units of heat are in milliamps. Useful changes in HEAT are 5 units or more to see an effect.
- **VELOCITY** (Range 0-255): The velocity of the glass carriage system is measured as the glass softens and begins to pull apart under a constant load. The velocity transducer is a patented approach (103) and this picks up on the velocity of the puller bars as the glass softens. (104)
- **PULL** (Range 0-255): This parameter controls the force of the hard pull. The units of PULL determine the current to the pull solenoid. Useful changes in PULL strength are 10 units or more to see an effect.
- **DELAY** (Range 0-255): DELAY is a cooling mode which controls the delay time between when the heat turns off and when the hard pull is activated. One unit of DELAY represents 1/2ms.

- TIME (Range 0-255): TIME is a cooling mode and controls the length of time the cooling air is active. One unit of TIME represents 1/2ms.
- PRESSURE (Range 0-999): This control sets the pressure generated by the air compressor during the active cooling phase of the pull cycle. The units of pressure are in psi. Changes of less than 10 units will not be noticeable.

To investigate the effect of each parameter on the pipette's tip surface properties, one parameter was varied whereas the others were held unchanged in every set of experiments. Delay and time are both cooling parameters. Time has a quite narrow working range, whereas delay provides a wider range of control. Therefore the effect of delay is investigated. Table 6.3 shows values of the parameters used in the experiments. Glass micropipettes pulled from borosilicate glass tubes have an outer diameter of 1.5 mm and an inner diameter of 0.86 mm (BF150-86-10, Sutter Instruments). The filament of the puller machine was FB230B (2.0 mm square box filament, 3.0 mm wide, Sutter Instruments). Pulling pipettes continuously will make the chamber warm and gradually decrease the heating time for subsequent pipettes. For this reason the chamber was left for 5 minutes to cool down after pulling every 5 pipettes.

Table 6.3 Pulling parameters values

Experiment	Heat	Velocity	Pull	Delay	Pressure
Effect of Heat	595, 600 605	10	0	1	500
Effect of Velocity	606	4, 8, 10, 12, 14	0	1	500
Effect of Pull	606	10	0, 10, 30	1	500
Effect of Delay	606	10	0	1, 20, 40	500
Effect of Pressure	606	10	0	1	300, 350, 400, 450

To test the reproducibility of the puller, 10 pipettes were pulled with a set of parameters and their tip sizes were measured by Scanning Electron Microscopy (SEM). Figure 6.2 is a summary of the statistics of the experiments. A few sudden variations in tip sizes are due mainly to the non homogeneities in the composition and molecular structure of borosilicate glass (99). In the experiments, pipettes with irregular sizes far from the expected value, were not used for reconstruction.

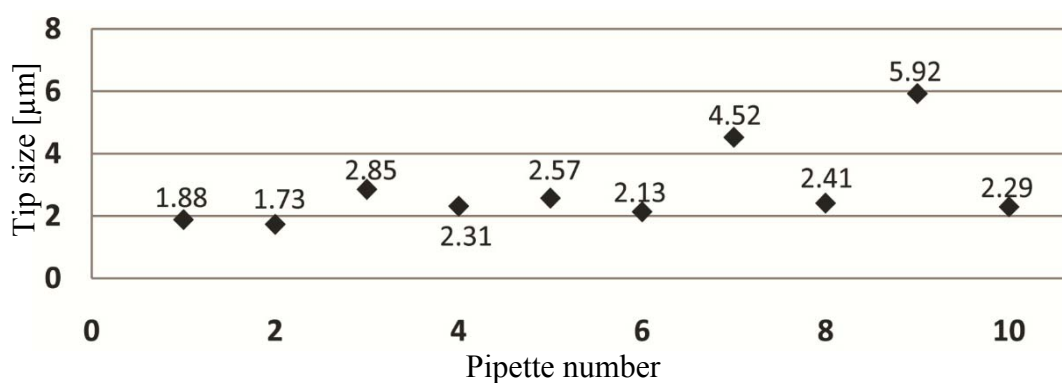


Figure 6.2 Pipette pulling experiment records. 10 pipettes were pulled with the same pulling parameters and their tip sizes were measured using SEM.

6.3.2 3D Reconstruction of Pipette Tips

To determine the three dimensional structure of pipette tips, the SEM stereoscopic technique was used in the investigation. Over 20 pipettes have been reconstructed. To capture high quality SEM images which satisfy stereoscopic technique requirements, glass micropipettes were coated with a thin layer of platinum (<5 nm). The SEM machine used for 3D reconstruction was “Quanta 3D FEG” (FEI, Hillsboro, Oregon). The important factors in the SEM stereoscopic technique are magnification, tilting angle and resolution. Since the maximum pixel resolution of

the machine is limited, different magnifications and tilting angles have been used to reconstruct every pipette's tip with maximum disparity and highest lateral and vertical resolution. Such a reconstruction could be expected to have the inaccuracy of less than 5% (71). Table 6.4 gives the values of tip diameter, tilting angle, magnification, lateral resolution and vertical resolution for 3 different sized reconstructed pipettes. Surface properties of the biggest and smallest pipette are shown in Table 6.5. Figure 6.3 shows the SEM stereo images and digital elevation model of the biggest one.

Table 6.4 Reconstruction information for 3 pipettes

Pipette number	Tip Diameter (μm)	Tilting Angle (left to right)	Magnification	Lateral Resolution	Vertical Resolution
1	34.5	10	5000	29 nm	41 nm
2	19.3	10	8000	18.1 nm	19.7 nm
3	3.7	10	50000	5.8 nm	8.2 nm

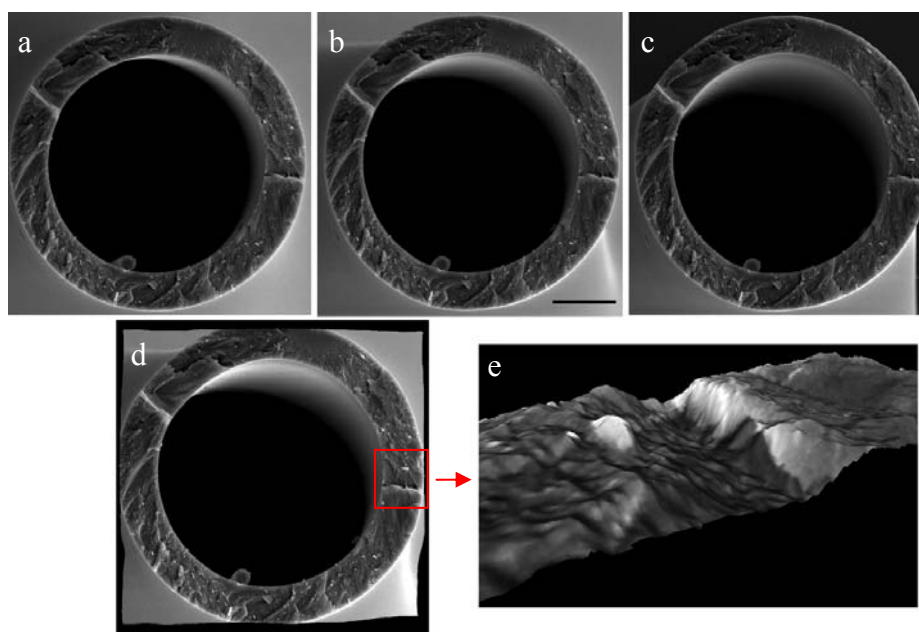


Figure 6.3 SEM stereoscopic images captured from different angles: -5 degrees (a), 0 degree (b) and 5 degrees (c), Digital elevation model created using MeX (d). The exploded view of the selected area. The bar represents 10 μm .

Table 6.5 The surface properties of the biggest and smallest pipettes presented in Table 6.4.

Name	Value ($D_t = 34.5 \mu\text{m}$)	Value ($D_t = 3.7 \mu\text{m}$)	Description
S_a	149.1 nm	30.8 nm	Average height of selected area
S_q	209.9 nm	42.0 nm	Root-mean-square height of selected area
S_p	1437.4 nm	304.1 nm	Maximum peak height of selected area
S_v	1409.3 nm	238.0 nm	Maximum valley depth of selected area
S_z	2846.7 nm	542.1 nm	Maximum height of selected area
S_{10z}	2304.3 nm	414.59 nm	Ten point height of selected area
S_{sk}	-0.2118	-0.514	Skewness of selected area
S_{ku}	7.0253	6.4208	Kurtosis of selected area
S_{dq}	0.5767	1.3246	Root mean square gradient
S_{dr}	13.129%	79.532%	Developed interfacial area ratio

6.3.3 Effect of Pulling Parameters of Pipette Surface Properties

The effect of each parameter is studied by investigating at least 3 reconstructions. Tip diameter (D_t) and average surface roughness (S_a) of all pipettes have been measured. Figures 6.4 to 6.8 show correlations between pulling parameters and D_t and S_a .

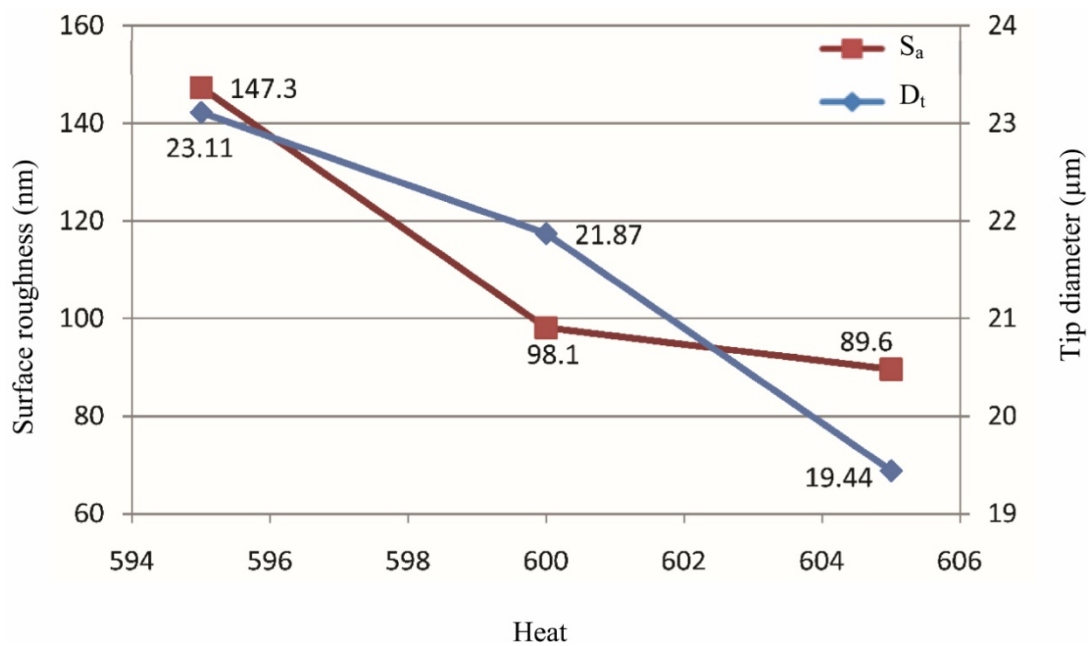


Figure 6.4 The effect of heat on tip diameter and average surface roughness. The heat is controlled by the level of electrical current supplied to the filament. The unit of heat is milliamp. Useful changes in heat are 5 units or more to see an effect. By increasing the heat, both S_a and D_t decreases.

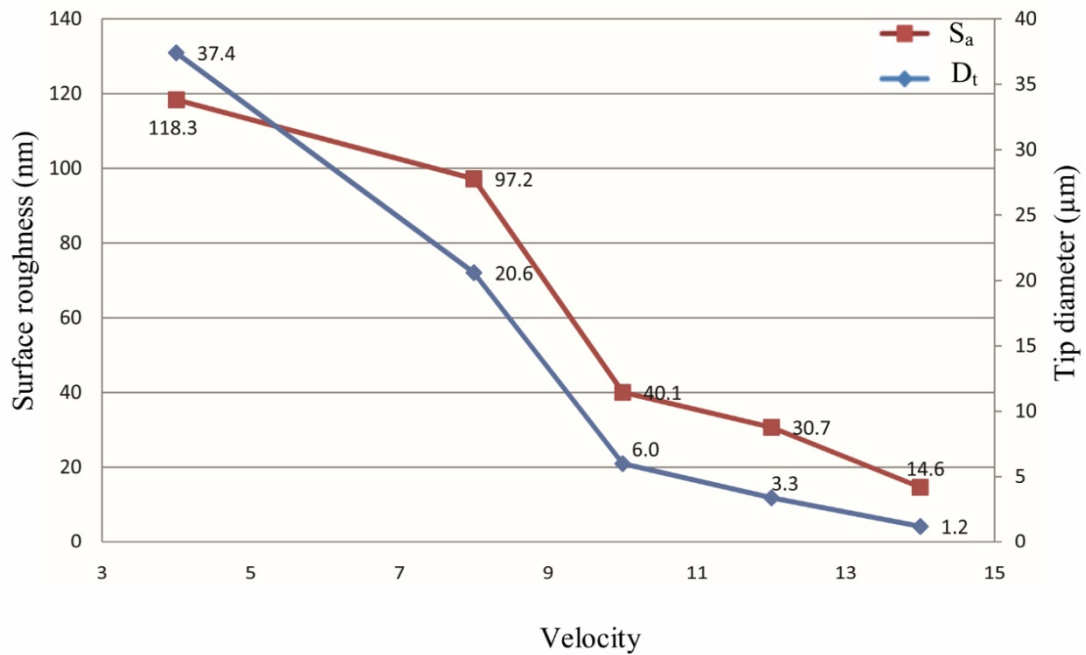


Figure 6.5 The effect of velocity on tip diameter and average surface roughness. This control measures the velocity of the glass carriage system as the glass softens. By increasing the velocity, both the tip size and the surface roughness decrease. The velocity has the most significant effect on the tip size and the surface roughness. A small change in velocity value decreases S_a and D_t rapidly.

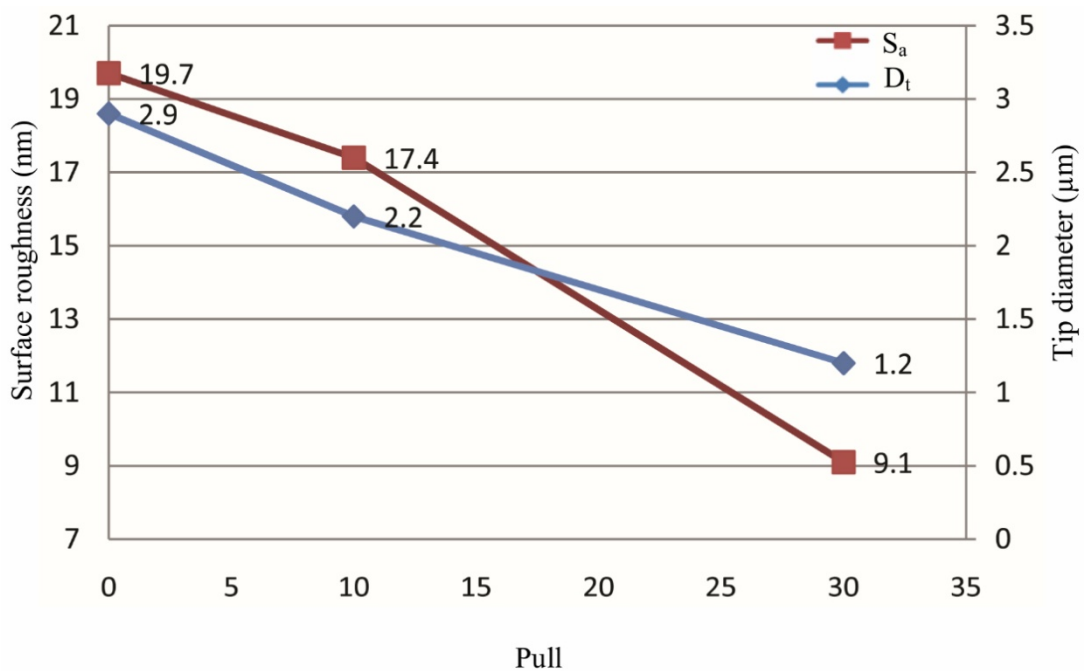


Figure 6.6 The effect of the pull on tip diameter and average surface roughness. This parameter controls the force of the hard pull. The amount of the pull determines the current to the pull solenoid. Useful changes in pull strength are 10 units or more to see an effect. By increasing the pull, both of the S_a and D_t decreases.

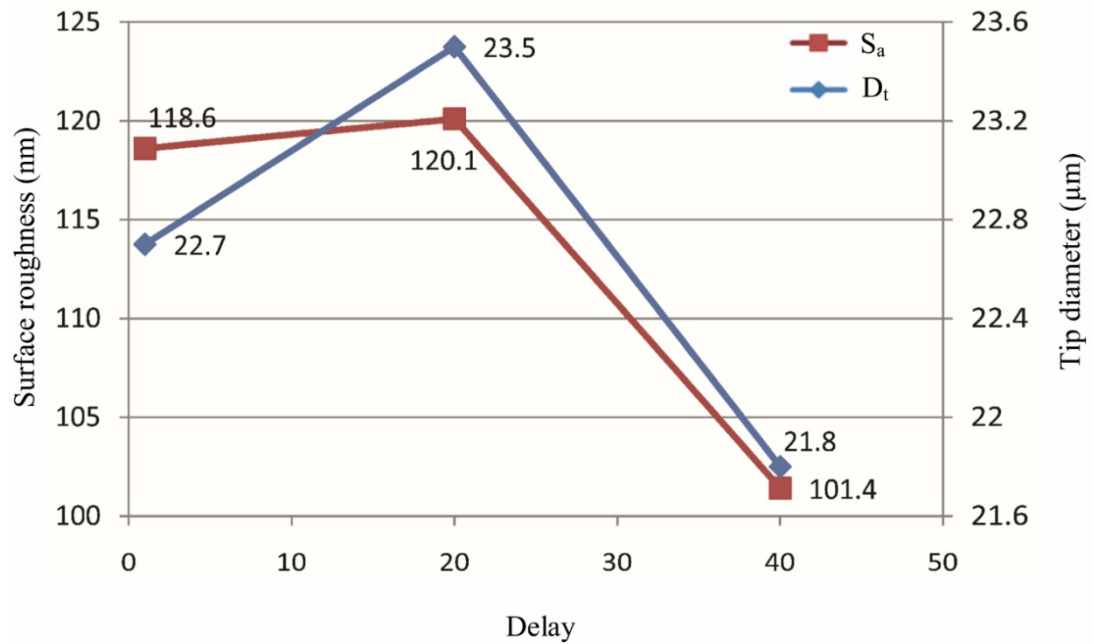


Figure 6.7 The effect of delay on tip diameter and average surface roughness. Delay is a cooling mode which controls the delay time between the time when the heat turns off and the time when the hard pull is activated. One unit of delay represents 1/2 ms. Delay is an effective means of controlling the pipette shank length which does not change the size of pipette tip notably.

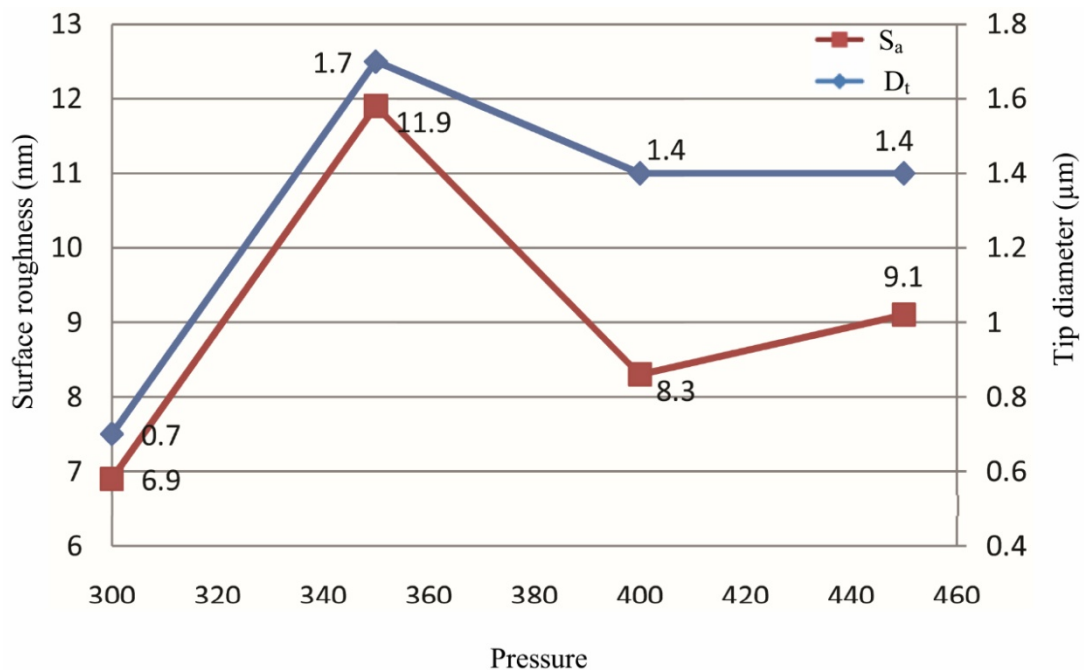


Figure 6.8 The effect of pressure on tip diameter and average surface roughness. This control sets the pressure generated by the air compressor during the active cooling phase of the pull cycle. The unit of pressure is psi. Changes of less than 10 units will not be noticeable. Pressure is another way of controlling the pipette shank length and does not change the size of pipette tip significantly.

As can be seen from figures 6.4 to 6.8 velocity has the most significant effect. A small increase in velocity significantly decreases D_t and S_a . The effects of pull and heat are very similar and not as significant as the effect of velocity. Delay and pressure are factors to change the shank length of the pipettes while keeping the tip size unchanged (65). Increasing delay and pressure will result in a shorter shank. Although these two factors do not change tip diameter significantly, it can be seen from figures 6.7 and 6.8 that the bigger pipette has a higher surface roughness. From figures 6.4 to 6.8 it can be understood that D_t and S_a have direct correlation. Figure 6.9 is obtained by plotting D_t versus S_a for 21 pipettes pulled with different pulling parameters. It can be seen that that average surface roughness of a pipette is strongly related to tip size. D_t and S_a have direct correlation i.e., by increasing the tip size, surface roughness also increases. This result is consistent with the results of Chapter 5 which states smaller pipettes form a better seal and lower leakage current.

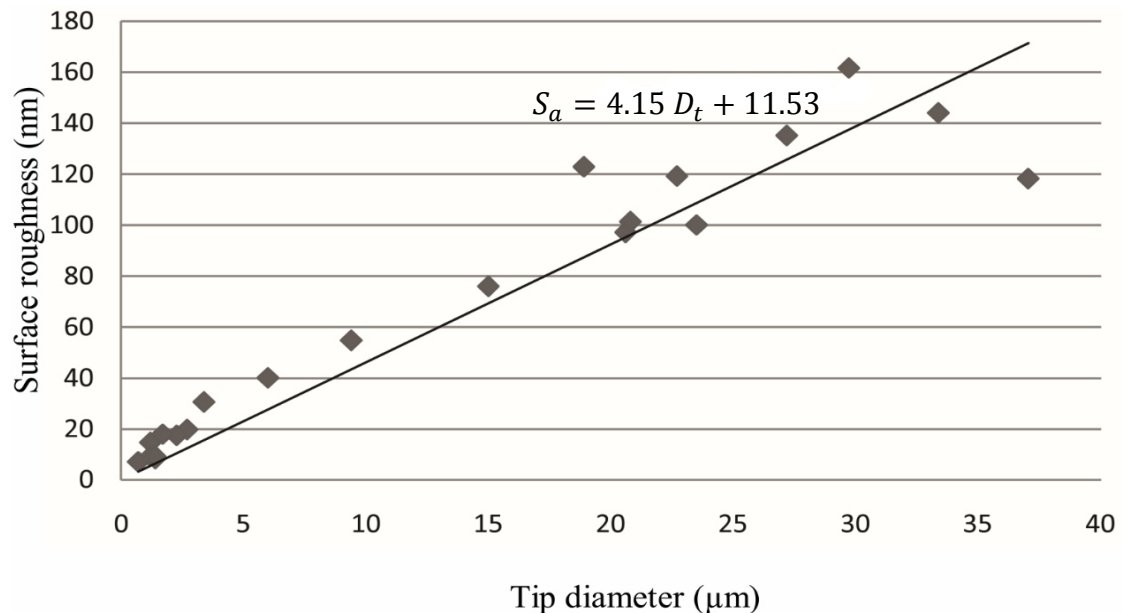


Figure 6.9 Average surface roughness of pipette tip (S_a) versus tip diameter (D_t). S_a is strongly dependent on D_t and has a direct correlation with it. A first degree polynomial equation fitted to data suggests that S_a can be estimated knowing the tip diameter of a given pipette with good approximation.

6.4 Effect of Pulling Direction on Pipette Surface Properties

It has been believed that pulling pipettes with a heating and pulling process results in a smooth surface (21). The surface properties of pipettes' inner walls were reported in section 5.4.2 and the effects of pulling parameters are discussed in the previous section. Here in order to determine the effect of pulling direction on the surface texture of a pipette inner wall, autocorrelation of a roughness model for the pipette inner surface is obtained. If the pulling direction is found to be effective on the surface properties then it can be used as a tool for controlling the surface properties. Figures 6.10 and 6.11 show the pipette inner wall and its autocorrelation roughness model.

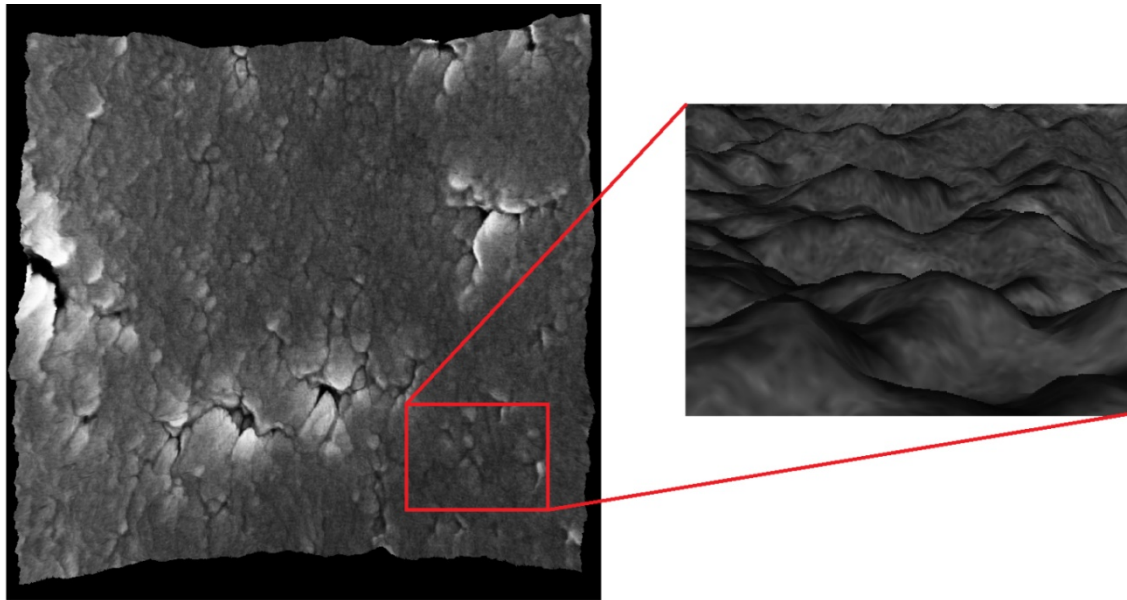


Figure 6.10 Digital elevation model of the inner wall surface of the pipette shown in figure 5.11. As is shown in the inset the surface doesn't have a defined lay and consisted of high frequency components.

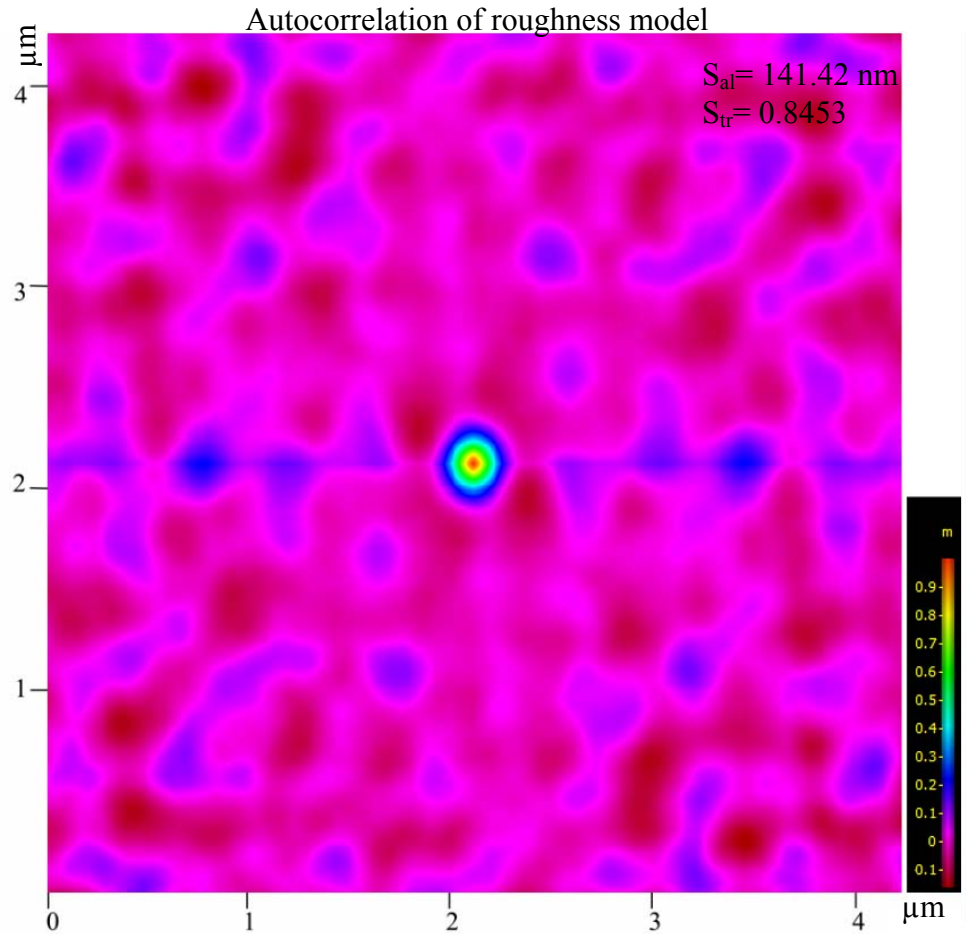


Figure 6.11 Autocorrelation of roughness model of the pipette inner wall. The plot shows that the surface doesn't have any texture orientation. Large value of Texture Aspect Ratio of the Surface (S_{tr}) indicates uniform texture in all directions i.e., no defined lay. Small value of Autocorrelation Length (S_{al}) denotes that the surface is dominated by high frequency components.

The autocorrelation plot suggests that the surface does not have any tendency of orientation and is not affected by pulling direction. This could be because micropipettes are fabricated by a heating and pulling process. Heating makes pipettes soften and no specific orientation could be achieved.

6.5 3D-Reconstruction of a Pipette Using FIB/SEM Nanotomography

As was mentioned in Chapter 2, the geometry of the patching site is an important factor in seal formation. Ideally a smooth round shape is preferred since a patching site with sharp corners and irregular shapes is believed to increase leakage. Micropipettes are produced from glass tubes with a circular cross section and it is assumed that the pipette tip is also circular. However, there has not been any report on the roundness of the pipette tip in the literature. In gigaseal formation the cell membrane has contact with the last one hundred microns of the pipette tip. Reconstruction of this area provides valuable information about the exact geometry of the contact area.

6.5.1 Effect of Omega Dot

A glass fibre is commonly fused along the inner bore of capillary tubing to facilitate the filling of micropipette tips with conducting solutions. This internal fibre is called Omega Dot (99). The omega dot increases the capillary action and facilitates the filling of pipettes by the solution. Figure 6.12 shows the effect of omega dot on the shape of the micropipette tip cross section. Omega dot changes the circular cross section of the pipette to an elliptical shape. The effect is more significant with the omega dot down.

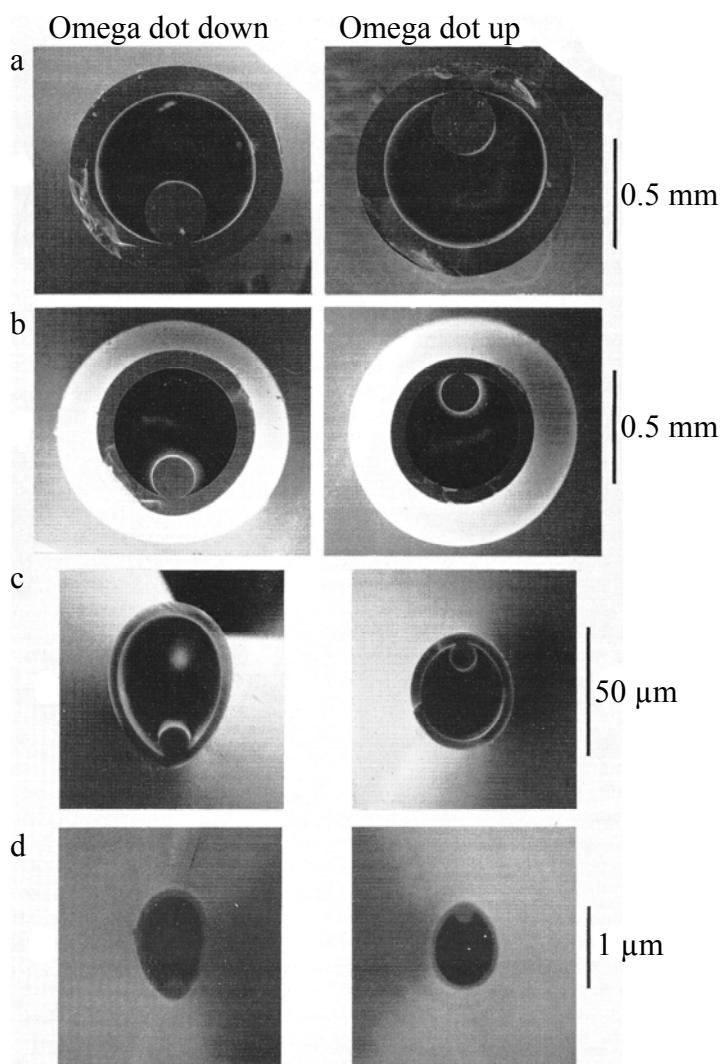


Figure 6.12 Cross-sections of micropipettes formed with omega dot either down toward the filament or upward away from it. The cross sections are shown at four different locations: (a) the capillary tubing prior to pulling, (b) the tubing softened by heat and attenuated only by the weak pull, the strong pull having been inactivated, (c) the broken back end of the tip mounted for SEM observation, and (d) the tip itself (99).

6.5.2 3D Reconstruction of a Pipette

A FEI dual beam Strata 235 focused ion beam (FIB) system was used as a nano tomography tool to obtain the 3D shape of a pipette tip. The process involves a cycle of milling a slice of the pipette using FIB, taking an SEM image of the new

surface, and then milling and imaging again to produce a stack of SEM images. A micropipette with a tip diameter of $1.3\ \mu\text{m}$ was placed facing the electron beam. Figure 6.13a shows the schematic of the pipette, electron beam and ion beam configuration. The angle between I-beam and E-beam was 52° . Therefore, the angle between the imaging plane and the sample was 38° , referring to figure 6.13b. This information was used later for reconstruction. Each slice of the sample was milled off using Ga^+ ion beam at 30 Kv and 100 pA for 90 s and dwell time of $1\ \mu\text{s}$ with overlap parameters of 50%. Sixty slices with a total thickness of $3\ \mu\text{m}$ were removed and SEM images of the slices taken. The pixel size of the SEM images was 4.5 nm. Figure 6.14 shows an image of the 20th slice after milling and its internal edge.

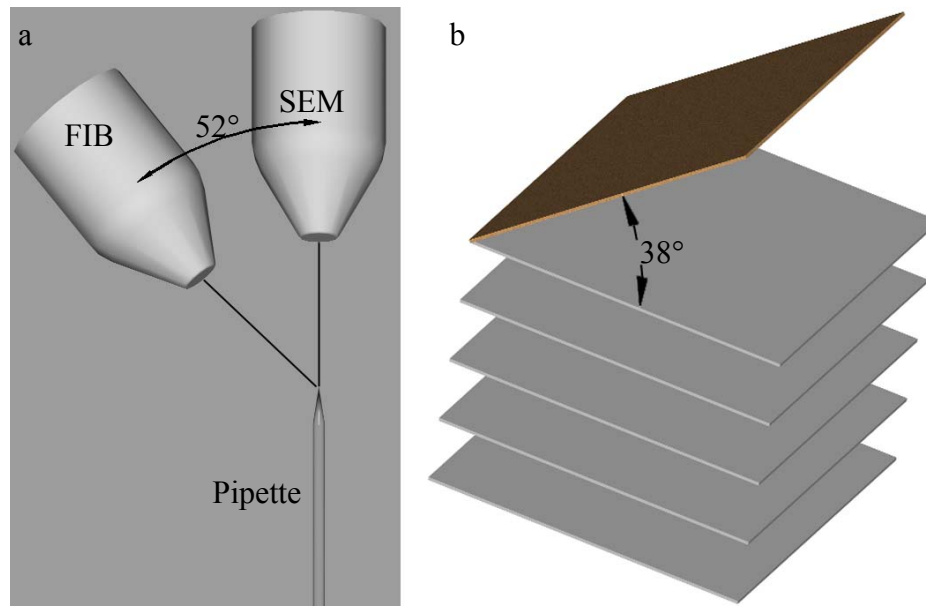


Figure 6.13 FIB nanotomography of a glass micropipette. a) schematic of pipette, E-beam and I-Beam configuration, (b) a schematic of projected plane and the sample slices planes. The brown face shows the projected planes.

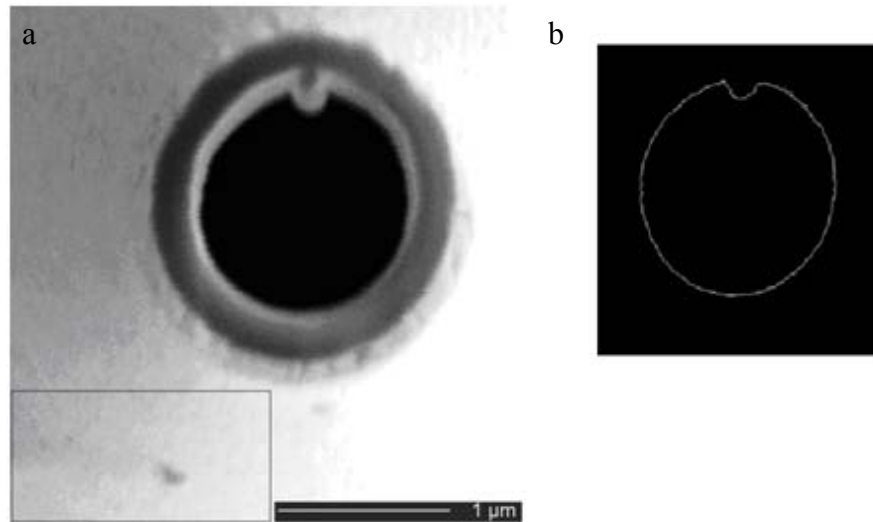


Figure 6.14 Edge detection by using Canny algorithm. a) An SEM image of a pipette after milling, the rectangle represents the area which has not been milled during slicing and not affected by the ion beam, b) detecting the edge of the internal wall of the pipette using Canny algorithm.

In order to be able to 3D reconstruct the tip, the following steps should firstly be carried out:

- Image alignment

A feature based alignment method has been used (105). A fixed feature which has not been milled during slicing and not affected by the ion beam is the bottom left side of the pipette in figure 6.14 which has been used for the alignment of the images.

- Edge detection

The edge of the internal circle of the pipette was detected using Canny algorithm (106).

The basic idea of this algorithm is to detect the zero-crossing of the second derivative of the smoothed images. It seeks out the zero-crossings of:

$$\partial^2(M * I)/\partial n^2 = \partial([\partial M/\partial n] * I)/\partial n$$

Where M and I are image matrix and unit matrix respectively and n is the direction of the gradient of the smoothed image. Edge detection was performed using the image processing tool box of MATLAB software for all of the slices.

- Back projection

As far as the image plane has an angle of 38° with respect to the sample slices (figure 6.13) one can calculate the position of each point of the sample slice. Assuming that x (horizontal) and y (vertical) axes are in the image plane and z is the norm of the surface, then:

$$x_{ssp} = x$$

$$y_{ssp} = y/\cos 38^\circ$$

where indices “ssp” is for the sample slice position. For zssp, the thickness of the slices are 50 nm so the relative distance between the slices remains 50 nm (or 11 pixels) and the initial angle of the image plane and projected plane is 38° .

Figure 6.15 shows the 3D structure of the pipette tip reconstructed using MATLAB. The units of X, Y, Z axes are in pixel and each pixel is 4.5 nm. In order to examine the shape of the pipette tip, a perfect circle was fitted to each slice based on the least squared fitted circle method (107) and maximum deviation of the pipette shape from the circle was obtained. Figure 6.16 shows the first slice image and fitted circle.

The maximum deviation from fitted circle is 43 nm for this slice. The average of maximum deviations of all slices was found to be 67 nm or 10% in roundness error.

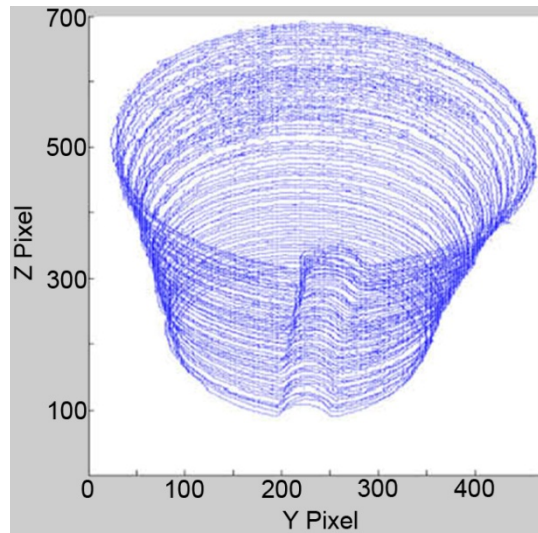


Figure 6.15 A 3D structure of the pipette tip after reconstruction.

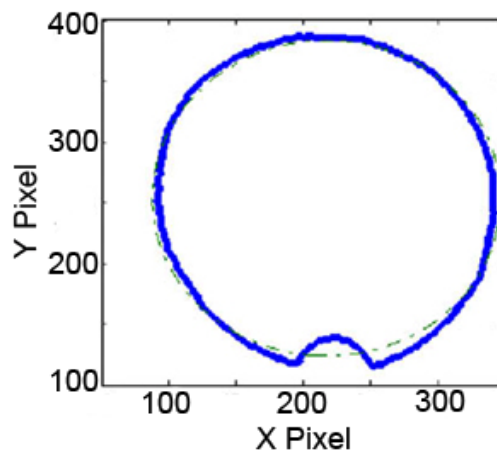


Figure 6.16 An image of the first slice and fitted circle. The fitted circle is shown in dashed line.

6.6 Tip Formation

Studies and observations carried out on the pipette's tip surface and geometry in this thesis have shed some light on the mechanism of tip formation and lead into new hypothesis for tip formation. In the literature two different mechanisms for micropipette tip separation have been discussed. One mechanism considers that tips separate while they are in a fluid phase (99) and another mechanism considers that separation happens in a solid phase by fracture (108). Brown et al have assumed that tip separation most probably happens while glass is in a fluid phase which is partly because of the appearance of micropipette tips under high resolution SEM. The tips are almost always formed at right angles to the long axis of the micropipette, and without major irregularities. This result may be expected if the two tips separate while still in the fluid phase and then harden shortly afterwards. In their model separation occurs when the thickness of the glass wall has become reduced to where it cannot be further attenuated at the prevailing viscosity (99). On the other hand in the model by Purves it is assumed that separation into two pipettes occurs by fracture when the stress exceeds the tensile strength of the glass (108). If the tips are separated by fracture then one could expect inconsistent fracture orientation and irregular or jagged edges. In both models it was assumed that the temperature and hence, viscosity of the glass, do not change during formation of the tips.

High resolution SEM images together with the 3D reconstruction technique have made it possible to precisely examine pipette tips in detail. Figure 6.17 shows SEM images of some big pipettes. Some common factors in all of them are cracks,

inconsistent fracture orientation and irregular or jagged edges. These factors are clearly symbols of fracture in the solid phase. It means that the tip is cooled down after the heat has turned off and fracture happens due to the hard pull of glass.

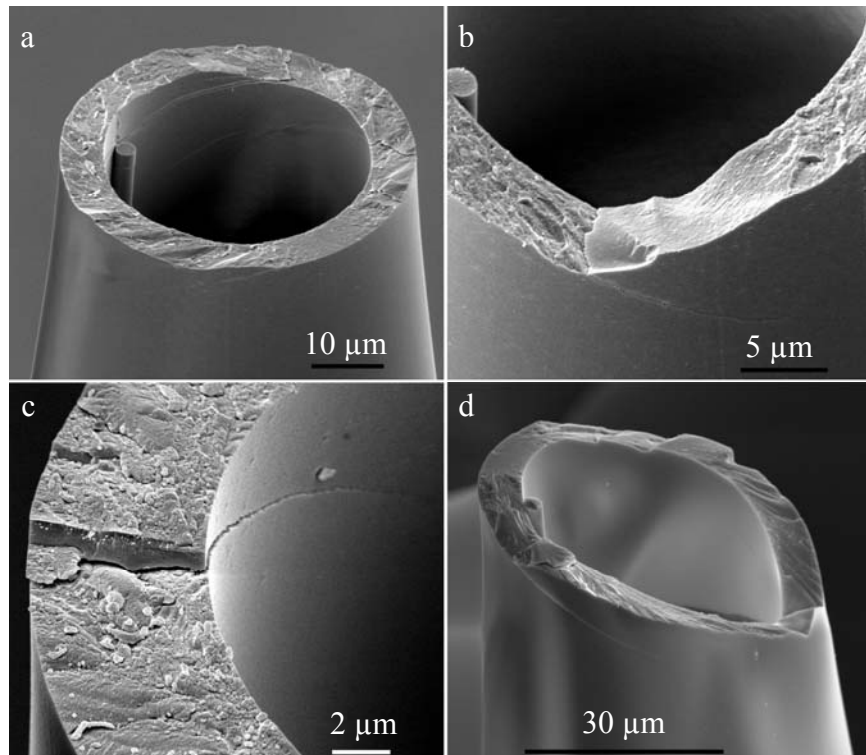


Figure 6.17 SEM images of some big pipettes ($D_t > 20 \mu\text{m}$). Some of the clear features of big size tips are: cracks, irregular, rough tips and inclined orientation of fracture.

Figure 6.18 shows SEM images of some small pipettes. Pipettes have smooth and round tips. There is no sign of cracks. Many pipettes were examined (more than 20) and it was found that similar to the results of Brown et al (99), the tips are almost always formed at right angles to the long axis of the micropipette, and without major irregularities. This suggests that for small pipettes the tips are formed while the glass is still in the fluid phase.

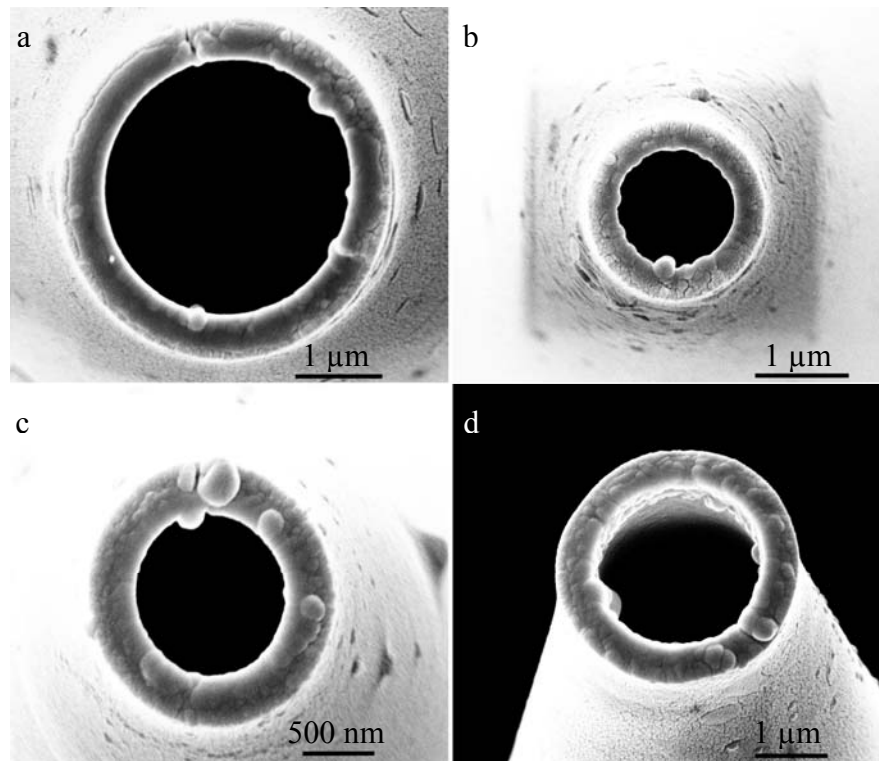


Figure 6.18 SEM images of some small pipettes ($D_t < 2 \mu\text{m}$). Some of the clear features of small size tips are: smooth and flat tips (in contrast with inclined of bigger pipettes) and dome shapes around the tip.

By comparing images of pipettes in figures 6.17 and 6.18 it can be hypothesized that the mechanism of tip formation is dependent on the tip size. For big pipettes (tip size $> 20 \mu\text{m}$) tips are formed by fracture in a solid phase while for small pipettes (tip size $< 2 \mu\text{m}$) the tips are formed while glass is still in a fluid phase.

For further investigation, tips of micropipettes were studied in more detail. If the tips are formed in a fluid phase then tip surface rearrange itself to minimize the free Gibbs energy, therefore tips should have a semispherical shape. This has been schematically shown in figure 6.19. While, if the tips are formed by fracture, then the irregular or jagged profiles are expected across the tip thickness.



Figure 6.19 A schematic of a micropipette tip. If the tip is formed in a fluid phase then the tip should have a semispherical shape.

In order to examine this hypothesis, tips of some big and small pipettes were 3D reconstructed using a SEM stereoscopic technique and profiles across their tip thickness were obtained. Figure 6.20 shows some tip profiles of a small pipette ($D_t = 2.7 \mu\text{m}$). As can be seen, the profiles are relatively smooth curves with a peak in the middle. This result could confirm that the tips are formed in a fluid phase.

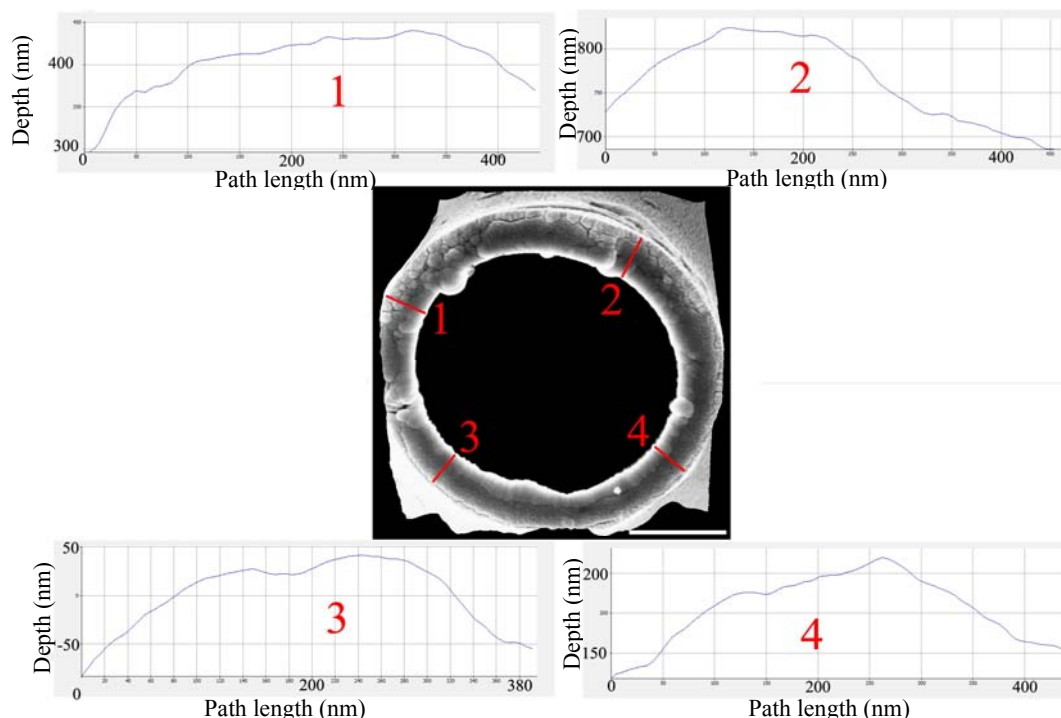


Figure 6.20 Digital elevation model of a small pipette tip ($D_t = 2.7 \mu\text{m}$) and 4 different profiles across the tip thickness. Profiles are relatively smooth curves with a peak in the middle. The bar represents $1 \mu\text{m}$.

Figure 6.21 shows some tip profiles of a big pipette ($D_t = 27.9 \mu\text{m}$). As can be seen, the profiles are irregular and jagged. This confirms the hypothesis that tips of bigger pipettes are formed in a solid phase.

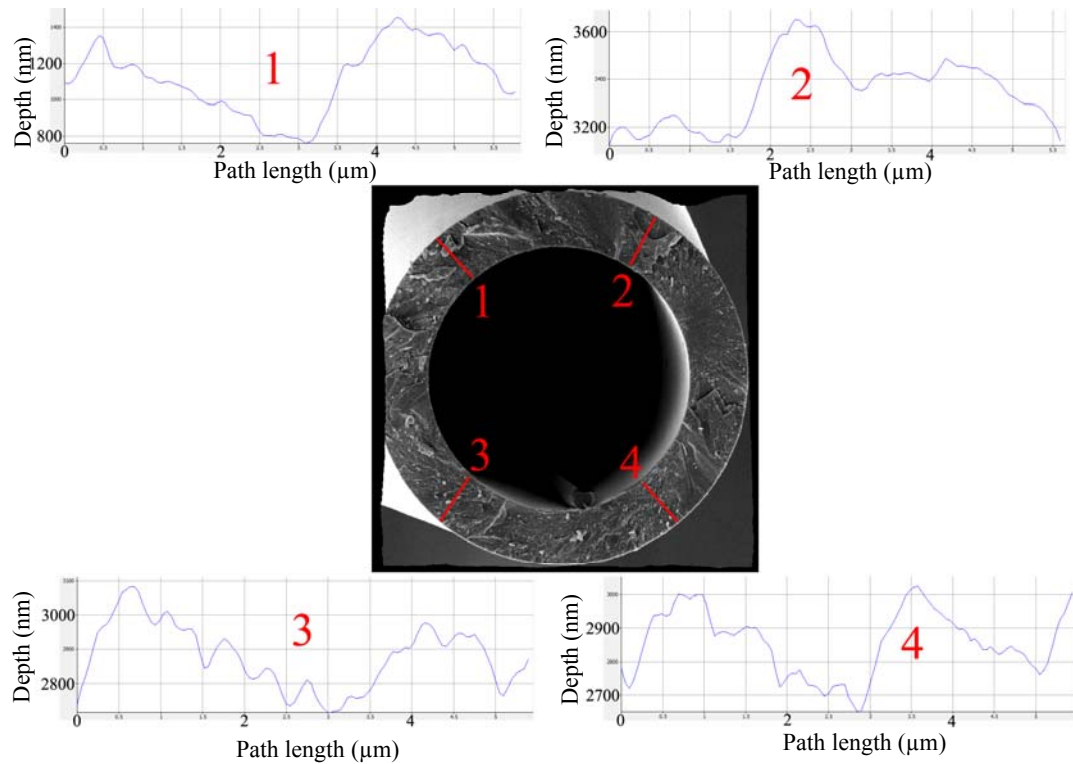


Figure 6.21 Digital elevation model of a big pipette tip ($D_t = 27.9 \mu\text{m}$) and 4 different profiles across the tip thickness. Profiles are irregular and jagged. The bar represents $10 \mu\text{m}$.

The profiles are very close to the semispherical shape for smaller pipettes which confirms the aforementioned hypothesis. The results also are consistent with previous findings and could explain why bigger pipettes have higher surface roughness (see Chapter 5). For the tip sizes between 2 to $20 \mu\text{m}$ both kinds of features were visible at the tip, therefore this range can be considered as the transient range from solid fracture to fluid separation.

6.7 Summary

In Chapter 6 various aspects of glass micropipettes are studied. Inside and outside walls' surface parameters of glass tubes before pulling, measured by laser interferometry, showed that both of these surfaces are rough which could be a result of the fabrication process of glass tubes. Glass micropipettes are fabricated from glass tubes by a heating and pulling process. Heat, velocity, pull, delay and pressure are the controllable parameters of the fabrication process. The effects of these parameters on tip size and surface roughness properties of pipettes were studied. It was found that there is a direct correlation between tip size and surface roughness of the pipette, i.e., by increasing the tip size, surface roughness also increases. Autocorrelation plot of the inner wall surface of a pipette showed that the surface does not have any tendency of orientation and is not affected by pulling direction. Roundness of the pipette in the contact area with a cell was also measured using FIB nanotomography and image processing techniques. It was found that although the original glass tubes are circular in cross section, the tips of micropipettes are not circular and have the average maximum deviations of 67 nm (10% in roundness error) for a micropipette with tip size of 1.3 μm . These studies helped in the better understanding of the mechanism of glass micropipettes' tip formation. The results show that two different mechanisms are involved in glass micropipette tip formation. The mechanisms are dependent on the tip size of the pipettes to be formed. If the parameters are set to produce big pipettes then tips are formed by fracture in a solid phase; while if they are set to produce small size pipettes, then the tips are formed in a liquid phase. The findings and results of this chapter explain sources of leakage in

seal formation and can be useful in various applications of glass micropipettes where surface properties and sizes are important.

CHAPTER 7: CONCLUSION AND FUTURE WORK

7.1 Conclusions

This PhD project is aimed at better understanding the mechanisms of gigaseal formation, and also to enhance seal formation in patch clamping using micro/nanotechnology in terms of both seal resistance and frequency of occurrence. The project furthermore aims to provide techniques which are readily applicable in practice for gigaseal formation improvement. The research has involved 3D reconstruction of tips using the Scanning Electron Microscope (SEM) stereoscopic technique and Focused Ion Beam (FIB) nanotomography; chemical treatment and FIB milling of micropipettes; studying the effect of pulling parameters on pipette surface properties and geometry; studying the mechanism of pipette tip formation; measuring inner and outer walls' surface properties; finite element modelling of patch clamping; conducting many patch clamping experiments and cell culture. The proposed approach uses micro/nano technology to study the influence of important factors such as roughness, hydrophilicity, and pipette tip size on gigaseal formation. Three dimensional reconstruction and nanotomography of glass micropipettes have revealed the details of the surface in contact with the cell membrane. FIB milling, plasma treatments and piranha solution treatment were used to alter the physical and chemical properties of the glass micropipettes. Extensive patch clamping experiments were conducted to investigate the effect of changes on seal resistance.

The significant contributions of the gigaseal formation research can be summarised as follows:

A. 3D Reconstruction of Micropipette Tip.

Tips of glass micropipettes were successfully reconstructed using the SEM stereoscopic technique. FIB nanotomography was also used to reconstruct the region of the pipette which is in contact with the cell membrane. Surface properties were then obtained from the reconstructed models.

B. Focused Ion Beam Polishing of Glass Micropipettes.

For the first time focused ion beam milling has been used as a micropipette's polishing tool. This will result in an ultimately smooth surface at the tips of micropipettes which enhance seal formation significantly.

C. Chemical Treatment of Glass Micropipettes.

A novel approach to alter surface chemistry of glass micropipettes, introduced by controlling etching time in piranha solution and oxygen plasma treatments. The approach makes only the patching site of pipettes highly hydrophilic and protects the rest of the pipette from treatment. Therefore the conductive bath solution will only

creep up from the pipette wall for a small distance which minimizes the pipette capacitance.

D. Study the Effect of Tip Size

The effect of tip size on surface roughness properties of the pipette tip and the pipette inner wall has been investigated. It was found that smaller pipettes have smoother surfaces which result in better sealing conditions.

E. Study the Effect of Pulling Parameters on Glass Micropipettes.

The effect of pulling parameters on the pipette tip surface roughness and geometry was studied. The study shows that there is a direct correlation between the size and surface roughness properties of micropipettes' tips.

F. Study the Mechanism of Pipette Tip Formation.

The mechanism of pipette tip formation is studied by investigating the tip of many pipettes using Scanning Electron Microscopy (SEM) and 3D reconstruction. It was found that the mechanism of tip formation (fracture in the solid phase or separation in the fluid phase) depends on the tip size of the pipettes.

G. Cell Culture and Patch Clamp Experiments.

Human Embryonic Kidney (HEK) cells were cultured on cover slips 2 to 3 days before the experiments. Patch clamp experiments were carried out using conventional and treated pipettes. FIB polished and piranha polished pipettes were able to improve the seal formation significantly in terms of both seal resistance and probability of seal formation.

Through repeated patch clamp experiments and characterization of micropipettes, all the project objectives have been met. The following conclusions can be drawn from the research.

1. Pipette tip roughness was found to be very important in seal formation. FIB polishing of pipettes proved successful in the formation of the high resistance seal required for single ion channel recording.
2. Surface hydrophilicity of patching plays an important role in seal formation. Treating pipettes with piranha solution is readily applicable in laboratories and increases the seal formation probability significantly.
3. Decreasing the tip size of micropipettes improves the seal formation. Tip size of micropipettes can be easily controlled by changing the pulling parameters to obtain pipettes with desired sizes.

4. Inner walls of micropipettes are also rough and surfaces do not have any tendency of orientation and are not affected by pulling direction.
5. Tip cross section is not circular and has the average of maximum deviations of 10% in roundness error.
6. Pulling parameters have influence on surface properties and tip size. Furthermore there is a direct correlation between size and surface roughness of micropipettes tips.
7. Finite Element modelling shows that cell membrane cannot fill cavities of the rough tip, which facilitates ions escape and compromising of the seal.
8. The mechanism of tip formation depends on tip size of the pipette to be formed. Large pipettes are very likely to be formed by fracture in the solid phase while for small pipettes separation happens while glass is still in the liquid phase.

Based on the experimental and analysis work presented in this thesis, FIB polishing and hydrophilic treatments of micropipettes prove to be effective, repeatable and yield high resistance seals. Furthermore, decreasing the tip size and piranha treatment of pipettes, can be easily applied in laboratories. Thus, the project aims

have been successfully met. The methodology and analysis adopted in the research are adequate in leading to the project aims. The treatment and fabrication processes developed in the research are applicable to planar and lateral patch clamping systems to improve the quality as well as throughput of recordings.

7.2 Suggestions for Future Work

This thesis represents a comprehensive research effort performed to explore gigaseal formation in patch clamping. As such, it should be viewed as a solid foundation for further work. Future research is needed, either to apply current findings into high throughput systems, or to complete works initiated in this PhD project which have not been completed because they are well beyond the project scope.

The following is a list of further research topics, which are identified:

1. In the current research, the surfaces of glass micropipettes were studied in detail. Techniques such as FIB nanotomography can be used for reconstruction of the interface between cell membrane and pipette wall. Such reconstruction provides valuable information about the nature of the interactions and how the membrane bonds to the pipette wall.
2. This thesis introduces the use of FIB milling as a polishing tool of glass micropipettes for the first time. FIB can be further used to reshape the tip by

creating a chamfer. This allows further movement of the cell membrane into the pipette and therefore increasing seal resistance.

3. Measuring the forces required for removing the membrane from micropipettes may give some clues about the nature of bonds involved in seal formation.

4. In Chapter 5 it was discussed that S_{dr} of a surface is an important factor in seal formation. Chemical treatments can be used for increasing the S_{dr} of glass micropipettes and therefore improving gigaseal formation.

5. The correct moment of suction application is important in successful seal formation. Better mechanisms for detecting the distance between tip and cell membrane can be helpful in achieving higher resistance seals.

REFERENCES

1. *Single-channel currents recorded from membrane of denervated frog muscle fibres.* **Neher, Erwin and Sakmann, Bert.** 1976, *Nature*, Vol. 260, pp. 799-802.
2. *Whole cell patch clamp recording performed on a planar glass chip.* **Fertig, Niels, Blick, Robert H and Behrends, Jan C.** 2002, *Biophysical Journal*, Vol. 82, pp. 3056–3062.
3. *A novel method for patch-clamp automation.* **Vasilyev, D, et al.** 2006, *European Journal of Physiology*, Vol. 452, pp. 240–247.
4. *A single cell electrophysiological analysis device with embedded electrode.* **Li, Sha and Lin, Liwei.** 2007, *Sensors and Actuators A*, Vol. 134, pp. 20–26.
5. **Molleman, Areles.** *Patch clamping: an introductory guide to patch clamp electrophysiology.* Chichester : John Wiley & Sons Ltd., 2003. 0-471-48685-X.
6. *Improved patch-clamp techniques for high-resolution current recording from cells and cell-free membrane patches.* **Hamill, O P, et al.** 1981, *European Journal of Physiology*, Vol. 391, pp. 85-100.
7. *CHANNELLING DRUG DISCOVERY current trends in ion channel drug discovery research.* **Owen, David and Silverthorne, Andrew.** 2, 2002, *Drug Discovery World*, Vol. 3 , pp. 48-61.

8. *Pharmaceutical Market Research*. s.l. : URCH Publishing, 2010. p. 142. 978-1-905751-06-8.
9. **Guyton, Arthur C and Hall, John E.** *Text book of medical physiology*. s.l. : W.B. Saunders company, 2000. 0-7216-8677-X.
10. Molecular view of the cell membrane. *In Encyclopædia Britannica*. [Online] <http://www.britannica.com/EBchecked/media/45550/A-molecular-view-of-the-cell-membrane-Intrinsic-proteins-penetrate>.
11. *Design and Fabrication of a Micromachined Planar Patch-Clamp Substrate With Integrated Microfluidics for Single-Cell Measurements*. **Matthews, Brian and Judy, Jack W.** 2006, JOURNAL OF MICROELECTROMECHANICAL SYSTEMS, Vol. 15.
12. *ION CHANNELS OF NOCICEPTION*. **McCleskey, Edwin W and Gold, S Michael.** 1999, annual review of physiology, Vol. 61, pp. 835–56.
13. *STRUCTURE AND REGULATION OF VOLTAGE-GATED Ca₂C CHANNELS*. **Catterall, William A.** 2000, Annual Review of Cell and Developmental Biology, Vol. 16, pp. 521–55.
14. *Fabrication of Si-based planar type patch clamp biosensor using silicon on insulator substrate*. **Zhang, Z L, et al.** 2008, Thin Solid Films, Vol. 516, pp. 2813-2815.
15. *Ion channel related diseases*,. **Dworakowska, B and Dolowy, K.** 3, 2000, Acta Biochimica Polonica, Vol. 47, pp. 685–703.

16. *Flux assays in high throughput screening of ion channels in drug discovery.* **Gill, Sikander, et al.** 5, 2003, Assay and drug development technologies, Vol. 1, pp. 709-717.
17. *HTS approaches to voltagegated ion channel drug discovery.* **Denyer, Jane, et al.** 7, 1998, Drug Discovery Today, Vol. 3.
18. *High-Throughput Screening for Ion Channel Modulators.* **FALCONER, MARGARET, et al.** 5, 2002, JOURNAL OF BIOMOLECULAR SCREENING, Vol. 7, pp. 460-465.
19. *Ion-channel assay technologies:quo vadis?* **Xu, Jia, et al.** 24, 2001, Drug discovery today, Vol. 6 , pp. 1278-1287.
20. *The patch clamp technique: Principles and technical considerations.* **Kornreich, Bruce G.** 2007, Journal of Veterinary Cardiology, Vol. 9, pp. 25-37.
21. *Flip the Tip: An Automated, High Quality, Cost-Effective Patch Clamp Screen.* **Lepple-Wienhues, Albrecht, et al.** 2003, Receptors and Channels, Vol. 9, pp. 13–17.
22. *An air-molding technique for fabricating PDMS planar patch-clamp Electrodes.* **Klemic, K, Klemic, J and Sigworth, F.** 2005, European Journal of Physiology, Vol. 449, pp. 564–572.
23. *Flyion ion channel solutions .* [Online] www.flyion.com.
24. *CYTOCENTERING: A novel technique enabling automated cell-by-cell patch clamping with the CYTOPATCH™ chip.* **Stett, A, et al.** 2003, Receptors and Channels, Vol. 9, pp. 59–66.

25. *Batch Fabrication of High-Performance Planar Patch-Clamp Devices in Quartz.*

Nagarah, John M, et al. 2010, *Advanced Material*, Vol. 22, pp. 4622–4627.

26. *Mammalian electrophysiology on a microfluidic platform.* **Ionescu-Zanetti, C,**

et al. 2005, *Proceeding of the national academy of science of the united states of America (PNAS)*, Vol. 102, pp. 9112–9117.

27. *Open-access microfluidic patch-clamp array with raised lateral cell trapping*

sites. **Lau, A Y, et al.** 2006, *Lab on a Chip*, Vol. 6, pp. 1510–1515.

28. *Realization of hollow SiO₂ micronozzles for electrical measurements on living*

cells. **Lehnert, T, et al.** 26, 2002, *APPLIED PHYSICS LETTERS*, Vol. 81, pp. 5063-5065.

29. *A Novel Silicon Patch-Clamp Chip Permits High-Fidelity Recording of Ion*

Channel Activity From Functionally Defined Neurons. **Py, Christophe, et al.** 4, 2010, *Biotechnology and Bioengineering*, Vol. 107, pp. 593–600.

30. *Single-Ion Channel Recordings on Quartz Substrates.* **Stava, Eric, et al.** 4, 2010,

Vol. 9, pp. 307-309.

31. *A chip-based biosensor for the functional analysis of single ion channels.*

Schmidt, C, Mayer, M and Vogel, H. 17, 2000, *Angewandte Chemie International Edition*, Vol. 39, pp. 3137-3140.

32. *Development of Patch-Clamp Chips for Mammalian Cell Applications.*

Martinez, Dolores, et al. 2010, *Micro and Nanosystems*, Vol. 2, pp. 274-279.

33. *A diamond-on-silicon patch-clamp-system.* **Kusterer, J, et al.** 2005, *Diamond &*

Related Materials, Vol. 14, pp. 2139 – 2142.

34. *High throughput ion-channel pharmacology: planar-array-based voltage clamp*. **Kiss, L, et al.** 1-2, 2003, ASSAY and Drug Development Technologies, Vol. 1, pp. 127-135.
35. *Multi-Patch: A chip-based ionchannel assay system for drug screening*. **Picollet-D'hahan, N, et al., [ed.]**. Alberta Canada : s.n., 2003. ICMENS International Conference on MEMS, NANO & Smart Systems. pp. 251 – 254.
36. *SURFACE MODIFICATION OF SiO₂ MICRO-NOZZLES FOR PATCH-CLAMP MEASUREMENTS ON-CHIP*. **Lehnert, T, Laine, A and Gijs, M A M**. California : s.n., 2003. 7th International Conference on Miniaturized Chemical and Blochemical Analysts Systems. pp. 1085-1088.
37. *Buried microfluidic channel for integrated patch-clamping assay*. **Ong, W, et al.** 2006, Applied physics letters, Vol. 89.
38. *A microfluidic model for single-cell capillary obstruction by Plasmodium falciparuminfected erythrocytes*. **Shelby, J Patrick, et al.** 25, 2003, Proceedings of the National Academy of Sciences, Vol. 100, pp. 14618–14622.
39. *Stabilization of High-Resistance Seals in Patch-Clamp Recordings by Laminar Flow*. **Sinclair, Jon, et al.** 2003, Analytical Chemistry, Vol. 75, pp. 6718-6722.
40. *High-fidelity patch-clamp recordings from neurons cultured on a polymer microchip*. **Martinez, Dolores, et al.** 2010, Biomedical Microdevices, Vol. 12, pp. 977–985.
41. *A novel holder allowing internal perfusion of patch-clamp pipettes*. **Lapointe, Jean Yves and Szabo, Gabor.** 1987, European journal of physiology, Vol. 410, pp. 212--216.

42. *A high-performance elastomeric patch clamp chip*. **Chen, Chihchen and Folch, Albert**. 2006, Lab on chip, Vol. 6, pp. 1338–1345.
43. *Applications of Piezo-Actuated Micro-Robots in Micro-Biology and Material Science*. **Breguet, Jean Marc, et al**. 2007. Proceedings of the 2007 IEEE International Conference on Mechatronics and Automation. pp. 57-62.
44. *Development of a novel automated ion channel recording method using "Inside-Out" whole-cell membranes*. **Vasilyev, D, Merrill, T L and Bowlby, M R**. 2005, Journal of Biomolecular Screening, Vol. 10.
45. *Population patch clamp improves data consistency and success rates in the measurement of ionic currents*. **Finkel, A, et al**. 5, 2006, Journal of biomolecular screening, Vol. 11, pp. 488-496.
46. *Automated patch clamping systems design using novel materials*. **Wilsona, S, et al**. Borovets, Bulgaria : s.n., 2007. 4M Annual Conference.
47. **Sakmann, Bert and Neher, Erwin**. *Single-Channel Recording*. Second Edition . s.l. : Springer, 2009. 978-1-4419-1230-5.
48. *The Quartz page*. [Online] www.quartzpage.de.
49. **Lodish, Harvey, et al**. *Molecular Cell Biology*. 6. s.l. : W.H.Freeman & Co Ltd, 2007.
50. *Ionic requirements for membrane-glass adhesion and gigaseal formation in patch-clamp recording*. **Priel, A, et al**. 2007, Biophysical Journal, Vol. 92, pp. 3893–3900.

51. *The Ultrastructure of Patch-clamped Membranes: A Study Using High Voltage Electron Microscopy.* **Ruknudin, A, Song, M J and Sachs, E.** 1, 1991, The Journal of Cell Biology, Vol. 112, pp. 125-134.
52. *Quantitative video microscopy of patch clamped membranes stress, strain, capacitance, and stretch channel activation.* **Sokabe, Masahiro, Sachs, Frederick and Jing, Zhongqi.** 1991, Biophysical journal, Vol. 59, pp. 722-728.
53. *Lipid-Glass Adhesion in Giga-sealed Patch-clamped Membranes.* **Opsahl, Lorinda R and Webb, Watt W.** s.l. : 66, 1994, Biophysical Journal, pp. 75-79.
54. *The structure and dynamics of patch-clamped membranes: a study using differential interference contrast light microscopy.* **Sokabe, M and Sachs, E.** 1990, The Journal of Cell Biology, Vol. 111, pp. 599-606.
55. *How do patch clamp seals form? A lipid bleb model.* **Milton, R L and Caldwell, J H.** 1990, European journal of philosophy, Vol. 416, pp. 758-765.
56. *The Breakdown of Cell Membranes by Electrical and Mechanical Stress.* **Akinlaja, Johannes and Sachs, Frederick.** 1998, Biophysical Journal, Vol. 75, pp. 247-254.
57. *Biophysics and Structure of the Patch and the Gigaseal.* **Suchyna, Thomas M, Markin, Vladislav S and Sachs, Frederick.** 2009, Biophysical Journal, Vol. 97, pp. 738-747.
58. *A Micromechanic Study of Cell Polarity and Plasma Membrane Cell Body Coupling in Dictyostelium.* **Merkel, Rudolf, et al.** 2000, Biophysical Journal, Vol. 79, pp. 707-719.

59. *Gadolinium Effects on Gigaseal Formation and the Adhesive Properties of a Fungal Amoeboid Cell, the Slime Mutant of Neurospora crassa.* **Barkovskaya, Dunina A Y, et al.** 2004, Membrane Biology, Vol. 198, pp. 77–87.
60. *A missing factor in chip-based patch clamp assay: gigaseal.* **Ong, W L, Yobas, L and Ong, W Y.** 2006, Journal of Physics, Vol. 34, pp. 187–191.
61. *Pressure polishing: a method for re-shaping patch pipettes during fire polishing.* **Goodman, M and Lockery, S R.** 2000, Journal of Neuroscience Methods, Vol. 100, pp. 13-15.
62. *Evaluating the process of polishing borosilicate glass capillaries used for fabrication of in-vitro fertilization (iVF) micro-pipettes.* **Yaul, M, Bhatti, R and Lawrence, S.** 2008, Biomed Microdevices, Vol. 10, pp. 123–128.
63. *Flexoelectricity of model and living membranes.* **Petrov, Alexander G.** 2001, Biochimica et Biophysica Acta, Vol. 1561, pp. 1-25.
64. *Electricity and mechanics of biomembrane systems: Flexoelectricity in living membranes.* **Petrov, Alexander G.** 2006, Analytica Chimica Acta, Vol. 568, pp. 70–83.
65. *Sutter instrument company.* [Online] www.sutter.com.
66. [Online] Sutter Instruments. www.sutter.com.
67. MeX catalouge. Graz, Austria : Alicona Imaging GmbH.
68. *Photogrammetry with the scanning electron microscope.* **Piazzesi, G.** 1973, Journal of Physics E: Scientific Instruments, Vol. 6, pp. 392–396.

69. *Investigation on the traceability of three dimensional scanning electron microscope measurements based on the stereo-pair technique.* **Bariani, P, et al.** 2005, Precision Engineering, Vol. 29, pp. 219–228.
70. *3D Reconstruction and Visualization of Microstructure Surfaces from 2D Images.* **Samak, D, Fischer, A and Rittel, D.** 1, 2007, Journal of Manufacturing Technology, Vol. 56, pp. 149-152.
71. *Critical factors in SEM 3D stereomicroscopy.* **Marinello, F, et al.** s.l. : 19, 2008, Measurement Science and Technology, pp. 1-12.
72. *MeXTM software.* Graz, Austria : Alicona Imaging GmbH.
73. *Estimating the Sensitivity of Mechanosensitive Ion Channels to Membrane Strain and Tension.* **Charras, Guillaume T, et al.** 2004, Biophysical Journal, Vol. 87, pp. 2870–2884.
74. *Numerical Simulation of Nanoindentation and Patch Clamp Experiments on Mechanosensitive Channels of Large Conductance in Escherichia coli.* **Tang, Y, et al.** 2009, Experimental Mechanics, Vol. 49, pp. 35–46.
75. *Finite element analysis of microelectrotension of cell membranes, Biomechanics and Modelling in Mechanobiology.* **Bae, Chilman and Butler, Peter J.** 2008, Vol. 7, pp. 379–386.
76. ABAQUS. *ABAQUS 6.4 user's manual.* Providence, RI. : ABAQUS Inc, 2004.
77. *Large Deformation Finite Element Analysis of Micropipette Aspiration to Determine the Mechanical Properties of the Chondrocyte.* **BAAIJENS, V P T, et al.** 4, 2005, Annals of Biomedical Engineering, Vol. 33, pp. 494-501.

78. *Contribution of the nucleus to the mechanical properties of endothelial cells.*

Caille, Nathalie, et al. 2002, Journal of Biomechanics, Vol. 35, pp. 177-187.

79. *Finite Element Simulation of the Micropipette Aspiration of a Living Cell*

Undergoing Large Viscoelastic Deformation. **Zhou, E H and Lim, C T.** 2005,

Mechanics of Advanced Materials and Structures, Vol. 12, pp. 501–512.

80. **Mofrad, R K and Kamm, Roger D.** *Cytoskeletal Mechanics.* s.l. : Cambridge

university press, 2006. 978-0-521-84637-0.

81. *CONTINUUM-BASED COMPUTATIONAL MODELS FOR CELL AND*

NUCLEAR MECHANICS. **VAZIRI, ASHKAN, GOPINATH, ARVIND and**

DESHPANDE, VIKRAM S. 6, 2006, JOURNAL OF MECHANICS OF

MATERIALS AND STRUCTURES, Vol. 2, pp. 1169-1191.

82. **Boal, David.** *Mechanics of the cell.* Cambridge : Cambridge university press,

2001. 978-0-521-79681-1.

83. *Mechanical properties of plasma membrane and nuclear envelope measured by*

scanning probe microscope. **YOKOKAWA, M, TAKEYASU, K and**

YOSHIMURA, S H. 2008, Journal of Microscopy, Vol. 232, pp. 82–90.

84. *The application of a homogeneous half-space model in the analysis of*

endothelial cell micropipette measurements. **Theret, D P, et al.** 1988, Journal of

Biomechanical engineering, Vol. 110, pp. 190–199.

85. *Stress And Strain in a Yeast Cell Under High Hydrostatic Pressure.* **Hartmann,**

Christoph and Delgado, Antonio. 2004, Proceedings in Applied Mathematics and

Mechanics , Vol. 4, pp. 316–317.

86. *Etch rates for micromachining processing.* **Williams, K R, Gupta, K and Wasilik, M.** 4, 1996, Journal of Microelectromechanical Systems, Vol. 5, pp. 256-269.
87. *Advances in Selective Wet Etching for Nanoscale NiPt Salicide Fabrication.* **Chu, Ming Mao and Chou, Jung Hua.** 2010, Japanese Journal of Applied Physics, Vol. 49, pp. 1-5.
88. *Cutting single-walled carbon nanotubes.* **Ziegler, Kirk J, et al.** 2005, Nanotechnology, Vol. 16, pp. 539–544.
89. *Effect of Surface Treatment on Diffusion and Domain Formation in Supported Lipid Bilayers.* **Seu, Kalani J, et al.** April 2007, Biophysical Journal, Vol. 92, pp. 2445–2450.
90. *Plasma-Assisted InP-to-Si Low Temperature Wafer Bonding.* **Pasquariello, Donato and Hjort, Klas.** 1, 2002, IEEE JOURNAL ON SELECTED TOPICS IN QUANTUM ELECTRONICS, Vol. 8, pp. 118-131.
91. **Bhushan, Bharat, [ed.].** *Springer Handbook of Nanotechnology.* New York : Springer, 2004. 3-540-01218-4.
92. *Improvement on Hydrophilic and Hydrophobic Properties of Glass Surface Treated by Nonthermal Plasma Induced by Silent Corona Discharge.* **Yamamoto, Toshiaki, et al.** 1, 2004, Plasma Chemistry and Plasma Processing, Vol. 24, pp. 1-12.
93. *The Analysis of Oxygen Plasma Pretreatment for Improving Anodic Bonding.* **Choi, Seung Woo, et al.** 1, 2002, Journal of The Electrochemical Society, Vol. 149, pp. 8-11 .

94. **Stout, K J and Blunt, L.** *Three-Dimensional Surface Topography*. London : Penton Press, 2000. 1857180267.
95. *The effect of surface treatment on the surface texture and contact angle of electrochemically deposited hydroxyapatite coating and on its interaction with bone-forming cells.* **Eliaz, N, et al.** 2009, *Acta. Biomater*, Vol. 5, pp. 3178–3191.
96. *Nanopipette delivery of individual molecules to cellular compartments for single-molecule fluorescence tracking.* **Bruckbauer, A, et al.** 2007, *Journal of Biophysical*, Vol. 93, pp. 3120–3131.
97. *Gene delivery to the eye using adeno-associated viral vectors.* **Keith, Martin R. G, Klein, R L and Quigley, H A.** 2002, *Methods*, Vol. 28, pp. 267–275.
98. *Intracytoplasmic sperm injection in the mouse.* **Kimura, Y and Yanagimachi, R.** 1995, *biology of reproduction*, Vol. 52, pp. 709-720.
99. **Brown, K T and Flaming, D G.** *Advanced Micropipette Techniques for Cell Physiology*. San Francisco : John Wiley & Sons, 1995.
100. *Microdroplets: A sea of applications?* **Huebner, A, et al.** 2008, *Lab on Chip*, Vol. 8, pp. 1244–1254.
101. *Scanning nanolithography using a material-filled nanopipette.* **Hong, M H, et al.** 2000, *Applied Physics letters*, Vol. 77, pp. 2604-2606.
102. *The scanned nanopipette: a new tool for high resolution bioimaging and controlled deposition of biomolecules.* **Ying, L, et al.** 2005, *Physical Chemistry Chemical Physics*, Vol. 7, pp. 2859-66.

103. **Flaming, Dale G.** *Method of forming an ultrafine micropipette.* 4600424 CA, 15 July 1986 .
104. **Oesterle, Adair.** *Personal communication.* s.l. : Sutter instruments , 24 January 2009.
105. *Focused-ion beam tomography.* **Kubis, A J, et al.** 7, 2004, Metallurgical and Materials Transactions A, Vol. 35, pp. 1935– 1943.
106. *A computational approach to edge detection.* **Canny, J.** 1986, IEEE Transaction Pattern Analysis and Machine Intelligence, Vol. 8, pp. 679–714.
107. *Least-squares fitting of circles and ellipses.* **Gander, W, Golub, G H and Strebel, R.** 1994, BIT Numerical Mathematics, Vol. 34, pp. 558–578.
108. *The mechanics of pulling a glass micropipette.* **Purves, Robert D.** March 1980, Biophysical Journal, Vol. 29, pp. 523-530.
109. *Mechanics and deformation of the nucleus in micropipette aspiration experiment.* **Vaziri, Ashkan and Kaazempur Mofrad, Mohammad R.** 2007, Journal of Biomechanics, Vol. 40, pp. 2053–2062.
110. **Timoshenko, S P and Goodier, J N.** *Theory of Elasticity.* New York : McGraw-Hill, 1970.

APPENDIX A

In Chapter 3 it was mentioned that in the stereoscopic technique, depth can be calculated from measuring the parallax movement of features from their location in the first image, to the new location in the second image.

Consider a fixed frame of reference having three orthogonal axes x , y , z , as depicted in figure A.1. Axis z coincides with the optic axis of the microscope and axis x is parallel to the tilt axis of the goniometric head. During the capturing of stereo images the sample will undergo different displacements whose composition will be equivalent to a rotation around the x axis, which will be called the virtual axis of the tilt, and a vertical translation along the z axis. The reference frame is considered as sliding up and down in such a way that the relative movement of the object will be only a rotation around the x axis. This simply means that the projection centre C moves along z during tilting and that different values of d must be considered, one for each new tilted position. Let P be a point on the object having cylindrical coordinates φ , R and a , relative to the tilt axis, as shown in figure A.1.

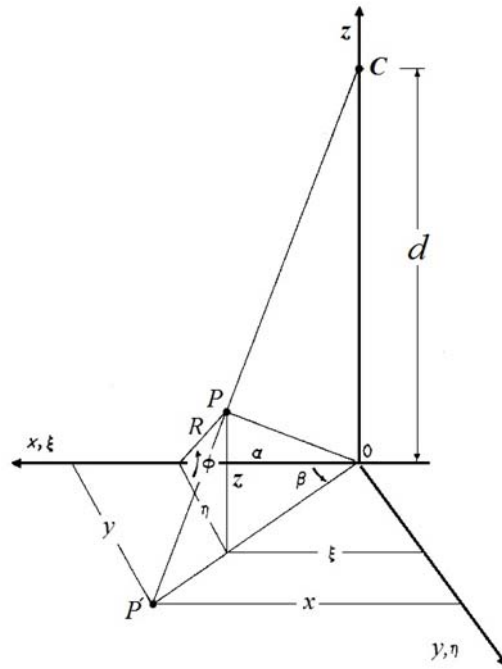


Figure A. 1 Coordinate axes for projection analysis.

The orthogonal coordinates of P are (68):

$$\zeta = a \qquad \eta = R \cos \varphi \qquad z = R \sin \varphi$$

Now the projection P' of P from the centre C on to the plane $z = 0$ has coordinates:

$$P'O = \frac{(a^2 + R^2 \cos^2 \varphi)^{1/2}}{1 - (R/d) \sin \varphi} \qquad \beta = \frac{R \cos \varphi}{a}$$

Or

$$x = \frac{a}{1 - (R/d) \sin \varphi} \qquad y = \frac{R \cos \varphi}{1 - (R/d) \sin \varphi}$$

Let us now consider the coordinates of projection P' as a function of the angle φ , and now introduce the tilt movement. As previously stated, the effect will be a shift along the z axis (thus determining a new working distance) and a rotation around the x axis by an angle equal to the angle of tilt. If we rotate the object around the x axis by an incremental quantity $\pm\Delta\varphi$, starting from the mean value φ , we obtain the following two sets of coordinates:

$$P(\varphi - \Delta\varphi): \begin{cases} x_1 = \frac{a}{1-(R/d_1) \sin(\varphi-\Delta\varphi)} \\ y_1 = \frac{R \cos(\varphi-\Delta\varphi)}{1-(R/d_1) \sin(\varphi-\Delta\varphi)} \end{cases}$$

$$P(\varphi + \Delta\varphi): \begin{cases} x_2 = \frac{a}{1-(R/d_1) \sin(\varphi+\Delta\varphi)} \\ y_2 = \frac{R \cos(\varphi+\Delta\varphi)}{1-(R/d_2) \sin(\varphi+\Delta\varphi)} \end{cases}$$

or, introducing the orthogonal coordinates ζ, η, z of $P(\varphi)$:

$$P(\varphi - \Delta\varphi): \begin{cases} x_1 = \frac{d_1 \zeta}{d_1 - z \cos \Delta\varphi + \eta \sin \Delta\varphi} \\ y_1 = \frac{d_1(\eta \cos \Delta\varphi + z \sin \Delta\varphi)}{d_1 - z \cos \Delta\varphi + \eta \sin \Delta\varphi} \end{cases}$$

$$P(\varphi + \Delta\varphi): \begin{cases} x_2 = \frac{d_2 \zeta}{d_2 - z \cos \Delta\varphi - \eta \sin \Delta\varphi} \\ y_2 = \frac{d_2(\eta \cos \Delta\varphi - z \sin \Delta\varphi)}{d_2 - z \cos \Delta\varphi - \eta \sin \Delta\varphi} \end{cases}$$

This gives four relationships in which x and y are the coordinates of the projections of point P on to the plane $z=0$. System (1) may be solved for the three unknowns

ζ, η, z :

$$z = \frac{(y_1 - y_2) \cos \Delta\varphi + y_1 y_2 (1/d_1 + 1/d_2) \sin \Delta\varphi}{\sin(2\Delta\varphi)(1 + y_1 y_2 / d_1 d_2) + \cos(2\Delta\varphi)(y_1 / d_1 - y_2 / d_2)}$$

$$\zeta = \frac{d_1 + d_2 - 2z \cos \Delta\varphi}{d_1 / x_1 + d_2 / x_2}$$

$$\eta = \frac{z\{(y_1 + y_2) \cos \Delta\varphi + (d_1 - d_2) \sin \Delta\varphi\} - (y_1 d_1 + y_2 d_2)}{(y_1 - y_2) \sin \Delta\varphi - (d_1 + d_2) \cos \Delta\varphi}$$

Therefore coordinates of point P were obtained. This can be done for all of the points in an SEM image to obtain the 3D structure of a given surface. Here this has been proved mathematically. Further information can be found in (68).